

AD-A207 542

KINEMATIC QUANTITIES DERIVED FROM A TRIANGLE OF VHF
DOPPLER WIND PROFILER. (U) PENNSYLVANIA STATE UNIV
UNIVERSITY PARK DEPT OF METEOROLOGY. C A CARLSON

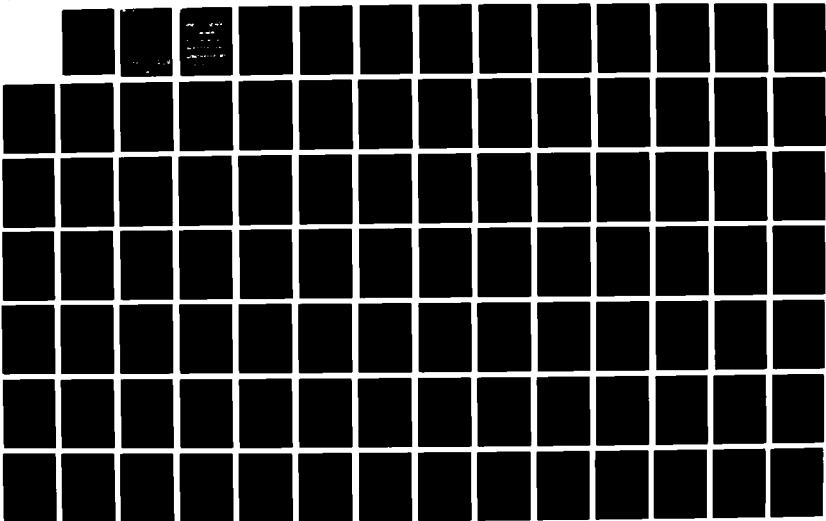
1/2

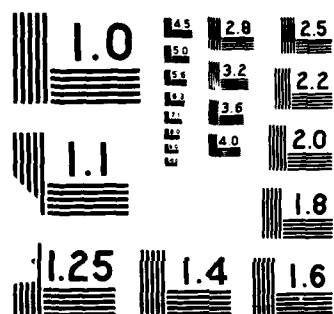
UNCLASSIFIED

AUG 87 SCIENTIFIC-1 AFGL-TR-87-0265

F/O 17/9

NL





AD-A207 542

**Stochastic Quantities Derived From a
Triangle of VHF Doppler Wind Profilers**

Catherine Ann Carlson

Pennsylvania State University
Department of Meteorology
University Park, PA 16802

August 1987

Scientific Report No. 1

APPROVED FOR PUBLIC RELEASE; DISTRIBUTION UNLIMITED


AIR FORCE GEOPHYSICS LABORATORY
AIR FORCE SYSTEMS COMMAND
UNITED STATES AIR FORCE
HANCOM AIR FORCE BASE, MASSACHUSETTS 01731-5000


DTIC
ELECTE
MAY 8 1989


S
Cb A D

89 5 5 068

"This technical report has been reviewed and is approved for publication"


ARTHUR JACKSON
Contract Manager


DONALD A. CHISHOLM, Chief
Atmospheric Prediction Branch


ROBERT A. MCCLACHEY, Director
Atmospheric Sciences Division

This document has been reviewed by the DOD Public Affairs Office (PAO) and is releasable to the National Technical Information Service (NTIS).

Qualified reporters may obtain additional copies from the Defense Technical Information Center. All others should apply to the National Technical Information Service.

If your address has changed, or if you wish to be removed from the mailing list, or if the addressee is no longer employed by your organization, please notify AFOSI/PAO, Room 3B-2A 01731-5000. This will assist us in maintaining a current mailing list.

Do not return copies of this report unless contractual obligations or notices on a specific document require that it be returned.

Unclassified

SECURITY CLASSIFICATION OF THIS PAGE

AD 4267542

REPORT DOCUMENTATION PAGE

1a. REPORT SECURITY CLASSIFICATION Unclassified			1b. RESTRICTIVE MARKINGS			
2a. SECURITY CLASSIFICATION AUTHORITY			3. DISTRIBUTION/AVAILABILITY OF REPORT Approved for public release; Distribution unlimited.			
2b. DECLASSIFICATION/DOWNGRADING SCHEDULE						
4. PERFORMING ORGANIZATION REPORT NUMBER(S)			5. MONITORING ORGANIZATION REPORT NUMBER(S) AFGL-TR-87-0265			
6a. NAME OF PERFORMING ORGANIZATION Pennsylvania State University		6b. OFFICE SYMBOL (If applicable)	7a. NAME OF MONITORING ORGANIZATION Air Force Geophysics Laboratory			
6c. ADDRESS (City, State, and ZIP Code) Department of Meteorology University Park, PA 16802			7b. ADDRESS (City, State, and ZIP Code) Hanscom AFB Massachusetts 01731-5000			
8a. NAME OF FUNDING/SPONSORING ORGANIZATION		8b. OFFICE SYMBOL (If applicable)	9. PROCUREMENT INSTRUMENT IDENTIFICATION NUMBER F19628-86-C-0092			
8c. ADDRESS (City, State, and ZIP Code)			10. SOURCE OF FUNDING NUMBERS			
			PROGRAM ELEMENT NO. 61102F	PROJECT NO. 2310	TASK NO. G8	WORK UNIT ACCESSION NO. BE
11. TITLE (Include Security Classification) Kinematic Quantities Derived From a Triangle of VHF Doppler Wind Profilers						
12. PERSONAL AUTHOR(S) Catherine Ann Carlson						
13a. TYPE OF REPORT Scientific Report #1		13b. TIME COVERED FROM 7/1/86 TO 6/30/87	14. DATE OF REPORT (Year, Month, Day) 1987 August		15. PAGE COUNT 146	
16. SUPPLEMENTARY NOTATION Submitted in partial fulfillment for Degree of Master of Science. This research was begun under, and partially supported by contract F19628-85-K-0011.						
17. COSATI CODES			18. SUBJECT TERMS (Continue on reverse if necessary and identify by block number)			
FIELD	GROUP	SUB-GROUP	wind profiler weather analysis vertical velocity			
			jet streams nowcasting precipitation			
			upper-level fronts weather forecasting divergence			
19. ABSTRACT (Continue on reverse if necessary and identify by block number) Using data from a triangle of VHF Doppler wind profilers, various kinematic quantities are calculated to investigate the mesoscale and synoptic-scale wind structure of jet streams, upper-level fronts, and synoptic-scale troughs. Hourly winds are used to compute horizontal divergence, relative vorticity, vertical velocity, and geostrophic and ageostrophic wind velocities. Kinematic vertical velocities are obtained at levels from the surface to 9 km by vertically integrating the horizontal divergence, applying the continuity equation for incompressible flow. As lower boundary conditions, orographic and frictional effects are applied from the surface to approximately 1.0 km above ground level. As an upper boundary condition, vertical velocities are forced to diminish to zero in the lower stratosphere. Three case studies are presented, using conventional rawinsonde, surface, and radar observations together with the winds and derived quantities obtained from the profiler network. Comparison of the synoptic-scale data with the profiler network data reveals that the two (OVER)						
20. DISTRIBUTION/AVAILABILITY OF ABSTRACT <input type="checkbox"/> UNCLASSIFIED/UNLIMITED <input type="checkbox"/> SAME AS RPT. <input type="checkbox"/> DTIC USERS			21. ABSTRACT SECURITY CLASSIFICATION Unclassified			
22a. NAME OF RESPONSIBLE INDIVIDUAL Arthur Jackson			22b. TELEPHONE (Include Area Code)		22c. OFFICE SYMBOL AFGL/LYP	

DD FORM 1473, 84 MAR

83 APR edition may be used until exhausted.
All other editions are obsolete.

SECURITY CLASSIFICATION OF THIS PAGE

Unclassified

Cont of Block 18:

vorticity
geostrophic wind
ageostrophic wind

Cont of Block 19:

data sets are generally consistent. Also, the profiler-derived kinematic quantities exhibit coherent vertical and temporal patterns, and these patterns change in a manner consistent with conceptual and theoretical models of the flow fields of various meteorological phenomena. *← RHT*

The temporal variations of the profiler-derived quantities are well correlated with the variations of the areal coverage of precipitation echoes over the profiler triangle during high-humidity periods. It is suggested that the profiler-derived quantities are of potential value to weather forecasters in that they enable the dynamic and kinematic interpretation of weather system structure and, thus, have nowcasting and short-term weather forecasting value.

2. VENTURER FORM	
FILL IN THE	
DATE	
TIME	
LOCATION	
OBSERVER	
EQUIPMENT	
REMARKS	
DIST	
SPECIAL	
A-1	



TABLE OF CONTENTS

	<u>Page</u>
LIST OF FIGURES	v
ACKNOWLEDGEMENTS	ix
CHAPTER 1 INTRODUCTION	1
1.1 History of the Problem of Studying Weather System Substructure	1
1.2 Background	2
1.3 Related Studies Using Doppler Wind Profiler Data	3
1.4 Purpose of This Study	8
CHAPTER 2 KINEMATIC QUANTITIES AND DIAGNOSIS OF WEATHER SYSTEMS	10
2.1 Introduction	10
2.2 Mean and Perturbation Wind Field	10
2.3 Divergence	12
2.4 Vertical Velocity	15
2.5 Vorticity	16
2.6 Geostrophic and Ageostrophic Winds	18
CHAPTER 3 METHODS OF CALCULATING KINEMATIC QUANTITIES WITH DOPPLER WIND PROFILERS	22
3.1 Profiler-Derived Horizontal Winds	22
3.2 Perturbation Wind	23
3.3 Horizontal Divergence	23
3.4 Vertical Velocity	26
3.5 Vorticity	31
3.6 Geostrophic and Ageostrophic Winds	33
CHAPTER 4 CASE STUDIES OF SYNOPTIC-SCALE FEATURES USING DOPPLER WIND PROFILER DATA	35
4.1 Case of September 22-23, 1985	35
4.2 Case of September 28-29, 1985	66
4.2.1 Low-Level Fronts and Troughs	72
4.2.2 Upper-Level Troughs and Jet Streaks	84
4.3 Case of October 22-23, 1985	100

TABLE OF CONTENTS (Continued)

	<u>Page</u>
CHAPTER 5 SUMMARY AND CONCLUSIONS	126
5.1 Assessment of Quality of the Derived Kinematic Quantities	126
5.2 Summary of Meteorological Observations with the Profiler Data	129
5.3 Overall Conclusions	132
BIBLIOGRAPHY	134

LIST OF FIGURES

<u>Figure</u>		<u>Page</u>
1.1	The Colorado wind profiler triangle located in northeastern Colorado	4
4.1	Surface pressure analyses	36
4.2	Time-height section of observed winds from the Platteville profiler during the period from 0300 UT 22 September 1985 to 1600 UT 23 September 1985 . . .	38
4.3	Time-height section from the Fleming profiler during the time period from 0300 UT 22 September 1985 to 1600 UT 23 September 1985	39
4.4	Time-height section of observed winds from the Flagler profiler during the time period from 0300 UT 22 September 1985 to 1600 UT 23 September 1985 . . .	40
4.5	National Meteorological Center (NMC) objective analyses of 300 mb height and temperature fields . .	43
4.6	Time-height section of profiler-derived geostrophic winds during the period from 0300 UT 22 September 1985 to 1400 UT 23 September 1985	48
4.7	Time-height section of the profiler-derived ageostrophic winds during the period from 0300 UT 22 September 1985 to 1400 UT 23 September 1985 . . .	50
4.8	Time-height section of the perturbation winds from the Platteville profiler during the period from 1600 UT 22 September 1985 to 1600 UT 23 September 1985	51
4.9	Time-height section of the perturbation winds from the Fleming profiler during the period from 1600 UT 22 September 1985 to 1600 UT 23 September 1985 . . .	52
4.10	Time-height section of the perturbation winds from the Flagler profiler during the period from 1600 UT 22 September 1985 to 1600 UT 23 September 1985 . . .	53
4.11	Time-height section of the profiler-derived relative vorticity field (units of $1 \times 10^{-5} \text{ s}^{-1}$) during the period from 0300 UT 22 September 1985 to 1500 UT 23 September 1985	55

LIST OF FIGURES (Continued)

<u>Figure</u>		<u>Page</u>
4.12	Time-height section of the profiler-derived horizontal divergence (units of $1 \times 10^{-5} \text{ s}^{-1}$) during the period from 0300 UT 22 September 1985 to 1500 UT 23 September 1985	57
4.13	NW-SE cross-sections of potential temperature (solid lines, K) and relative humidity (dashed lines, %)	59
4.14	Time-height section of profiler-derived kinematic vertical velocities (cm/s) during the period from 0300 UT 22 September 1985 to 1500 UT 23 September 1985, and a plot of percent areal coverage of the profiler triangle by precipitation echo from the Limon, CO, weather radar	61
4.15	Skew-T log-P diagrams from Denver, CO	62
4.16	Surface pressure analyses	67
4.17	WNW-ESE cross-sections of potential temperature (solid lines, K) and relative humidity (dashed lines, %)	70
4.18	NMC objective analyses of 700 mb height and temperature fields	73
4.19	Time-height section of observed winds from the Platteville profiler during the period from 1200 UT 28 September 1985 to 0000 UT 30 September 1985 . . .	77
4.20	Time-height section of observed winds from the Fleming profiler during the period from 1200 UT 28 September 1985 to 0000 UT 30 September 1985 . . .	78
4.21	Time-height section of observed winds from the Flagler profiler during the period from 1200 UT 28 September 1985 to 0000 UT 30 September 1985 . . .	79
4.22	Time-height section of perturbation winds from the Platteville profiler during the period from 0000 UT 29 September 1985 to 0000 UT 30 September 1985 . . .	81
4.23	Time-height section of perturbation winds from the Fleming profiler during the period from 0000 UT 29 September 1985 to 0000 UT 30 September 1985 . . .	82

LIST OF FIGURES (Continued)

<u>Figure</u>		<u>Page</u>
4.24	Time-height section of the perturbation winds from the Flagler profiler during the period from 0000 UT 29 September 1985 to 0000 UT 30 September 1985	83
4.25	NMC objective analyses of 300 mb height and temperature fields	85
4.26	Time-height section of the profiler-derived geostrophic winds during the period from 1200 UT 28 September 1985 to 2300 UT 29 September 1985 . . .	89
4.27	Time-height section of the profiler-derived ageostrophic winds during the period from 1200 UT 28 September 1985 to 2300 UT 29 September 1985 . . .	90
4.28	Time-height section of the profiler-derived relative vorticity field (units of $1 \times 10^{-5} \text{ s}^{-1}$) during the period from 1200 UT 28 September 1985 to 0000 UT 30 September 1985	92
4.29	Time-height section of profiler-derived horizontal divergence (units of $1 \times 10^{-5} \text{ s}^{-1}$) during the period from 1200 UT 28 September to 0000 UT 30 September 1985	94
4.30	Time-height section of the profiler-derived kinematic vertical velocities (cm/s) during the period from 1200 UT 28 September 1985 to 2200 UT 29 September 1985, and a plot of percent areal coverage of the profiler triangle by the precipitation echo	95
4.31	Skew-T log-P diagrams from Denver, CO	97
4.32	WNW-ESE cross-sections of potential temperature (solid lines, K) and relative humidity (dashed lines, %)	101
4.33	300 mb height (solid lines, m) and isotach (dashed lines, m/s) analyses	104
4.34	Time-height section of the observed winds from the Platteville profiler during the period from 1200 UT 22 October 1985 to 1200 UT 23 October 1985	108

LIST OF FIGURES (Continued)

<u>Figure</u>		<u>Page</u>
4.35	Time-height section of the observed winds from the Fleming profiler during the period from 1200 UT 22 October 1985 to 1200 UT 23 October 1985	109
4.36	Time-height section of the observed winds from the Flagler profiler during the period from 1200 UT 22 October 1985 to 1200 UT 23 October 1985	110
4.37	Time-height section of profiler-derived geostrophic winds during the period from 1200 UT 22 October 1985 to 0900 UT 23 October 1985	113
4.38	Time-height section of profiler-derived ageostrophic winds during the period from 1200 UT 22 October to 0900 UT 23 October 1985	115
4.39	Time-height section of the profiler-derived relative vorticity field (units of $1 \times 10^{-5} \text{ s}^{-1}$) during the period from 1200 UT 22 October 1985 to 1000 UT 23 October 1985	117
4.40	Time-height section of the profiler-derived horizontal divergence (units of $1 \times 10^{-5} \text{ s}^{-1}$) during the period from 1200 UT 22 October 1985 to 1000 UT 23 October 1985	120
4.41	Time-height section of the profiler-derived kinematic vertical velocities (cm/s) during the period from 1200 UT 22 October 1985 to 1000 UT 23 October 1985	121
4.42	Skew-T log-P diagrams from Denver, CO	123

ACKNOWLEDGEMENTS

The author offers her gratitude to Dr. Gregory S. Forbes, advisor of the thesis, for his guidance and patience throughout the course of the thesis research. I am also grateful to Dr. Dennis W. Thomson and Dr. John J. Cahir for their guidance and contributions during the research. I would like to thank A. Person, S. Williams, B. Peters, W. Syrett, and P. Neiman for their technical assistance, and A. S. Frisch and R. Strauch of NOAA/ERL Wave Propagation Laboratory for providing the data from the Fleming, Platteville, and Flagler profilers. Finally, I wish to thank William M. Lapenta for his encouragement and support during the thesis project.

The research was supported by the Air Force Geophysics Laboratory under contracts F19628-85-K-0011, and F19628-86-C-0072.

CHAPTER 1

INTRODUCTION

1.1 History of the Problem of Studying Weather System Substructure

Upper-level winds are currently measured only twice daily with expendable rawinsondes. Stations in the national network are spaced 300 to 500 km apart. The resulting temporal and spatial resolution allows the detection of synoptic-scale features such as jet streams, fronts, and trough-ridge systems which have horizontal scales on the order of 1000 km and time spans on the order of a few days. But the mesoscale structures of these features, which are on the order of 100 km or less, often go undetected due to the relatively coarse temporal and spatial resolution.

The analysis of mesoscale structure generally has been limited to measurements obtained from special mesoscale rawinsonde networks like those set up during Project Stormy Spring, AVE (Atmospheric Variability Experiment), and SESAME (Severe Environmental Storms and Mesoscale Experiment), and to aircraft measurements. Shapiro (1974, 1978) and Shapiro and Kennedy (1981, 1982) used the NCAR Sabliner to observe the mesoscale wind structure associated with upper-level fronts, jet streaks, and synoptic-scale waves. With the recent development of Doppler wind profilers, the meteorologists now have the opportunity to observe the mesoscale time variations of these features as they pass through the profiler beams. Further, when mesoscale networks of wind profilers are deployed, even more can be learned about the mesoscale structure of these features.

1.2 Background

Gage and Balsley (1978) summarized the historical development of the wind profiler technique. Unlike microwave (3 to 10 cm wavelength) Doppler weather radars, which are most sensitive to hydrometeors, the wind profilers (33 cm to 6 m wavelength) are sensitive principally to clear air eddies and turbulence.

The Doppler wind profiler derives its signal from the backscatter of the transmitted signal by inhomogeneities in the radio refractive index. These inhomogeneities are the result of turbulence-scale variations in the temperature and humidity. Gage and Balsley (1978), Balsley (1981), and Balsley and Gage (1982) reviewed the measurement technique used by the various profiling systems.

Larsen and Röttger (1982) and Hogg et al. (1983) discuss the techniques and systems employed to resolve the horizontal winds using UHF and VHF wind profilers. The most common and inexpensive method uses a phased dipole array as an antenna which phases the transmitted pulse so that it produces a beam pointed about 15° off-zenith. Two off-zenith beams are used to determine the horizontal wind vector, and a zenith-pointing beam is used to measure the vertical velocity.

The Wave Propagation Laboratory (WPL), located in Boulder, Colorado, has been operating a network of UHF and VHF Doppler radar wind profilers since 1983. Strauch et al. (1984) describe the instrument designs, the data processing and averaging techniques, and the performance characteristics of the Colorado wind profilers.

Measurements used in this thesis were obtained using the three Doppler wind profilers sited near Fleming, Flagler, and Platteville, Colorado. The distance between each of these profilers is approximately 160 km, less than half the distance between the rawinsonde sites in the national network. The location of these profilers with respect to the Continental Divide is shown in Figure 1.1.

The three Doppler wind profilers all have phased dipole arrays for antennae. All operate at approximately 50 MHz, and transmit both 3 μ s and 9 μ s pulses. The 3 μ s pulse provides high-resolution data, sampling the troposphere at 290 m intervals starting about 1.7 km above ground level or 3.0 km above sea level. The 9 μ s pulse gives low-resolution data, sampling the troposphere at 870 m intervals starting about 2.6 km above ground level or 4.0 km above sea level. High-resolution data samples the troposphere from 3 to 9 km for 22 levels at hourly intervals, and will be used most extensively in this thesis.

1.3 Related Studies Using Doppler Wind Profiler Data

Since the late 1970's, various observations of front and jet stream passages have been reported using a single Doppler wind profiler. Rüster and Czechowsky (1979) observed a jet stream passage with the SOUSY VHF radar facility located in West Germany. The Doppler wind profiler measurements at the jet stream level agreed well with the rawinsonde data observations. They also found that this profiler, having 150 m vertical resolution, was able to observe a 100 m layer of strong vertical shear located just below the jet stream.

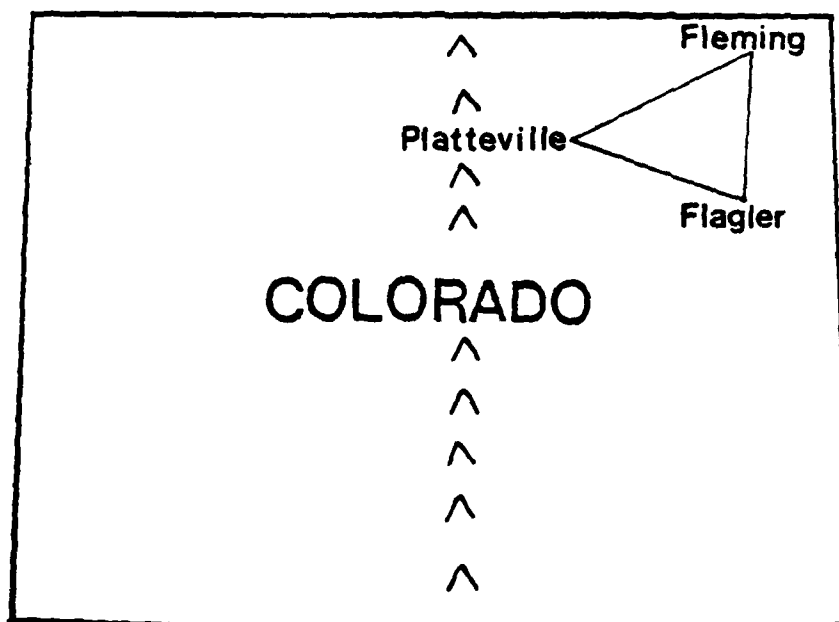


Figure 1.1 The Colorado wind profiler triangle located in northeastern Colorado.

Röttger (1979) and Röttger and Schmidt (1981) observed warm frontal passages with the same system. Both the horizontal and vertical winds, and the radar reflectivities from the vertical beam were used to analyze frontal characteristics. They found that the profiler-deduced information indicating the location and intensity of the frontal zone was consistent with rawinsonde data.

Green et al. (1978) used the Sunset profiler located in Colorado to monitor a jet streak passage, and found sharp wind speed increases and decreases with time at the jet streak level. With the use of the three-beam system, Green et al. were also able to qualitatively infer that the direct transverse circulation located in the entrance region of the jet streak had passed over the profiler site. Forbes (1986) observed the coupling of upper and lower jet streak circulations with one of the Pennsylvania State University profilers. The low-level profiler winds backed to the southwest as the exit region of a northerly jet streak moved over the profiler site. The direction of the low-level winds was consistent with the return branch of an indirect transverse circulation located in an exit region of a jet streak.

Using the Colorado profiler network, Shapiro et al. (1984) presented a case study of an upper-level frontal passage and an associated jet streak, which were located in a strong upper-level trough. They used the hourly averaged winds from the Cahone, Lay Creek, Stapleton, and Fleming profilers and the surrounding rawinsonde sites to construct a cross-section of winds and potential temperature through the frontal zone. The cross-section illustrated the weak wind speeds and wind shift associated with the upper-level

trough axis, and the strong (35 m/s) jet streak located west of the frontal zone in the cold air. The Lay Creek and Cahone time-height sections of the jet streak also revealed a 1 km layer of strong vertical wind shear located beneath the jet streak.

Stankov and Shapiro (1986) used the Stapleton (UHF) wind profiler to investigate the passage of a surface cold front. Profiler soundings were taken every 1.2 minutes at 100 m intervals for a depth from about 1.5 to 3.5 km above ground level. They used a time-space conversion technique to derive horizontal divergence, the vertical component of vorticity, and vertical velocity from the temporal variations of the horizontal wind. For these computations they assumed that the front-parallel gradients were much smaller than the front-normal gradients, and that the front remained in a steady state as it passed over the profiler. With these assumptions, Stankov and Shapiro found large cyclonic cross-front vorticity and convergence at the leading edge of the front, and large anticyclonic cross-front vorticity and divergence behind the front. They also found rising motions using the kinematic method, on the order of 1.5 m/s at the front with weaker sinking motions behind the front. They compared their kinematically derived vertical velocities with the profiler measured vertical velocities, and found good agreement except for the lowermost 1 km.

The Colorado profiler network also has provided meteorologists with an opportunity to calculate two-dimensional derived quantities such as horizontal divergence, vorticity, kinematic vertical velocities, and ageostrophic and geostrophic winds. Zamora and Shapiro (1984) calculated horizontal divergence and absolute

vorticity using the line integral method (see Section 3.3 for a detailed explanation) with the Lay Creek, Cahone, and Fleming profilers. A comparison of the divergence and vorticity values obtained from this profiler triangle to those computed with rawinsonde data showed that the profiler triangle derived quantities were consistent with the rawinsonde-based quantities. Zamora and Shapiro also showed correlation was evident between maximum positive values of the profiler-derived divergence at 9 km and the occurrence of severe weather near the profiler triangle.

Smith and Schlatter (1986) used a Kinematic Analysis Model (KAM) developed at Purdue University to calculate horizontal divergence, vorticity, and vertical velocities. To compute divergence and vorticity, KAM used the u and v components from the Fleming, Platteville, and Flagler profilers and expanded the u and v components for each site into a first order Taylor series, solving six equations for six unknowns and the partial derivatives. Assuming that w was equal to zero from the surface to 1500 m, KAM kinematically solved for the vertical velocity field. For a case study in which an approaching short-wave trough touched off thunderstorms in the profiler triangle, Smith and Schlatter compared the profiler-derived quantities to those derived from a rawinsonde triangle. The profiler-derived divergence field had strong convergence values and upward motions from 700 mb to 300 mb at the time the thunderstorms were present, while the rawinsonde network had weak divergence below 500 mb and weak convergence above 500 mb at this time. Weak downward motions were also present in the rawinsonde triangle.

Zamora et al. (1987) calculated horizontal divergence, absolute vorticity, absolute vorticity advection, deformation, and areal-averaged ageostrophic and geostrophic winds using the Lay Creek, Fleming, and Cahone profilers. A linear vector point function (LVPF), similar to the line integral method in that the winds are assumed to vary linearly from point to point, was used to calculate the above quantities. They presented two cases which showed that the above quantities, and their variations in time, were consistent with the synoptic-scale conditions. They also found that these quantities revealed mesoscale structure in the jet stream which was unresolved by the rawinsonde network. Zamora et al. also mentioned that the magnitudes of the ageostrophic winds and absolute vorticity advections were suspect due to their assumption that vertical motions were negligible when calculating these quantities.

1.4 Purpose of This Study

The purpose of this thesis is to investigate the synoptic-scale and mesoscale wind structure of jet streams, upper-level fronts, and synoptic-scale troughs using a triangle of VHF Doppler wind profilers. Specifically, kinematic quantities such as horizontal divergence, relative vorticity, and vertical velocity, as well as the ageostrophic and geostrophic winds, are used to diagnose these features. The hourly, high-resolution horizontal winds from the Fleming, Platteville, and Flagler profilers are used primarily in the computation of the kinematic quantities. Horizontal divergence and relative vorticity are computed using a line integral method and finite differencing technique. The geostrophic and ageostrophic

winds are computed by evaluating the derivatives of the equation of motion with a finite differencing technique. Assuming the atmosphere is incompressible, vertical velocities are derived by vertically integrating the continuity equation.

The principles of these methods for calculating kinematic quantities are discussed in Chapter 2. Chapter 3 discusses the application of these methods to Doppler wind profiler data.

Three case studies, which combine the conventional rawinsonde, surface and radar observations with the observed winds and derived quantities of the Doppler wind profiler network, are presented in Chapter 4. Chapter 5 summarizes and presents the conclusions.

CHAPTER 2

KINEMATIC QUANTITIES AND DIAGNOSIS OF WEATHER SYSTEMS

2.1 Introduction

Kinematic quantities are those which can be determined from the motions of a fluid without reference to the existing forces which cause the motion. Basically, kinematic quantities provide a geometric description of the velocity pattern of a fluid. In meteorology, kinematic quantities are among the most useful tools for analyzing patterns of the wind field, and in particular, for examining important characteristics such as vorticity and divergence. These quantities and others will be discussed in more detail in the following sections.

2.2 Mean and Perturbation Wind Field

The total (i.e., observed) wind velocity at a particular point in space and time can be written as

$$\underline{v} = \bar{\underline{v}} + \underline{v}' \quad , \quad (1)$$

where the total velocity field is equal to the sum of the time or space averaged velocity, $\bar{\underline{v}}$, and the varying perturbation velocity, \underline{v}' . The equation can be rearranged to solve for the perturbation field,

$$\underline{v}' = \underline{v} - \bar{\underline{v}} \quad . \quad (2)$$

In this form, the mean flow field often represents the zonal wind while the perturbation flow field represents the disturbance embedded in the zonal field.

In order to obtain a precise representation of the perturbation field, an appropriate averaging period must be chosen. For time series observations from an individual station, the appropriate averaging period will be dependent upon the wavelength of the meteorological disturbance of interest and the speed of propagation of the disturbance associated with that perturbation. For a wave-like disturbance having wavelength L and propagation speed C , the disturbance has period $T = LC^{-1}$. Hence, an averaging period that is an integer multiple of T will isolate the wave disturbance from the steady mean flow, U , by averaging out the sinusoidal perturbations. That is, if $\underline{v} = U\hat{i} + V \cos 2\pi ft\hat{j}$, where V is the amplitude of the wave perturbation, then

$$\begin{aligned}\bar{\underline{v}} &= \int_0^T \underline{v} dt \left[\int_0^T dt \right]^{-1} = \int_0^T U dt \left[\int_0^T dt \right]^{-1} \hat{i} \\ &+ \int_0^T V \cos 2\pi f t dt \left[\int_0^T dt \right]^{-1} \hat{j} \quad .\end{aligned}$$

Since $f=1/T$ and U is a constant,

$$\bar{\underline{v}} = U T T^{-1} \hat{i} + V (T-T) T^{-1} \hat{j} = U \hat{i}$$

$$\underline{v}' = \underline{v} - \bar{\underline{v}} = \underline{v} - U \hat{i} = V \cos 2\pi f t \hat{j} \quad .$$

In practice, any averaging period $\geq T$ effectively reveals the mesoscale feature as the perturbation wind, but may include a small wave (phase) bias. In meteorology, this process can be effectively used to differentiate the mesoscale perturbations from the slowly varying synoptic scale pattern.

2.3 Divergence

Divergence is a scalar quantity resulting from a vector operation which describes the rate of expansion or compression of a vector field. By definition, the divergence of \underline{F} is

$$\nabla \cdot \underline{F} = \frac{\partial F}{\partial x} + \frac{\partial F}{\partial y} + \frac{\partial F}{\partial z} \quad , \quad (3)$$

where \underline{F} represents a three-dimensional vector. The mass continuity equation for a fluid is

$$\frac{\partial \rho}{\partial t} = - \nabla \cdot (\rho \underline{V}) \quad , \quad (4)$$

which indicates that if the fluxes through the sides of a volume of fluid do not balance, then the mass within the volume must increase or decrease. This can also be written

$$\frac{\partial \rho}{\partial t} = - \underline{V} \cdot \nabla \rho - \rho \nabla \cdot \underline{V} \quad ,$$

or

$$\frac{\partial \rho}{\partial t} = - \rho \nabla \cdot \underline{v} \quad ,$$

or

$$- \frac{1}{\rho} \frac{d\rho}{dt} = \nabla \cdot \underline{v} \quad . \quad (5)$$

Since for most applications the atmosphere can be considered incompressible at any particular level, equation (5) simplifies to the continuity equation

$$\frac{\partial u}{\partial x} + \frac{\partial v}{\partial y} + \frac{\partial w}{\partial z} = 0 \quad . \quad (6)$$

The equation can be rewritten in terms of horizontal divergence

$$\text{DIV} \equiv \frac{\partial u}{\partial x} + \frac{\partial v}{\partial y} = - \frac{\partial w}{\partial z} \quad , \quad (7)$$

where horizontal divergence is compensated by vertical shrinking of a column of air, and horizontal convergence is compensated by vertical stretching of a column of air. The magnitude of synoptic scale divergences is typically on the order of $1 \times 10^{-5} \text{ s}^{-1}$.

When deep layers of the atmosphere are involved, and vertical motions are present, vertical variations of air density must also be considered. The continuity equation for incompressible motion then becomes, from equation (4),

$$0 = - w \frac{\partial \rho}{\partial z} - \rho(\text{DIV}) - \rho \left(\frac{\partial w}{\partial z} \right)$$

or

$$\frac{\partial w}{\partial z} + \frac{w}{\rho} \frac{\partial \rho}{\partial z} = - \text{DIV} \quad . \quad (8)$$

The vertical advective term, involving vertical velocity and vertical gradients of air density, has a magnitude typically 10% (or less) of the first term and is usually of the opposite sign.

Dines' compensation law states that there exists at least one sign reversal of divergence with height such that the net mass in a column does not tend to be depleted or accumulated appreciably with time. A consequence of this law is that there also exists at least one level where divergence is equal to zero, a level of non-divergence.

In the earth's atmosphere, this level of non-divergence (LND) is often found near the 600 mb level. From equations (7) and (8), the maximum vertical velocity is found near this level. Synoptic-scale upward motion is associated with horizontal convergence at low levels while horizontal divergence is occurring above the LND. This pattern is often found to the east of a 500 mb trough axis and above a developing low pressure system. Conversely, synoptic scale downward motion is associated with horizontal divergence at or near the surface with horizontal convergence occurring above the LND. This condition often occurs west of a 500 mb trough axis and above a developing high pressure system. Analysis of the divergence patterns in the atmosphere can be very helpful in diagnosing vertical motion fields and, thus, cloud cover and precipitation patterns.

2.4 Vertical Velocity

The vertical velocity is the component of the wind oriented along the local vertical axis. Synoptic-scale vertical velocities are on the order of magnitude of a few centimeters per second, much smaller and more difficult to measure than synoptic-scale horizontal motions. Because of this difficulty, it has been necessary to develop indirect methods to ascertain the vertical motion field.

The kinematic method is one example of an indirect method of computing vertical velocities of the atmosphere. It will be used later in this thesis. The continuity equation (7), is integrated vertically from the ground (z_0) to some level h . The integral becomes

$$\int_{z_0}^h \frac{\partial w}{\partial z} dz = - \int_{z_0}^h \left(\frac{\partial u}{\partial x} + \frac{\partial v}{\partial y} \right) dz \quad , \quad (9)$$

where z is height and w is the vertical component of the wind.

Integrating the left side, the equation simplifies to

$$w(h) = w(z_0) - \int_{z_0}^h \text{DIV} \partial z = w(z_0) - \overline{\text{DIV}} (h - z_0) \quad , \quad (10)$$

where $\overline{\text{DIV}}$ is the layer averaged horizontal divergence, and w_0 is the vertical velocity at ground level. w_0 is assumed to equal zero for most cases except where the terrain may be steep enough to force a vertical component to the primarily horizontal flow.

When the integral is performed over a deep layer, vertical density variations must also be considered and equation (8) is non-

linear in w . Since the vertical advective term is of secondary importance, a mean vertical velocity can be used, giving

$$w(h) = w(z_0) + \bar{w}^{z_0, h} \ln \left(\frac{\rho_0}{\rho_h} \right) - \overline{\text{DIV}} (h - z_0) \quad (11)$$

This equation can be solved by iteration, first using $w(z_0)$ as an approximation of \bar{w} to obtain $w(h)$, then re-calculating for \bar{w} , and repeating until trial values of $w(h)$ converge to within reasonable limits.

Dines' compensation law stated previously requires that the vertically integrated horizontal divergence equal zero in the layer from the surface to the top of the atmosphere or to some level aloft where w equals zero. The latter level is usually chosen to be in the lower stratosphere near 14 km (or 100 mb). In practice, the largest synoptic scale vertical motions are found near the level of non-divergence with the smallest synoptic-scale vertical motions found at the ground and in the stratosphere.

2.5 Vorticity

Vorticity measures the rotation of a fluid. The vorticity or curl of a vector $\underline{F} = F_1 \hat{i} + F_2 \hat{j} + F_3 \hat{k}$ can be written as

$$\nabla \times \underline{F} = \left(\frac{\partial F_3}{\partial y} - \frac{\partial F_2}{\partial z} \right) \hat{i} + \left(\frac{\partial F_1}{\partial z} - \frac{\partial F_3}{\partial x} \right) \hat{j} + \left(\frac{\partial F_2}{\partial x} - \frac{\partial F_1}{\partial y} \right) \hat{k} \quad (12)$$

where \hat{i} , \hat{j} , and \hat{k} are unit vectors and \underline{F} is a three-dimensional vector. Three-dimensional atmospheric vorticity is obtained by

substituting \underline{V} for \underline{F} . In most instances, meteorologists are concerned with the vertical component of vorticity, $\hat{k} \cdot \nabla \times \underline{V}$. The vertical component is

$$\xi = \hat{k} \cdot \nabla \times \underline{V} = \frac{\partial v}{\partial x} - \frac{\partial u}{\partial y} \quad (13)$$

The magnitude of synoptic scale relative vorticity is on the order of $1 \times 10^{-5} \text{ s}^{-1}$. Absolute vorticity is obtained by adding the Coriolis parameter $f = 2\Omega \sin \phi$, where ϕ is latitude and Ω is the rotation rate of the earth, 2π per 24 hours.

Diagnosis of vorticity is important for locating and studying the development of mid-latitude cyclones and anticyclones. Positive relative vorticity indicates cyclonic or counterclockwise circulation. Conversely, negative relative vorticity indicates anticyclonic or clockwise circulation. Upper-level (500 mb) troughs and surface low pressure systems are associated with positive relative vorticity whereas upper-level (500 mb) ridges and surface high pressure systems are associated with negative relative vorticity.

Most mid-latitude weather disturbances are embedded in a zonal flow that is westerly and increases in speed with height in the troposphere, yet disturbances propagate with approximately the mid-tropospheric velocity at the LND. This means that air flows through the trough aloft from west to east, and must experience an increase of vorticity as it moves toward the trough axis from the west and a decrease of vorticity as it "outruns" the trough to its east. These increases and decreases of vorticity are largely accomplished through horizontal convergence and divergence, respectively; much like a

skater spinning faster as his or her arms are contracted toward the body and spinning slower when the arms are extended. In the area ahead of the trough in the upper troposphere, where the wind would advect the cyclonic vorticity eastward away from the trough axis, positive vorticity advection (PVA) is counteracted by divergence which in turn produces upward motion. Similar arguments can be made for negative vorticity advection (NVA) and for other levels. Hence, diagnosis of vorticity advections is useful for analyzing vertical motions in synoptic-scale wave systems induced by large-scale patterns of divergence and convergence.

2.6 Geostrophic and Ageostrophic Winds

The observed winds represent the sum of various steady and varying components. The equations of horizontal motion are

$$\frac{du}{dt} = -\frac{1}{\rho} \frac{\partial P}{\partial x} + fv + F_x$$

and

$$\frac{dv}{dt} = -\frac{1}{\rho} \frac{\partial P}{\partial y} - fu + F_y, \quad (14)$$

where the terms on the left-hand side are accelerations of the wind, the terms involving P (atmospheric pressure) are the pressure-gradient forces, the terms involving f are the Coriolis forces, and the terms F_x and F_y represent the sum of other forces (including frictional and turbulent processes) which can yield accelerations or decelerations.

A fair approximation of the atmosphere in many instances is that the flow is frictionless and unaccelerated, such that the pressure gradient and Coriolis force terms are in nearly exact balance. This balance is referred to as geostrophic balance. The geostrophic wind components are

$$u_g = -\frac{1}{f\rho} \frac{\partial P}{\partial y} \quad \text{and} \quad v_g = \frac{1}{f\rho} \frac{\partial P}{\partial x} \quad (15)$$

The actual wind \underline{V} can be interpreted as being composed of two components, one geostrophic and the other ageostrophic, $\underline{V} = \underline{V}_g + \underline{V}_{ag}$. Substituting into the equations of motion,

$$\begin{aligned} \frac{d(u_g + u_{ag})}{dt} &= -\frac{1}{\rho} \frac{\partial P}{\partial x} + fv + F_x \\ &= -\frac{1}{\rho} \frac{\partial P}{\partial x} + fv_g + fv_{ag} + F_x = fv_{ag} + F_x \end{aligned} \quad (16)$$

Hence,

$$v_{ag} = \frac{1}{f} \frac{d(u_g + u_{ag})}{dt} - \frac{1}{f} F_x \quad (17)$$

Similarly,

$$u_{ag} = -\frac{1}{f} \frac{d(v_g + v_{ag})}{dt} - \frac{1}{f} F_y \quad (18)$$

Equations (17) and (18) suggest several sources of ageostrophic winds. When friction is present, it is possible to have unaccelerated flow with

$$v_{ag} = -\frac{1}{f} F_x \quad \text{and} \quad u_{ag} = -\frac{1}{f} F_y \quad (19)$$

It is also possible to have ageostrophic flow without friction, even if the ageostrophic component is steady, with

$$\begin{aligned} v_{ag} &= \frac{1}{f} \frac{du_g}{dt} & ; & & u_{ag} &= -\frac{1}{f} \frac{dv_g}{dt} \\ &= -\frac{1}{f} \frac{d}{dt} \left(\frac{1}{\rho f} \frac{\partial P}{\partial y} \right) & & & &= \frac{1}{f} \frac{d}{dt} \left(\frac{1}{\rho f} \frac{\partial P}{\partial x} \right) \\ &= -\frac{1}{\rho f^2} \frac{\partial}{\partial y} \left(\frac{\partial P}{\partial t} \right) & & & &= \frac{1}{\rho f^2} \frac{\partial}{\partial x} \left(\frac{\partial P}{\partial t} \right) \quad (20) \end{aligned}$$

The latter expressions, derived via several approximations, are referred to as the isallobaric wind components.

At locations where friction and other forces (F_x and F_y) are negligible,

$$v_{ag} = \frac{1}{f} \frac{du}{dt} \quad \text{and} \quad u_{ag} = -\frac{1}{f} \frac{dv}{dt} \quad (21)$$

Expanding the total derivative of the horizontal equations of motion, and solving for the ageostrophic components, the final result reduces to

$$u_{ag} = -\frac{1}{f} \left[\frac{\partial v}{\partial t} + u \frac{\partial v}{\partial x} + v \frac{\partial v}{\partial y} + w \frac{\partial v}{\partial z} \right] \quad (22)$$

$$v_{ag} = \frac{1}{f} \left[\frac{\partial u}{\partial t} + u \frac{\partial u}{\partial x} + v \frac{\partial u}{\partial y} + w \frac{\partial u}{\partial z} \right] \quad (23)$$

Thus, horizontal ageostrophic motions result from the imbalance between the local rate of change of the horizontal wind, and the effects of horizontal and vertical advection of variations in the wind.

Equations (21)-(23) suggest other conditions during which ageostrophic winds might be present; specifically, when winds vary rapidly in space and time. Jet streams and streaks are candidates. Blackadar (1957) found that inertial oscillations are often present in the ageostrophic wind field which, if conditions are favorable, produce a nocturnal jet at low levels in the atmosphere. Ageostrophic motions are also important in the vicinity of jet streaks (e.g. Murray and Daniels, 1953; Uccellini and Johnson, 1979).

CHAPTER 3

METHODS OF CALCULATING KINEMATIC QUANTITIES WITH
DOPPLER WIND PROFILERS

3.1 Profiler-Derived Horizontal Winds

The hourly profiler-derived horizontal wind is an averaged wind determined according to the number of independent samples taken within the hour which agree to within a specified tolerance. Twelve independent samples from each beam and each altitude are measured during the period of an hour (Strauch et al., 1985). The 12 samples from each beam are compared to one another, and those samples whose values fall to within a 4 m/s tolerance are retained for the computation of the hourly profiler-derived horizontal wind. The number of samples meeting the tolerance requirement and, thus, used to compute the "hourly average" wind velocity component is referred to as the consensus number for that beam. When consensus numbers are low, the computed hourly wind may not be a useful measure of the wind during the hour when conditions were varying considerably.

The consensus numbers can be used as a method of quality control of the profiler data. The algorithm at the profiler sites automatically eliminated hourly horizontal wind data if the consensus number in either beam was less than or equal to three. In this thesis, a more stringent criterion was used and data points were flagged as questionable if the consensus number in either off-zenith beam was less than seven. To avoid removing good data, yet eliminate unrealistic values, the flagged data were checked for time and space continuity. Although the checking was done subjectively

for the research in this thesis,¹ flagged winds were eliminated if their direction or speed varied by more than 30° or 10 m/s, respectively, from the nearest high-consensus wind observation.

If one or two consecutive hourly values were missing at some level due to removal of flagged data, a linear temporal interpolation (using the values at times straddling the gap) was used to fill the missing data point(s). A five-point (1-3-5-3-1 weighting) low-pass filter was then applied to the profiler data to reduce the potential impact of high-frequency noise.

3.2 Perturbation Wind

Perturbation winds were calculated using (2) at the three profiler sites for each of the profiler levels. The mean u and v components were obtained by time averaging over a 24-hour period at each site, level by level. In this case, the 24-hour averaging period was selected primarily for display purposes, as that was the largest interval which could be practically displayed. Determination of the optimal time averaging period was outside the scope of this particular thesis project. The use of a running mean was rejected primarily because it complicates the interpretation of the results.

3.3 Horizontal Divergence

Two techniques were used to calculate horizontal divergence with a triangle of Doppler radar wind profilers. The first method, using a line integral technique, is based on Gauss's Theorem,

¹Objective filtering schemes were developed as part of the M.S. Thesis of William Syrett (1987).

$$\oint_L \vec{V} \cdot \hat{n} \, d\ell = \int_A \nabla \cdot \vec{V} \, dA = \text{DIV} \cdot A \quad , \quad (24)$$

which relates the sum of the fluxes through the sides of a finite surface area to the net flux divergence of the area. The unit vector, \hat{n} , is directed normal to the surface and outward. The second method uses an interpolation and finite differencing technique to calculate derivatives from a triangle of data points. The application of these two techniques to a triangle of Doppler radar wind profilers will be described in more detail in the following paragraphs.

The first step of the line integral involves computing the perpendicular component of the wind at each profiler site for the respective side of the triangle. Because the legs of the triangle cannot possibly all be normally oriented north-south or east-west, it is necessary to compute the angles of the sides of the triangles and then compute the angles between the wind vectors and the sides of the triangle. The perpendicular components were obtained by taking the sine of these angles. Either positive or negative values were assigned depending on whether or not the component was away from or pointing toward the side of the triangle, respectively.

The next step was to average the perpendicular components for each side, assuming linear variation along the side, and to weight these side-averaged components by multiplying each averaged component by the distance between the two profiler sites forming the side. These weighted averages were added together and divided by the area of the triangle. The equation for the above method is

$$\begin{aligned}
\nabla \cdot \underline{v} = & \left[\frac{A}{2} (|v_1| \sin \alpha_{1a} + |v_2| \sin \alpha_{2a}) \right. \\
& + \frac{B}{2} (|v_2| \sin \alpha_{2b} + |v_3| \sin \alpha_{3b}) \\
& \left. + \frac{C}{2} (|v_3| \sin \alpha_{3c} + |v_1| \sin \alpha_{1c}) \right] / \left(\frac{1}{2} AB \sin \alpha_{ab} \right) \quad . \quad (25)
\end{aligned}$$

A, B, and C denote the distances between the profiler sites for the respective sides of the triangle, the subscripts 1, 2, and 3 denote the vertices of the triangle, and the subscripts a, b, and c represent the sides of the triangle used for the calculations.

The first step of the finite differencing technique involved converting the latitude and longitude coordinates of the three profiler sites to a Cartesian coordinate system. The origin of the coordinate system was located at the southwest corner of the triangle with the western site intersecting the y axis ($x=0$) and the southern site intersecting the x axis ($y=0$). The equations used for the conversions were

$$\begin{aligned}
X &= 111.0 | ((LON - LONMIN) (\cos(LATCEN))) | \\
Y &= 111.0 (LAT - LATMIN) \quad , \quad (26)
\end{aligned}$$

where LAT and LON represent the latitude and longitude of each site, LATMIN and LONMIN represent the minimum latitude and longitude of the three profiler sites, and LATCEN is the average latitude of the three profiler sites. The centroid of the triangle was computed using the following equations

$$\begin{aligned}
 XCEN &= \frac{X_1 + X_2 + X_3}{3} \\
 YCEN &= \frac{Y_1 + Y_2 + Y_3}{3}
 \end{aligned}
 \tag{27}$$

The next step was to determine the intersections of the lines $X=XCEN$ and $Y=YCEN$ with the sides of the triangle. An intersection was resolved if the value of $XCEN$ or $YCEN$ fell between the X and Y values of the two profiler sites defining the particular side of the triangle. The values of the u component and the v component of the wind vector were interpolated to each of the four points of intersection, $(XCEN, YMIN)$, $(XCEN, YMAX)$, $(XMIN, YCEN)$, and $(XMAX, YCEN)$. The derivatives $\partial u / \partial x$ and $\partial v / \partial y$ were then computed using the equations

$$\begin{aligned}
 \frac{\partial u}{\partial x} &= \frac{u(XMAX, YCEN) - u(XMIN, YCEN)}{XMAX - XMIN} \\
 \frac{\partial v}{\partial y} &= \frac{v(XCEN, YMAX) - v(XCEN, YMIN)}{YMAX - YMIN}
 \end{aligned}
 \tag{28}$$

The values of horizontal divergence for each of the 22 profiler levels were calculated using equation (7) and either equation (24) or (28). Differences in divergence calculated from the two techniques were negligible. The finite differencing method is somewhat more readily adaptable to any other triangle.

3.4 Vertical Velocity

Vertical velocities were obtained from a triangle of Doppler radar wind profilers through implementation of the kinematic method

discussed in Section 2.4. The horizontal divergence values obtained from the line integral method and finite differencing technique were integrated vertically from 3 km to 9 km above mean sea level. To determine w_0 , orographic and friction-induced vertical velocities were applied at the surface and at the top of the Ekman layer, respectively.

When the divergence is integrated upward to obtain vertical velocities at successively higher levels, small errors in measured divergence may accumulate. As a consequence, calculated vertical velocities may remain appreciable in the lower stratosphere where they really are probably nearly zero. To enforce the upper boundary condition, the vertical velocity at a level in the lower stratosphere ($z_{STR}=14$ km) was forced to equal zero using a technique much like O'Brien's second-order adjustment scheme (1970). This requires an adjustment of the mean divergence. The correction scheme adjusted the divergence values at each profiler level by a constant,

$$DIV_{corrected} = DIV_{measured} - \Delta D \quad . \quad (29)$$

The constant was calculated using the equation

$$\Delta D = - \frac{w(z_{STR})}{z_{STR} - z_0} \quad . \quad (30)$$

The correction factors were computed using low resolution wind profiler data. The value of z_{STR} was 14.0 km MSL and the value of z_0 was 4.0 km MSL, the lowest altitude at which divergence was calculated from the low resolution profiler data. The correction

factors were applied to the high resolution divergence data. The correction factor varied with time, but was typically $\pm 1.0 \times 10^{-5} \text{ s}^{-1}$.

Several approaches were investigated to deal with the portion of the atmosphere between the ground and 3.0 km which the profiler did not sample. One method used the divergence calculated from the surface observation network. A second approach used the component of the surface wind perpendicular to the terrain. A third approach used surface vorticity and its relation to friction-induced divergence. The total vertical velocity at altitude h was taken to be, from equation (7),

$$w(h) = w_{\text{TER}} + \Delta w \Big|_{z_0}^{3.0 \text{ km}} + \int_{3.0 \text{ km}}^h \text{DIV} \, dz \quad . \quad (31)$$

w_{TER} represents terrain-induced vertical velocity. Δw represents the increment of vertical velocity in the layer between the surface and the level of the lowest profiler measurement.

Surface data from all nearby reporting stations in the National Weather Service, FAA, and DOD networks were incorporated with the profiler data to calculate the orographic and friction-induced vertical velocities via these approaches. The GST and FIT algorithms found on PROMETS (The Pennsylvania State University Department of Meteorology, Research, Operational Meteorology, Education and Trainig System) were used to interpolate the surface station data to a 30x40 grid of values. The GST routine is a nearest-neighbor analysis and smoothing scheme used to obtain data values at a 30x40 grid. One grid interval was approximately 55 km for the map background used. This gridded data was used as the first guess field for the FIT

program which applies a Bergthorssen-Cressman-Doos (BCD) distance-squared weighting scheme to perform the analysis, and is similar to the method of successive corrections devised by Cressman (1959). Three passes of the BCD analysis were applied to the data using a radius of influence equal to six grid lengths for the first pass, three for the second pass, and one for the third pass. A 1-4-1 low-pass filter was finally applied to smooth out high-frequency noise.

To calculate vertical velocities induced by the terrain, w_{TER} , the u and v components of the wind were bilinearly interpolated to the centroid of the triangle using the values at the four grid points surrounding the centroid. The interpolated u and v components and the three profiler site elevations (h) were used in the following equation,

$$w_{TER} = V_{SFC} \cdot \nabla h = u \frac{\partial h}{\partial x} + v \frac{\partial h}{\partial y} \quad (32)$$

The derivatives of $\partial h / \partial x$ and $\partial h / \partial y$ were calculated using the finite differencing technique discussed in Section 3.3. The elevations of the three profiler sites were used to interpolate the heights of the four points of intersection where the lines $X=XCEN$ and $Y=YCEN$ intersected the sides of the profiler triangle. The following equations were used for the calculation of the derivatives

$$\frac{\partial h}{\partial x} = \frac{h(XMAX, YCEN) - h(XMIN, YCEN)}{XMAX - XMIN}$$

$$\frac{\partial h}{\partial y} = \frac{h(XCEN, YMAX) - h(XCEN, YMIN)}{YMAX - YMIN} \quad (33)$$

Two methods were applied for the inclusion of frictional effects on the vertical motion field, which contribute to Δw in equation (31). The first method indirectly accounted for frictional effects by incorporating frictionally-induced surface divergence and convergence into the vertical integration. The surface divergence was combined with the lowest-level profiler divergence to give the average divergence value within the Ekman layer (Holton, 1979). This value of divergence was used in the vertical integration as the mean divergence for the layer between the surface and the lowest profiler level. The integral of this divergence gives Δw in equation (31).

The second method of treating friction-induced vertical velocity involved computing a parameterized version of the friction-induced vertical velocity for the top of the Ekman layer, based on the relative vorticity at the top of the Ekman layer, ξ_e . One parameterization, taken from Nastrom et al. (1985), was

$$w_{\text{FRIC}} = \frac{RTF\xi_e}{g2f_0} \quad , \quad (34)$$

where F represents a frictional coefficient with the value of 8×10^{-6} s, g is the acceleration due to gravity, R is the gas constant, and f_0 is the Coriolis parameter. The temperature and surface relative vorticity values, T and ξ , used were surface values obtained from PROMETS grid analysis and bilinear interpolations from the four grid points surrounding the centroid of the triangle. A typical value of the friction-induced vertical velocity using the equation above was approximately ± 0.4 cm/s. A second and similar parameterization, taken from Holton (1979), was

$$w_{\text{FRIC}} = \xi_g |K/2f|^{1/2}, \quad (35)$$

where K represents a friction coefficient with a value of $5.0 \text{ m}^2/\text{s}$, and ξ_g is the geostrophic relative vorticity. The observed vorticity was substituted for the geostrophic value in equation (35). A typical value of the friction-induced vertical velocity using the second equation was on the order of magnitude of $\pm 0.2 \text{ cm/s}$. The relative vorticity at the top of the Ekman layer for both equations was obtained by interpolation between the surface vorticity and the computed vorticity at the lowest level of the profiler data. The value of w_{FRIC} was substituted into Δw of equation (31) to represent the frictional contribution to vertical velocity.

Both the surface divergence and surface relative vorticity values were acquired from PROMETS using the software routines SFC and VOR. The gridded u and v components previously mentioned were used for the calculations of both the surface divergence and surface relative vorticity. These are computed via grid-point computations of a form (7) and (12). The computed surface divergence and vorticity values were bilinearly interpolated to the centroid of the triangle from the four surrounding grid points.

3.5 Vorticity

Both a line integral method and a finite differencing technique were implemented to compute relative vorticity. The line integral method used to calculate relative vorticity is based on Stoke's Theorem,

$$\oint \vec{v} \cdot d\vec{\ell} = \int_A (\nabla \times \vec{v}) \cdot \hat{n} dA = \xi \cdot A \quad (36)$$

Stoke's Theorem relates the sum of the vector components tangent to a closed surface contour to the average relative vorticity about an axis \hat{n} normal to the surface bounded by the line integral.

The first step of the line integral technique involved calculating the component of the wind vector parallel to the respective side of the triangle for each profiler site, based upon the cosine of the angle between the wind vector and the side of the triangle. The components were assigned positive or negative values depending on whether or not the components pointed counter-clockwise or clockwise, respectively.

As with the horizontal divergence calculations, the components were averaged for each side and weighted by multiplying the averaged component by the distance between the two profiler sites. These weighted averages were added together and divided by the area of the triangle. The equation for this method was

$$\begin{aligned} \xi = & \left[\frac{A}{2} (|v_1| \cos \alpha_{1a} + |v_2| \cos \alpha_{2a}) \right. \\ & + \frac{B}{2} (|v_2| \cos \alpha_{2b} + |v_3| \cos \alpha_{3b}) \\ & \left. + \frac{C}{2} (|v_3| \cos \alpha_{3c} + |v_1| \cos \alpha_{1c}) \right] / \left(\frac{1}{2} AB \sin \alpha_{ab} \right) \quad (37) \end{aligned}$$

where A, B, and C denote the distances between the profiler sites for the respective sides of the triangle, the subscripts 1, 2, and 3

denote the vortices of the triangle, and the subscripts a, b, and c represent the sides of the triangle used for the calculations.

The finite differencing technique used to calculate the relative vorticity was comparable to the technique used to calculate the horizontal divergence. The equations applied to obtain the derivatives $\partial v / \partial x$ and $\partial u / \partial y$ were

$$\begin{aligned}\frac{\partial v}{\partial x} &= \frac{v(XMAX, YCEN) - v(XMIN, YCEN)}{XMAX - XMIN} \\ \frac{\partial u}{\partial y} &= \frac{u(XCEN, YMAX) - u(XCEN, YMIN)}{YMAX - YMIN}\end{aligned}\quad (38)$$

The values of the relative vorticity for each of the 22 profiler levels were calculated using equation (11).

3.6 Geostrophic and Ageostrophic Winds

To determine the ageostrophic winds from a triangle of Doppler radar wind profilers, the following equations were applied:

$$\overline{u}_{ag} = -\frac{1}{f} \left[\frac{\partial \overline{v}}{\partial t} + \overline{u} \frac{\partial \overline{v}}{\partial x} + \overline{v} \frac{\partial \overline{v}}{\partial y} + \overline{w} \frac{\partial \overline{v}}{\partial z} \right] \quad (39)$$

$$\overline{v}_{ag} = \frac{1}{f} \left[\frac{\partial \overline{u}}{\partial t} + \overline{u} \frac{\partial \overline{u}}{\partial x} + \overline{v} \frac{\partial \overline{u}}{\partial y} + \overline{w} \frac{\partial \overline{u}}{\partial z} \right] \quad (40)$$

In this context the overbar denotes the triangle-average value or centroid value of the velocity component (rather than a single station temporal average).

These equations were used to calculate ageostrophic winds pertaining to the centroid of the triangle. The finite differencing technique described in Section 3.3 was used to compute the derivatives $\partial u/\partial x$, $\partial u/\partial y$, $\partial v/\partial x$, and $\partial v/\partial y$. To calculate the mean u and v components for the centroid, the two u and v components for a side were averaged. The side averages were then weighted by multiplying the length of the side and the averaged component. The derivatives $\partial u/\partial t$ and $\partial v/\partial t$ were computed using a centered-in-time finite differencing scheme. The vertical velocity was computed from the method described in Section 3.4. The derivatives $\partial u/\partial z$ and $\partial v/\partial z$ were computed at 600 m intervals using the mean u and v components for the centroid. The geostrophic components were derived by subtracting the ageostrophic components from the triangle-averaged u and v components.

Once the geostrophic wind components are calculated, the magnitude and direction of the gradient of the pressure or geopotential field over the triangle is known from equation (15). Additionally, but not treated in this thesis, once the geostrophic wind is known as a function of height, the horizontal temperature gradient can be determined from the vertical shear of the geostrophic wind (Neiman, 1987).

CHAPTER 4

CASE STUDIES OF SYNOPTIC-SCALE FEATURES USING DOPPLER
WIND PROFILER DATA

4.1 Case of September 22-23, 1985

In this case study, five synoptic-scale features which passed through the profiler triangle are examined: a weak surface cold front, a second and stronger surface cold front, an amplifying upper-level trough, and two jet streaks. In order to better demonstrate the interpretation of profiler data corresponding to these features, this section proceeds feature by feature rather than strictly by chronology.

The case begins at 0300 UT² on 22 September 1985 with a weak synoptic-scale surface cold front located just east of the profiler triangle, and extending from North Dakota to New Mexico and back into Utah. At this time it was co-located with a lee trough on the east slopes of the Rockies. Two weak low-pressure disturbances were situated to the northeast and southwest of the profiler triangle, as depicted in Fig. 4.1a. These disturbances touched off rainshowers in the profiler triangle. This weak cold front continued to move through the profiler triangle, and by 1500/22 was located from Kansas to New Mexico to Arizona, as shown in Fig. 4.1b. By 2100/22, this front had slowed down, reaching the position shown in Fig. 4.1c.

Figures 4.2, 4.3, and 4.4 illustrate the profiler winds at the three stations. During the time period from 0400/22 until the passage of the second, stronger synoptic-scale cold front, the Flagler winds at 4 km backed to a south-southwest direction. The

²UT represents Universal Time and for the remainder of this chapter the time will be denoted in the format 0300/22 which represents 0300 UT 22 September 1985.

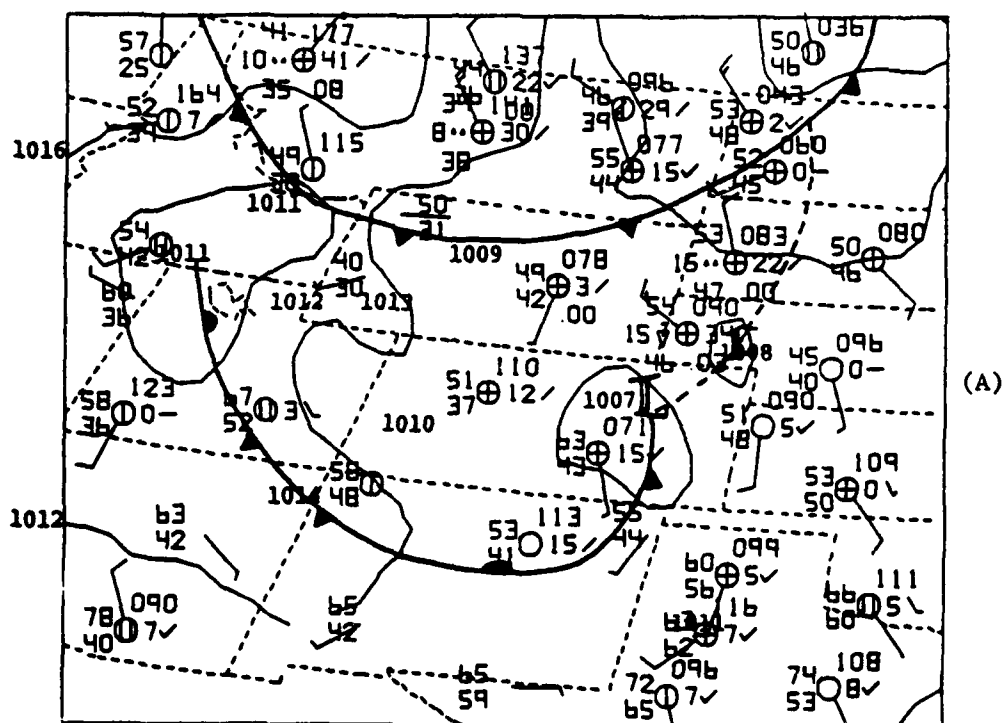


Figure 4.1 Surface pressure analyses. (A) valid 0300 UT 22 September 1985, (B) 1500 UT 22 September 1985, and (C) 2100 UT 22 September 1985.

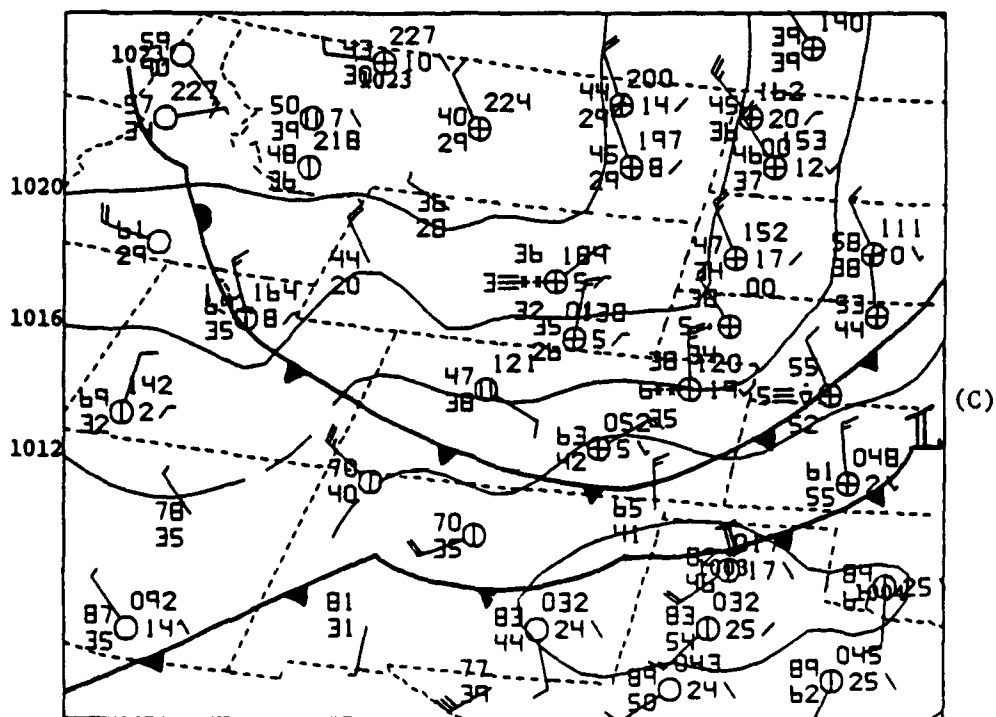
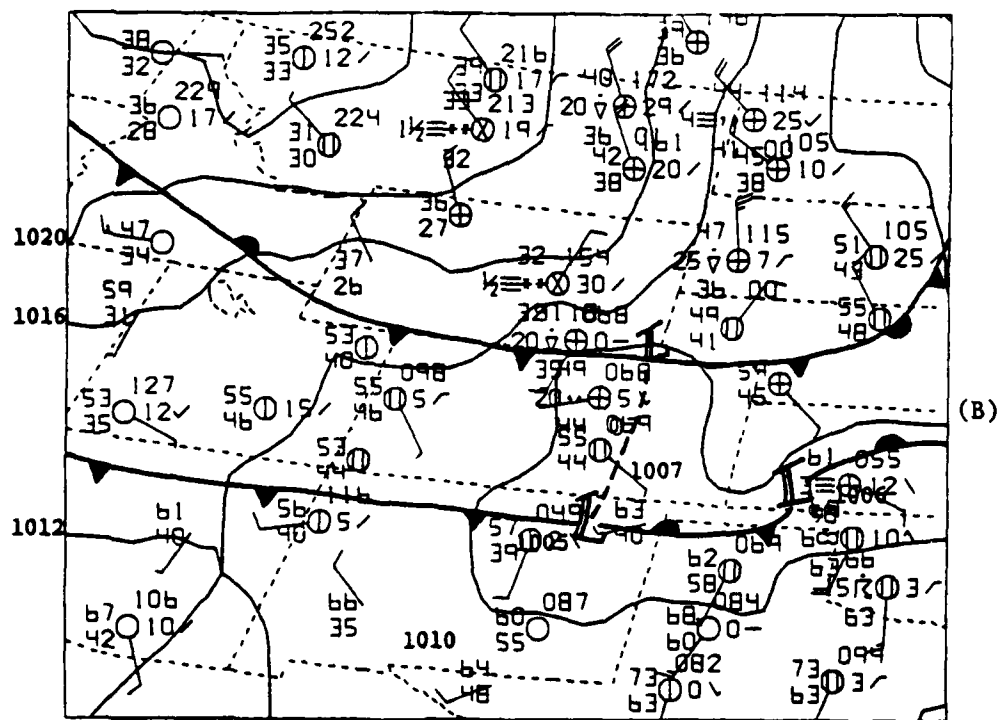


Figure 4.1 (B) and (C)

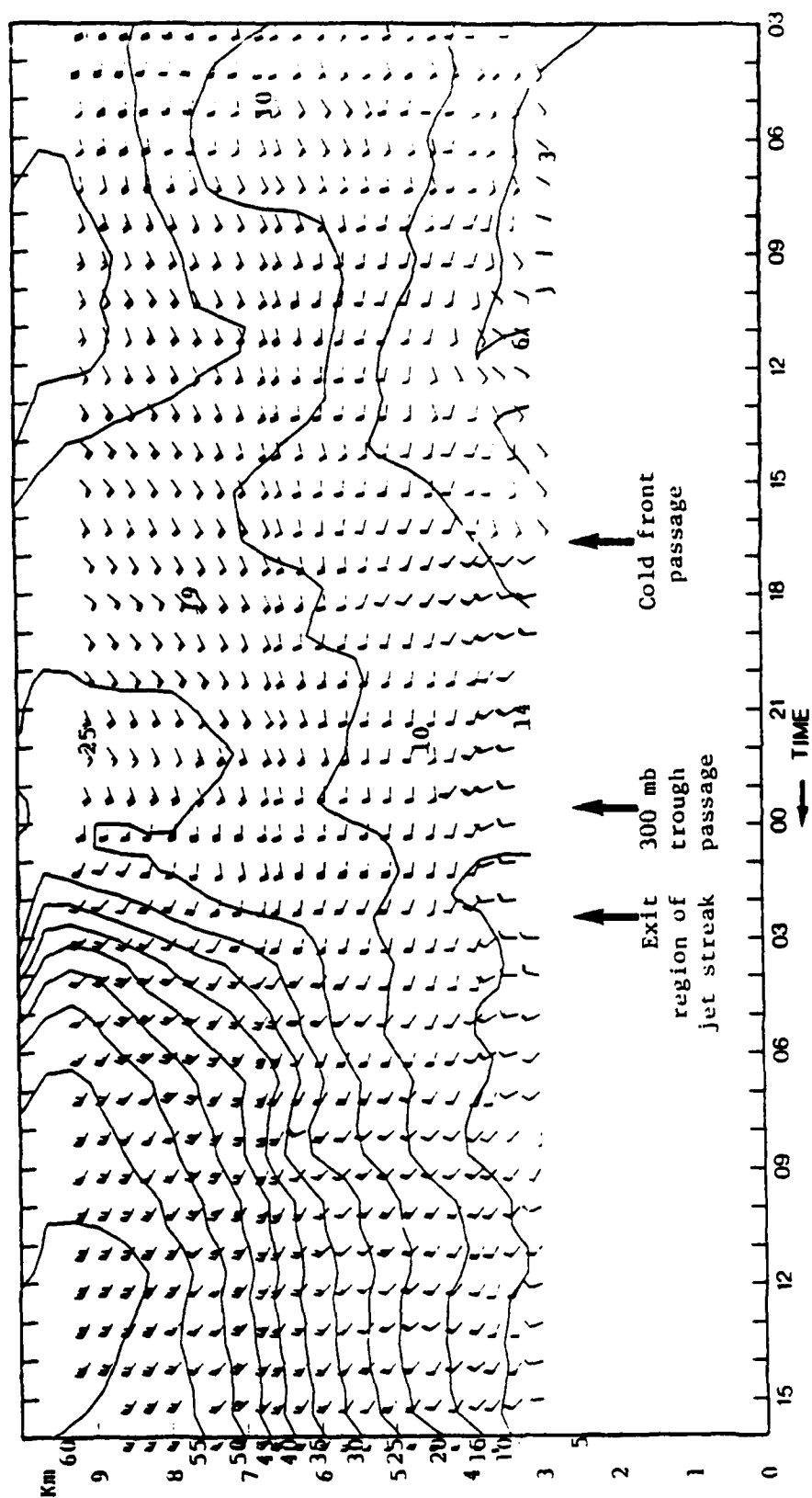


Figure 4.2 Time-height section of observed winds from the Platteville profiler during the period from 0300 UT 22 September 1985 to 1600 UT 23 September 1985. One flag represents 5.0 m/s. One pennant represents 27.0 m/s. A wind from the south points toward the top of the page. Contour interval is 5 m/s.

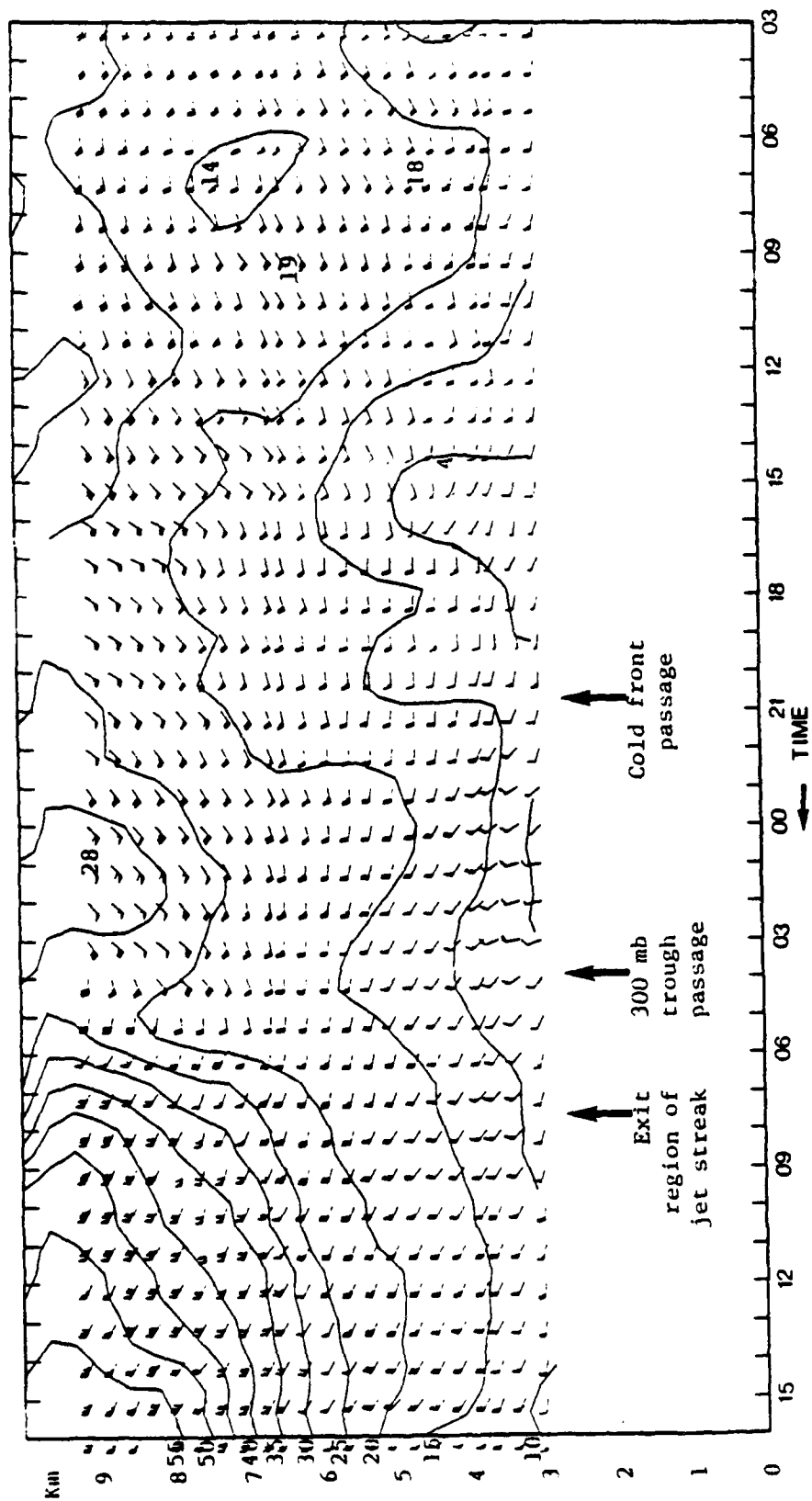


Figure 4.3 Time-height section from the Fleming profiler during the time period from 0300 UT 22 September 1985 to 1600 UT 23 September 1985. Conventions as in Fig. 4.2.

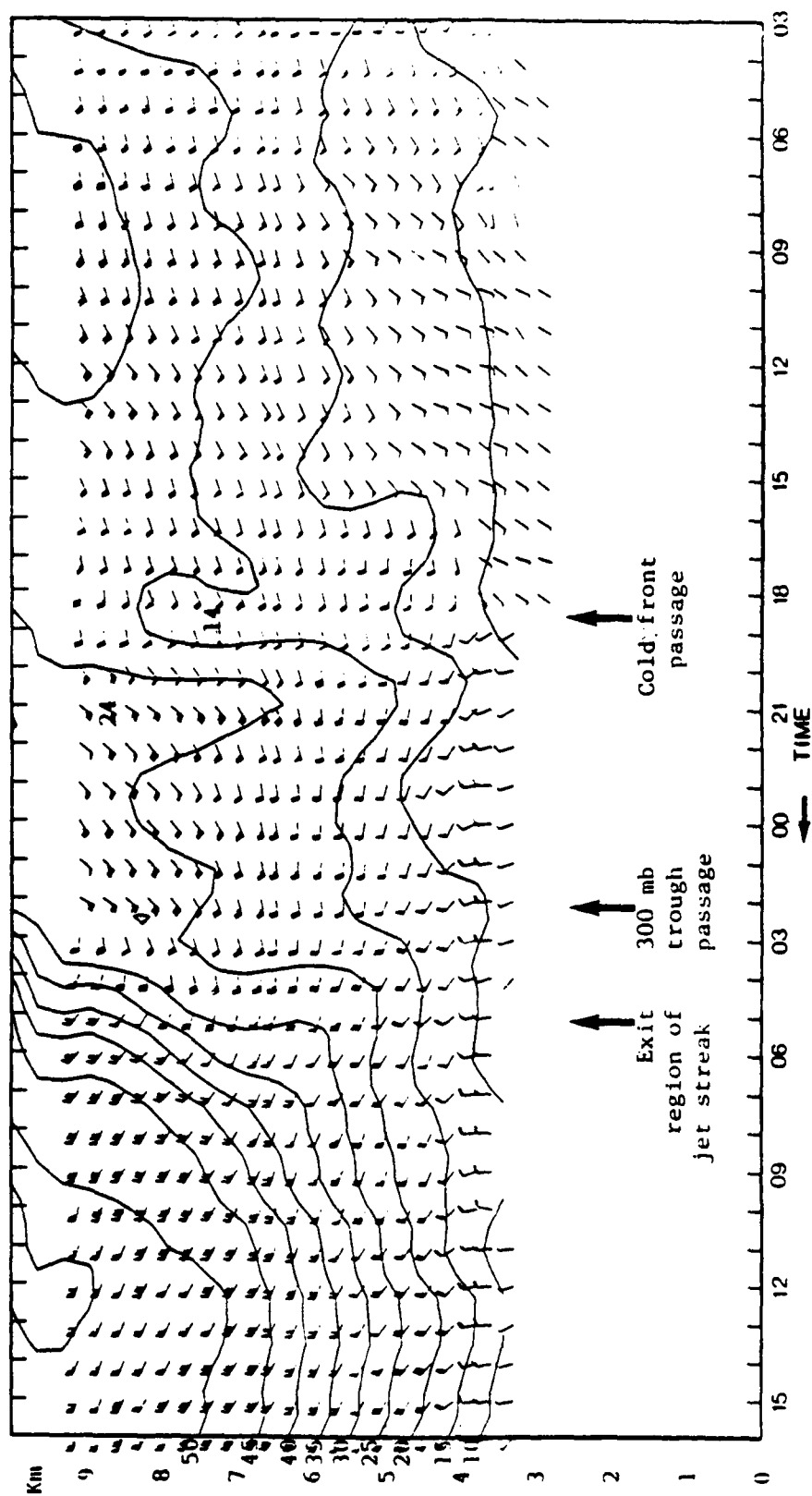


Figure 4.4 Time-height section of observed winds from the Flagler profiler during the time period from 0300 UT 22 September 1985 to 1600 UT 23 September 1985. Conventions as in Fig. 4.2.

Platteville winds at 4 km backed briefly to the southwest at 0400/22, but after 0400/22 veered to the west-northwest for about five hours. During this period, the Fleming winds at 4 km backed to the west-southwest until 0600/22, and then veered to the west and west-northwest for several hours. Since the Flagler (the profiler farthest to the southeast) winds were southwest during this period, it can be discerned that a trough was present over the triangle.

The trough at 4 km revealed by the profiler triangle data can be interpreted as either the quasi-stationary mid-tropospheric portion of the weak cold front or as the lee trough, or some combination of the two. The profiler data from Platteville and Fleming, which show a sloping wind speed maximum extending from 9 km to the lowest gate, support the interpretation that the trough was associated with the weak cold front. What is quite clear is that after 0600/22, the advancing portion of the weak cold front of Fig. 4.1 was shallow, since the veering windshift did not pass Flagler at 4 km.

The second, stronger cold front was located in northern Wyoming at 0300/22, shown in Fig. 4.1a. Fig. 4.1b shows that this cold front moved to the Wyoming-Colorado border by 1500/22. This cold front entered the profiler triangle between 1600/22 and 1700/22 at the Platteville site, as indicated by the veering of the winds in time from the southwest to northwest. As the front and its accompanying trough approached, winds at levels up to 4 km backed for several hours at Platteville and Fleming, where winds had previously veered in association with the preceding trough. The

cold front then passed Flagler between 1800/22 and 1900/22, and passed Fleming by 2100/22.

The strong cold front had a southwest-to-northeast orientation through the profiler triangle as shown in Fig. 4.1c. This cold front was somewhat deeper, and North Platte had a wind shift to northwest at 850 mb by 1200/22. After this frontal passage, a surface high pressure system moved into the profiler triangle from the northwest, and dominated the surface conditions for the remainder of the case.

The other three features of this case can be seen in Fig. 4.5. The 300 mb winds measured by the National Weather Service (NWS) rawinsonde network at 1200/22 are shown in Fig. 4.5a. The rawinsonde network showed a 300 mb short-wave trough with an imbedded jet streak approaching the profiler triangle. The wind speeds at the core of the jet streak were approximately 70 m/s (135 kts). At this time the core of the jet streak was located over the Oregon-Idaho border. The Denver rawinsonde, in advance of the trough axis, indicated a 22 m/s (45 kts) southwesterly wind which was consistent with the winds in the profiler triangle at 9 km.

The winds on the 300 mb chart in Fig. 4.5b for 0000/23 show the axis of the upper-level trough between Denver and Grand Junction, Colorado. It was probably not far from Denver. The contours of the height of the 300 mb surface are too smooth and falsely suggest that the trough axis is just east of Denver. With the strong jet streak on its west flank, the trough was digging and heights were falling in advance of and even near the trough axis.

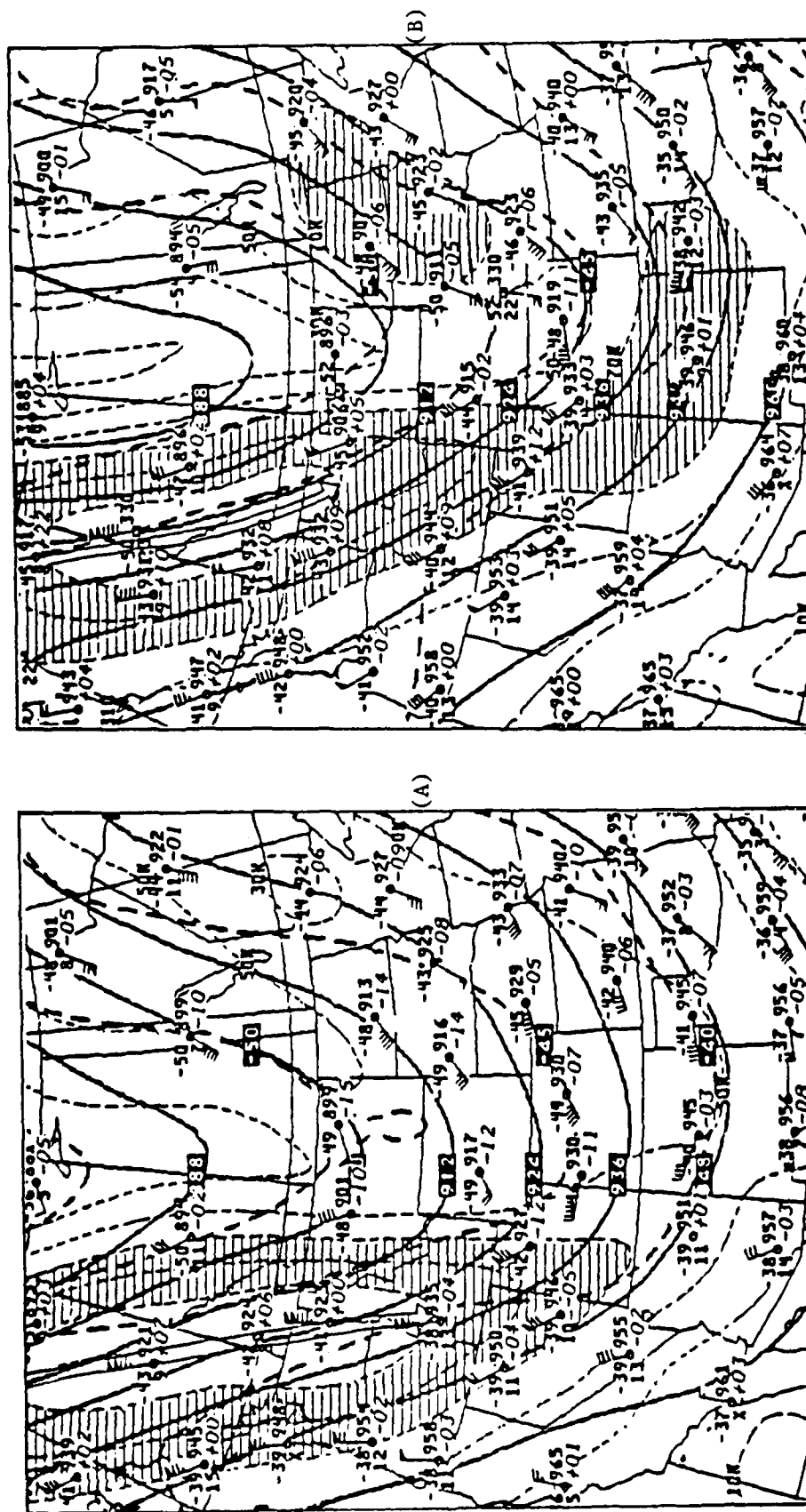


Figure 4.5 National Meteorological Center (NMC) objective analyses of 300 mb height and temperature fields. (A) valid 1200 UT 22 September 1985, (B) 0000 UT 23 September 1985, and (C) 1200 UT 23 September 1985.

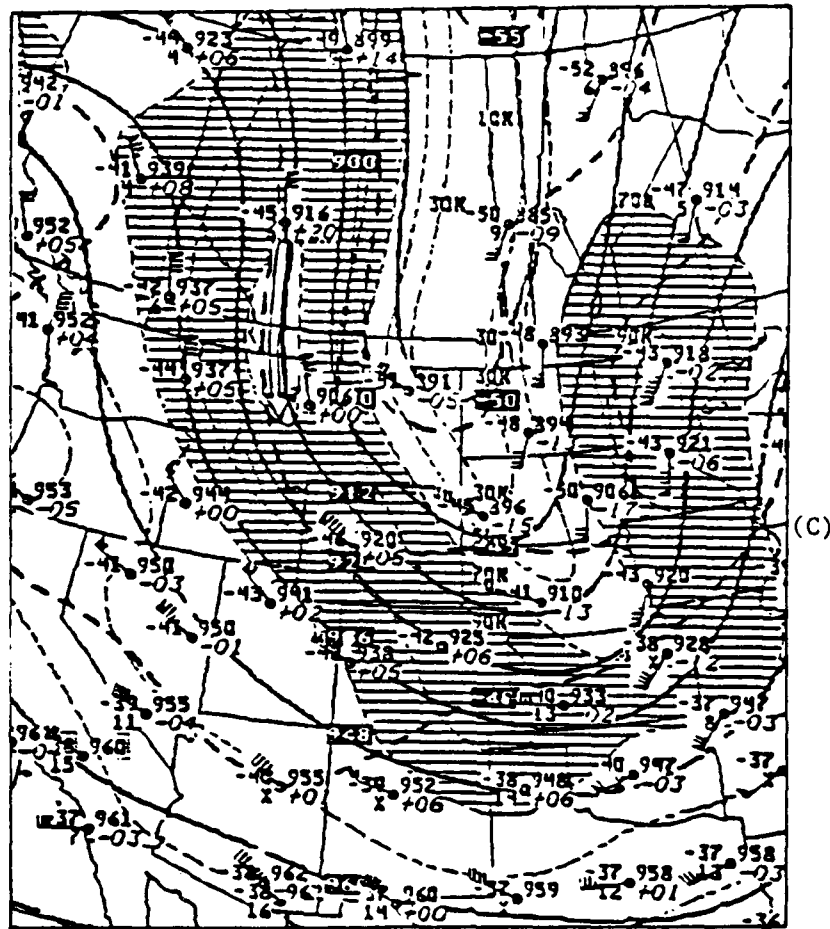


Figure 4.5 (C)

The Denver rawinsonde site reported a 110 meter height fall between 1200/22 and 0000/23.

The profiler data show that the 300 mb trough was just approaching the Denver area. At 9 km, the trough axis passed through Platteville, Flagler, and Fleming at 0000/23, 0300/23, and 0400/23, respectively. A 500 mb trough axis had passed through the profiler triangle earlier; however, it was not as sharp as the 300 mb trough passage. At 5.6 km, the axis of the 500 mb trough passed through Flagler at 1600/23 and Fleming at 1700/23. The timing of the 500 mb trough axis passage was difficult to determine at the Platteville site.

Based upon the 300 mb analysis, the core of the jet streak with maximum winds of approximately 70 m/s appeared to have moved north and east into western Montana. Such a movement would be quite anomalous, considering that the steering flow on the west side of the trough was from the northwest. It will subsequently be seen that this analysis was wrong.

A new jet streak developed to the northeast of the profiler triangle by 0000/23. All three profiler sites showed evidence of a southwesterly wind maximum associated with this developing jet streak. The Fleming profiler site, located the farthest north in the triangle, had the strongest (30 m/s) southwesterly wind maximum.

With the passage of the 300 mb trough axis, a strong northwesterly flow moved into the profiler triangle. The Denver rawinsonde, at 1200/23, was unable to measure the winds at 9 km. The contoured isotach analysis in Fig. 4.5c yields an interpolated wind speed of 45 m/s in the profiler triangle. From this analysis, the

core of the jet streak appeared to have unexpectedly remained stationary over western Montana. However, the profiler winds at 1200/23 were 65, 55, and 50 m/s for the Platteville, Flagler, and Fleming sites, respectively. Thus, the objective analysis of the rawinsonde network data had misrepresented the strength of the jet stream by up to 20 m/s over the profiler network, and the core of the jet stream had actually slipped between the rawinsonde sites to reach Colorado. The misleading 300 mb isotach analysis occurred because the core of the jet stream could not be resolved by the coarsely spaced rawinsonde sites.

Another feature not expected based upon the rawinsonde isotach analysis was the rapidity of increase of the wind speed observed by the profilers. In a six-hour period, the wind speed changed by 35, 30, and 25 m/s at the Platteville, Flagler, and Fleming sites, respectively, at 9 km. The time-space-converted horizontal gradients indicated by these changes are approximately 14 to 20 m/s per 100 km.

At each site, the large gradient of wind speed began two hours after the passage of the 300 mb trough axis, as indicated by the time of most rapid change of wind direction. The two-hour lag between the trough axis passage and the arrival of the jet streak in the profiler triangle (as manifested by the onset of the rapid speed increases) indicated that the jet streak had not yet entered the base of the 300 mb trough, but was still slightly to the west of the trough axis. Thus, the trough was still in the process of digging.

By combining the profiler triangle data with the rawinsonde network data in Fig. 4.5c, the core of the jet streak was determined to be on the western side of the profiler triangle at 1200/23. This placement put the profiler triangle in the left exit region of an elongated jet streak, stretching from western Montana to southwestern Wyoming to northern Colorado.

Idealized models of jet streak circulations indicate that the left exit region of a jet streak can be characterized by a cross-gradient flow toward the axis of the jet streak into the right exit region at upper levels, and vice versa at lower levels. Indeed, three profiler sites, during the rapid change of wind speed with time, showed a northerly cross-gradient flow across the northwest-to-southeast-oriented jet streak axis at 9 km. The low-level cross-gradient flow, which in this case would appear as a southwesterly or westerly flow, was not evident in the low-level profiler winds.

Having now introduced the weather features and compared the raw profiler and rawinsonde wind observations for these various features, let us proceed to assessing the value of various profiler-derived quantities in interpreting the various features. Quantities assessed are geostrophic and ageostrophic winds, perturbation winds, relative vorticity, divergence, and vertical velocity.

The profiler-derived geostrophic winds, relevant at the center of the profiler triangle, are depicted in Fig. 4.6. The 4 km geostrophic winds, at the beginning of the case, showed a period when the winds backed, and then veered until 0800/22, when the 4 km winds backed as the trough associated with the strong cold front moved

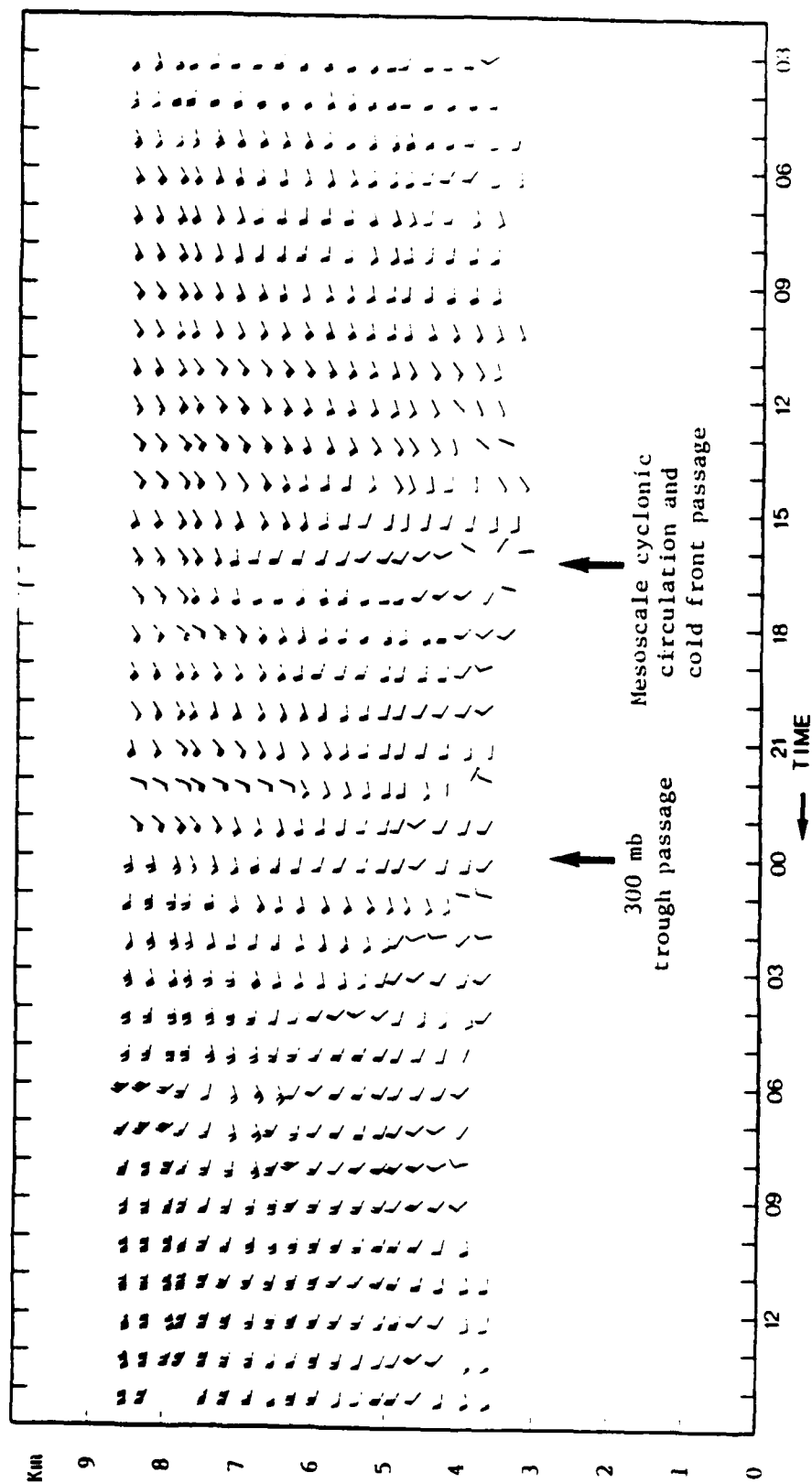


Figure 4.6 Time-height section of profiler-derived geostrophic winds during the period from 0300 UT 22 September 1985 to 1400 UT 23 September 1985. Conventions as in Fig. 4.2.

into the profiler triangle. At 1600/22, when the strong cold front entered the profiler triangle, a cyclonic circulation appeared in the 3-4 km geostrophic winds.

As the upper-level features moved into the profiler network, the geostrophic winds differed greatly from the observed winds, indicating that strong ageostrophic motions were present. During the period when the observed winds were influenced by the developing southwesterly jet streak located northeast of the profiler triangle, the geostrophic winds were more southerly and not as strong as the observed winds. As the short-wave trough with its imbedded jet streak moved into the profiler network, the geostrophic winds were more westerly and stronger than the observed winds.

Figure 4.7 illustrates the ageostrophic winds for the case. Although the ageostrophic winds appear to be chaotic at first glance, upon closer inspection the easterly flow associated with the transverse circulations in both jet streaks is apparent. From 1600/22 to 2000/22, a weak northeasterly ageostrophic wind prevailed at 8.5 km which was consistent with the direct circulation found in the entrance region of a jet streak moving northeastward. At 0000/23, strong southeasterly to northeasterly ageostrophic winds were present from 5 to 8.5 km. These ageostrophic winds were consistent with the indirect transverse circulation in the exit region of the northwest-to-southeast-oriented jet streak.

The perturbation winds (relative to the 24-hour mean) for the time period from 1600/22 to 1600/23 for the three stations are depicted in Figs. 4.8, 4.9, and 4.10. The perturbation winds enhanced

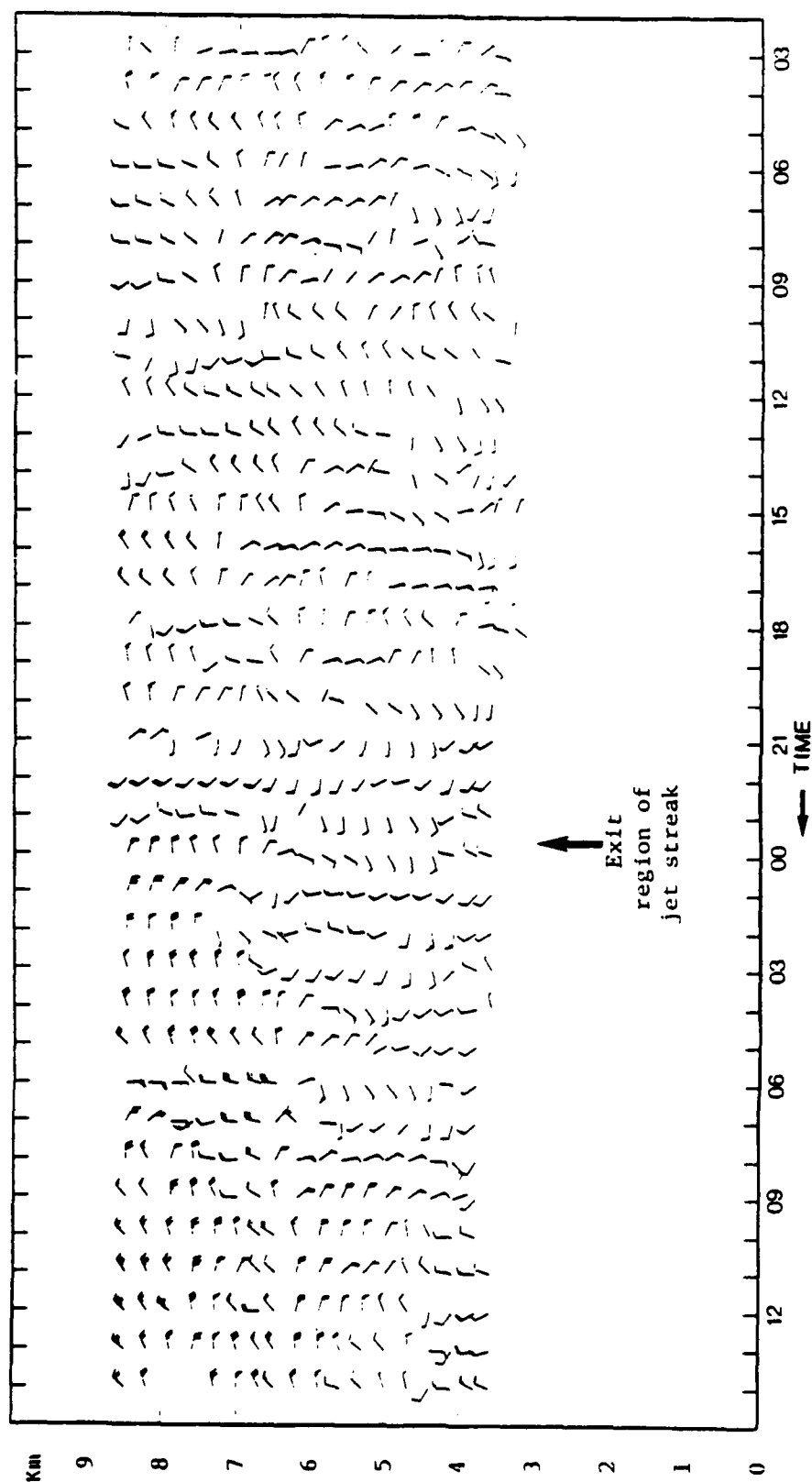


Figure 4.7 Time-height section of the profiler-derived ageostrophic winds during the period from 0300 UT 22 September 1985 to 1400 UT 23 September 1985. Convention as in Fig. 4.2.

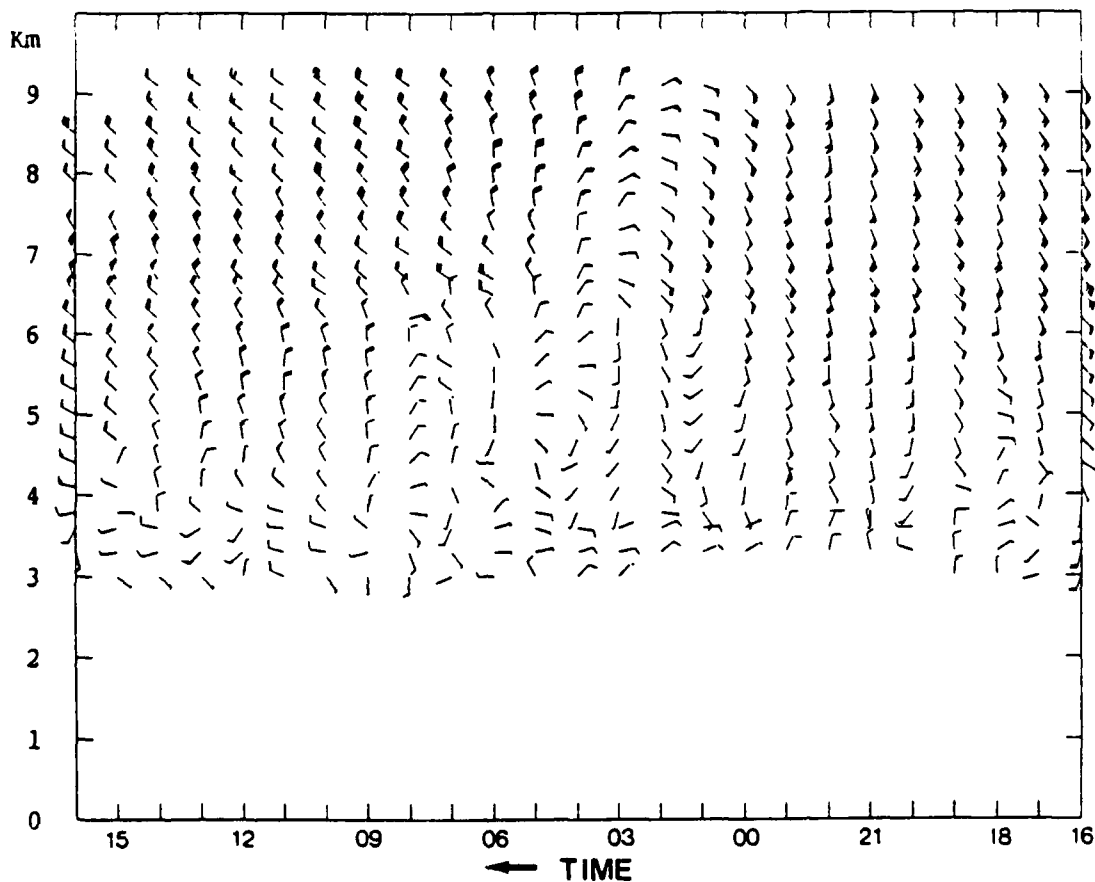


Figure 4.8 Time-height section of the perturbation winds from the Platteville profiler during the period from 1600 UT 22 September 1985 to 1600 UT 23 September 1985. Convention as in Fig. 4.2.

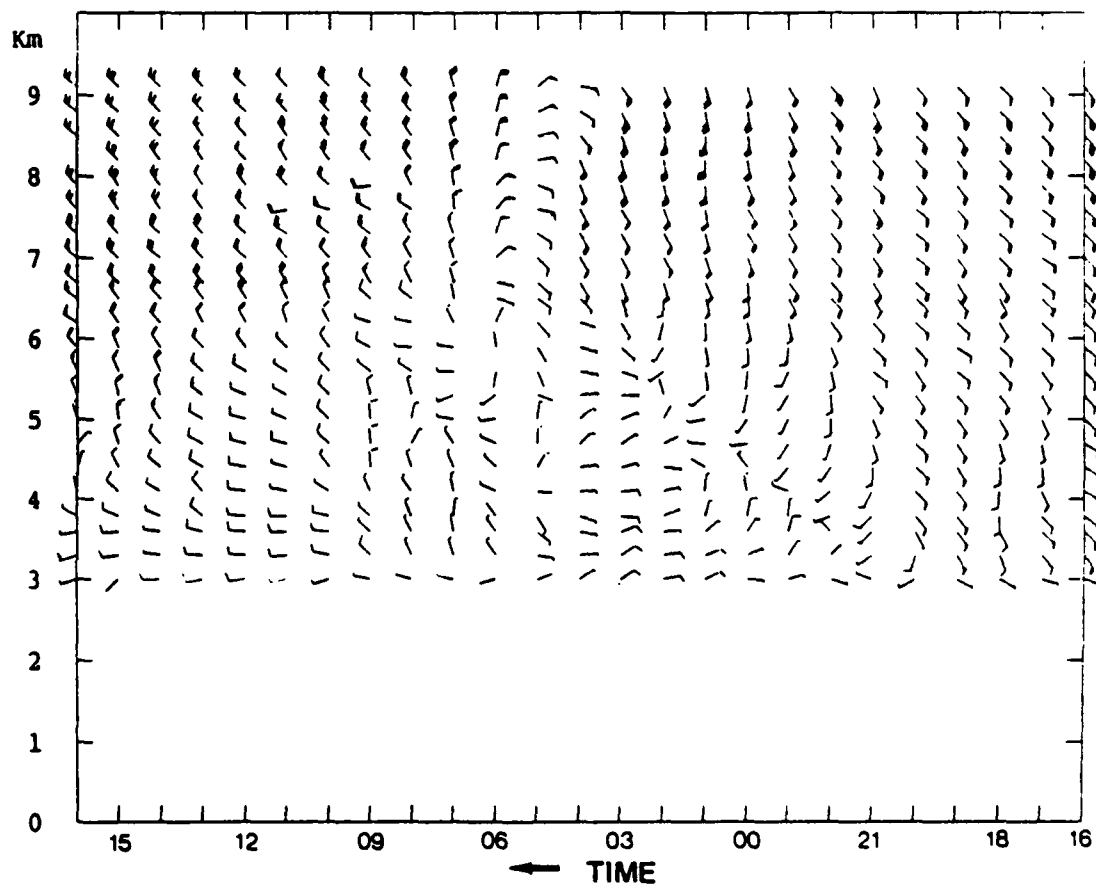


Figure 4.9 Time-height section of the perturbation winds from the Fleming profiler during the period from 1600 UT 22 September 1985 to 1600 UT 23 September 1985. Convention as in Fig. 4.2.

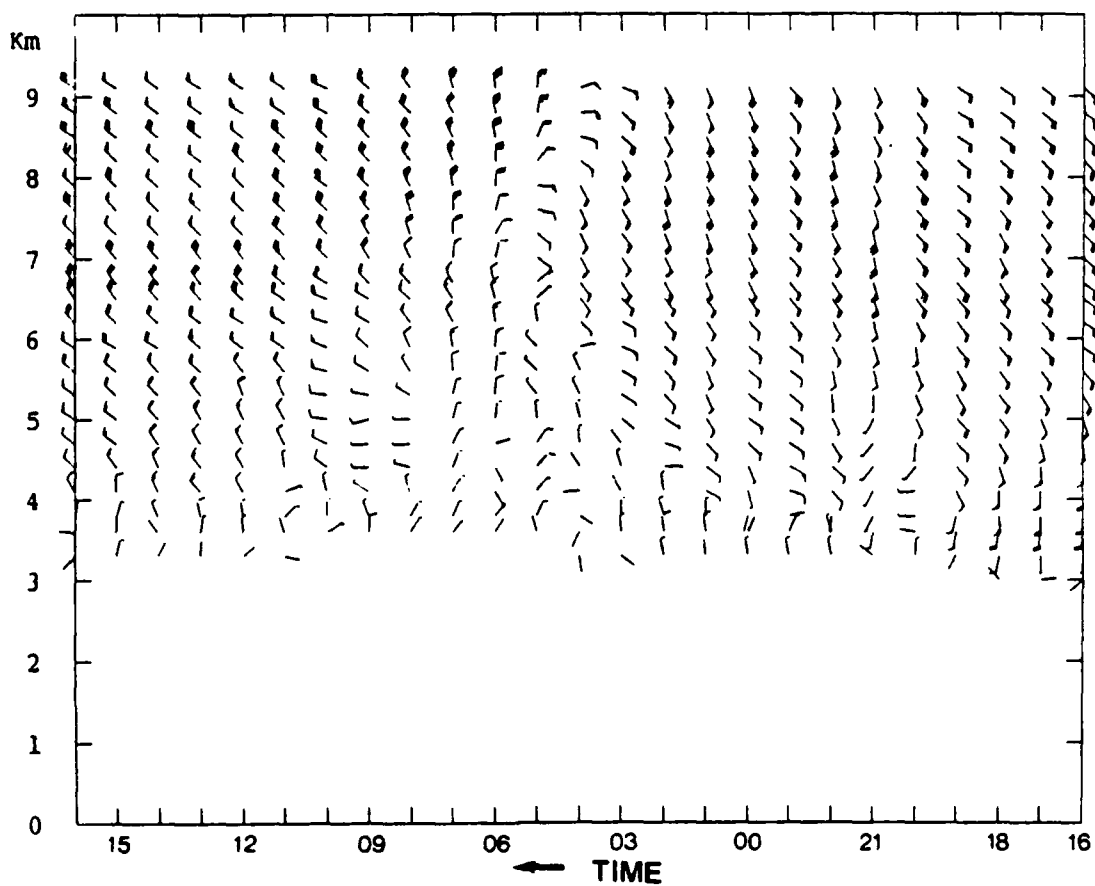


Figure 4.10 Time-height section of the perturbation winds from the Flagler profiler during the period from 1600 UT 22 September 1985 to 1600 UT 23 September 1985. Convention as in Fig. 4.2.

the signature of the change of the flow from the southeast to the northwest accompanying the passage of the upper-level trough.

The values of the profiler-derived relative vorticity field are shown in Fig. 4.11. During the time period from 0300/22 to 1500/22, the relative vorticity values were negative or small and positive. These values indicated an anticyclonic flow about the profiler triangle. Beginning at 0900/22, the values at all levels became less negative, indicating, from spatial interpretation, that positive vorticity advection (PVA) had started. The PVA was consistent with the backing of the profiler winds from the west to the southwest as the 300 mb trough approached, and was strongest at the 9 km level two hours prior to the passage of the trough axis at Platteville. The PVA was also strong in the lower levels prior to the cold frontal passage with a maximum occurring near 5 km at 1600/22.

The largest positive vorticity maximum observed by the profiler network, $23 \times 10^{-5} \text{ s}^{-1}$, occurred at the base of the 300 mb trough at 8-9 km at 0200/23 to 0300/23. Apparently associated with PVA ahead of this trough, a surface low pressure system had begun to develop as a frontal wave in southwestern Kansas at 2100/22. This wave was probably induced because, as the upper-air trough and its associated PVA moved through the profiler network and onto the Great Plains, the region of PVA had gained on and caught up to the first weak cold front that had become quasi-stationary in Kansas.

After the passage of the strong synoptic-scale cold front at about 1700/22, the low-level relative vorticity values became

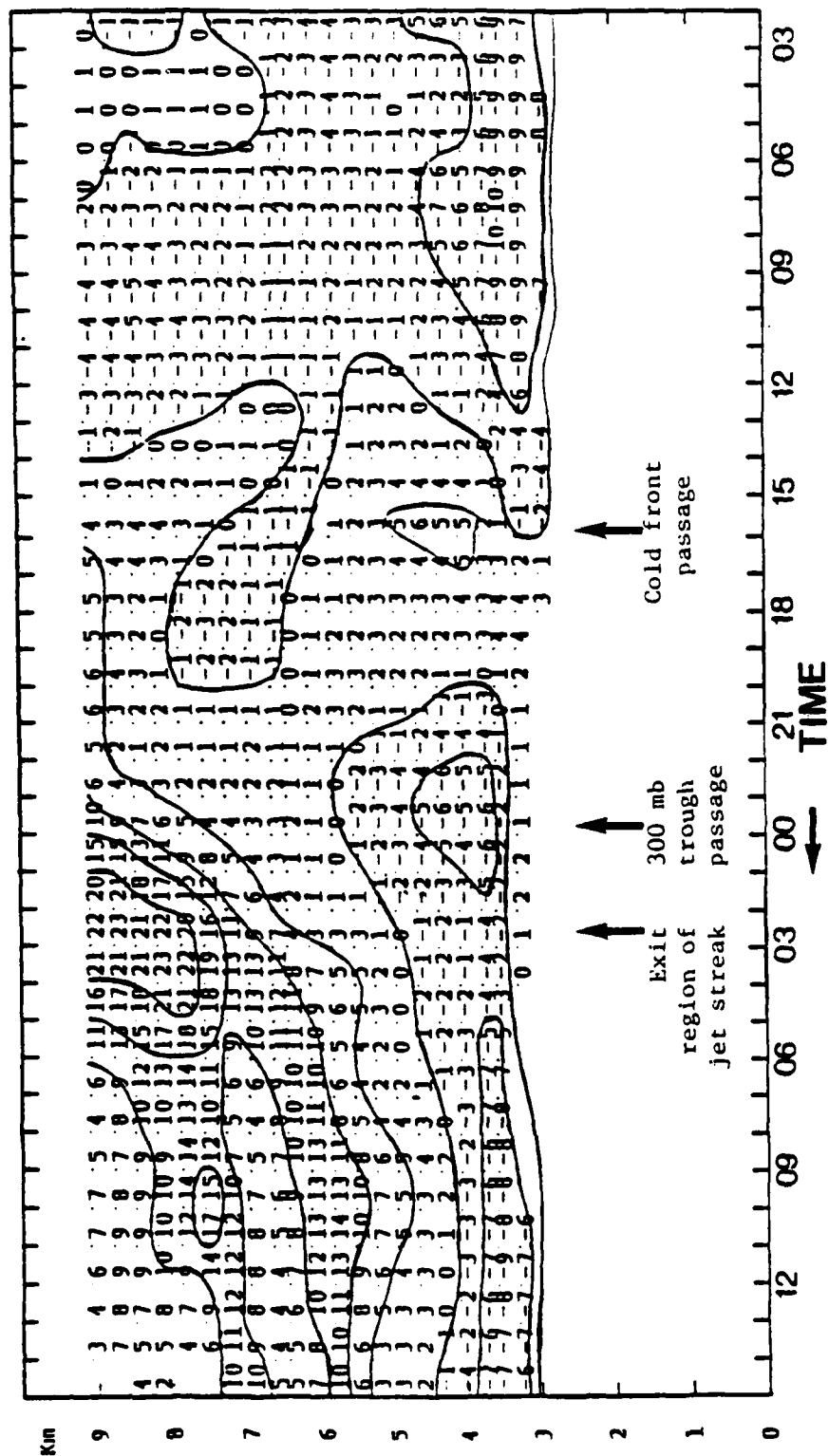


Figure 4.11 Time-height section of the profiler-derived relative vorticity field (units of 10^{-5} s^{-1}) during the period from 0300 UT 22 September 1985 to 1500 UT 23 September 1985. Contour interval is $5 \times 10^{-5} \text{ s}^{-1}$. Positive values denote cyclonic vorticity and negative values denote anticyclonic vorticity.

negative; negative vorticity advection (NVA) was occurring behind the front. NVA also occurred after the passage of the 300 mb trough.

The profiler-derived divergence field is shown in Fig. 4.12. A thin layer of convergence at the beginning of the period (0300/22) was associated with the weak cold front and its disturbances which produced showers around the profiler triangle. During the period from 0800/22 to 1500/22, where the convergence zone sloped forward and upward in space or descended from 5 to 3 km in time, the convergence zone appeared to have the characteristics of a warm front. This was during the period following the first (weak) cold front passage when the profiler winds backed to southwesterly as the trough of the strong cold front approached. The remnants of the weak cold front may have been retreating as a warm front at this time.

Once the second, stronger cold front entered the profiler triangle at 1600/22, the convergence zone reversed its slope and deepened in time, indicating the slope of the cold front. As expected, the slope of the preceding warm frontal surface does not appear as steep as the slope of this cold frontal surface.

An area of larger convergence values from 3 to 5 km was located in the transition period from the warm to cold frontal slope. A mesoscale low pressure system apparently passed through the profiler triangle during that time, but it could not be resolved by the surface station or rawinsonde network then. However, it was readily identified by the $6 \times 10^{-5} \text{ s}^{-1}$ relative vorticity maximum in the profiler network at 1600/22 near 4-5 km. By 0000/23,

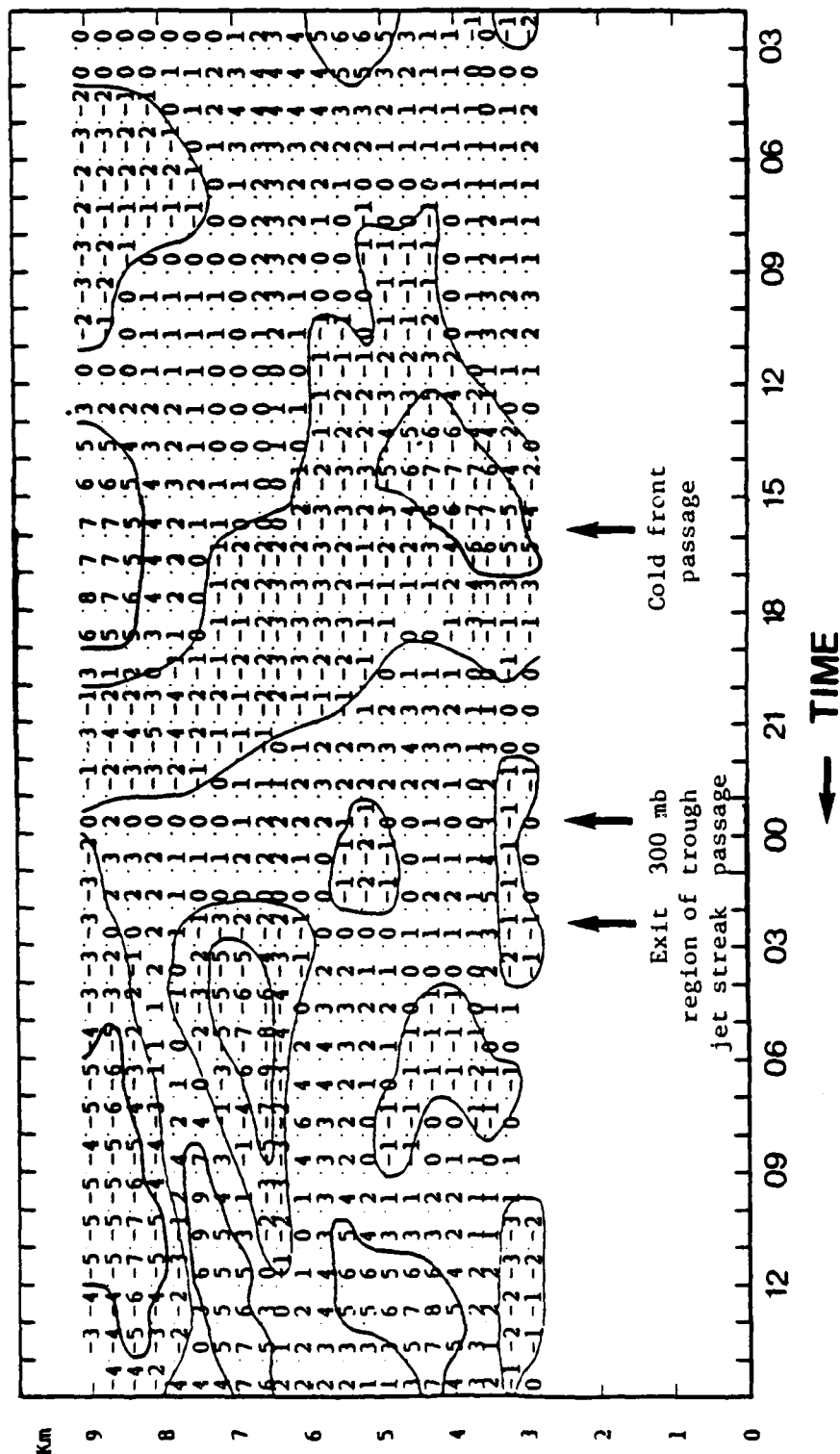


Figure 4.12 Time-height section of the profiler-derived horizontal divergence (units of $1 \times 10^{-5} \text{ s}^{-1}$) during the period from 0300 UT 22 September 1985 to 1500 UT 23 September 1985. Contour interval is $5 \times 10^{-5} \text{ s}^{-1}$. Positive values denote divergence and negative values denote convergence.

the 700 mb rawinsonde winds showed a cyclonic rotation in eastern Kansas which may have evolved earlier near the profiler network.

The convergence zone above 5 km in Fig. 4.12 may have been associated with a developing upper-level front. The cross-section of potential temperature, in Fig. 4.13a, extending from Spokane, Washington, to Victoria, Texas, showed a surface cold front approaching Denver. At the same time, an upper-level front, represented by sloping isentropes in the 300 mb layer, was approaching Denver at 1200/22. The 0000/23 cross-section of potential temperature, in Fig. 4.13b, showed the surface cold front through Denver and approaching Amarillo, Texas. The slope and the intensity of the upper-level front had become steeper with time, and had moved south of Denver to near Amarillo.

Following the passage of the upper-level front and the movement of the jet streak into the profiler triangle, belts of vorticity, convergence, and divergence were generated at various levels of the atmosphere, most notably at 6-8 km after 0600/23. The divergence belts were associated with inferred PVA, and the convergence with NVA. These vorticity, convergence, and divergence features have not been investigated but may have been waves associated with the jet stream.

The profiler-derived vertical velocities are illustrated in Fig. 4.14. At the beginning of the period, a small area of upward motion extended to 5 km in the profiler triangle. The thermodynamic sounding in Figure 4.15a showed a deep planetary boundary layer extending to 500 mb over the Denver area. The Limon, Colorado, WSR-57 weather radar picked up precipitation echoes over the

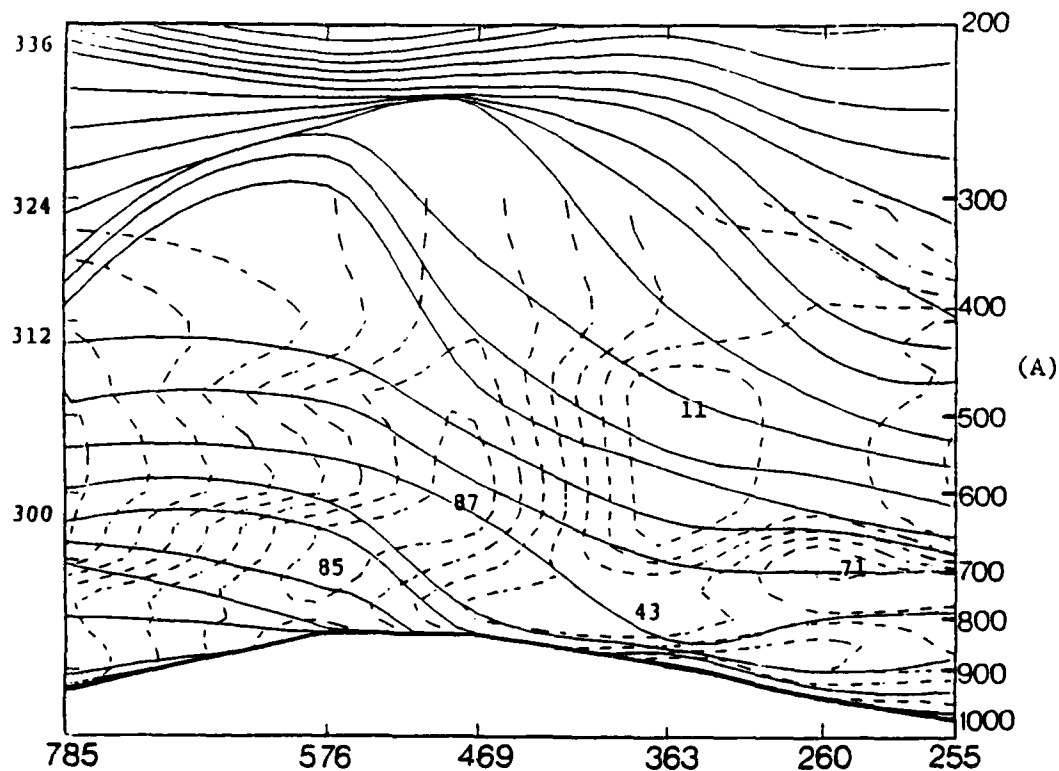


Figure 4.13 NW-SE cross-sections of potential temperature (solid lines, K) and relative humidity (dashed lines, %). Observing stations include Spokane, WA. (785), Lander, Wy. (576), Denver, Co. (469), Amarillo, Tx. (363), Nenana, Ak. (260), and Victoria, Tx. (255). (A) 1200 UT 22 September 1985, and (B) 0000 UT 23 September 1985.

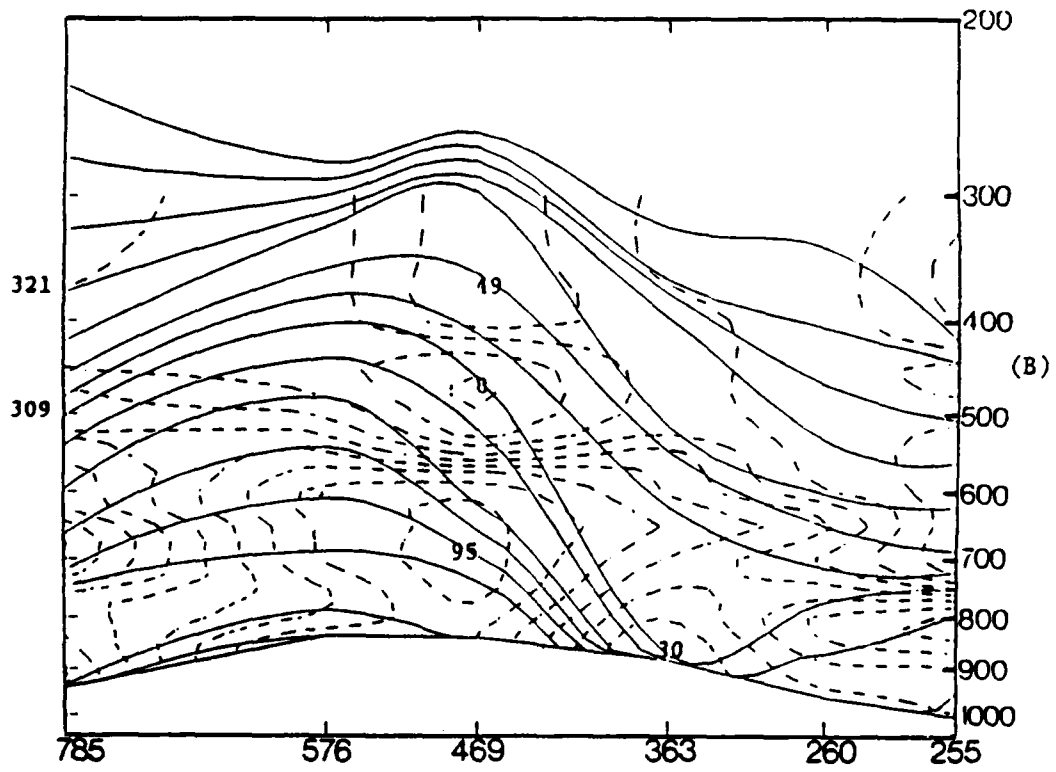


Figure 4.13 (B)

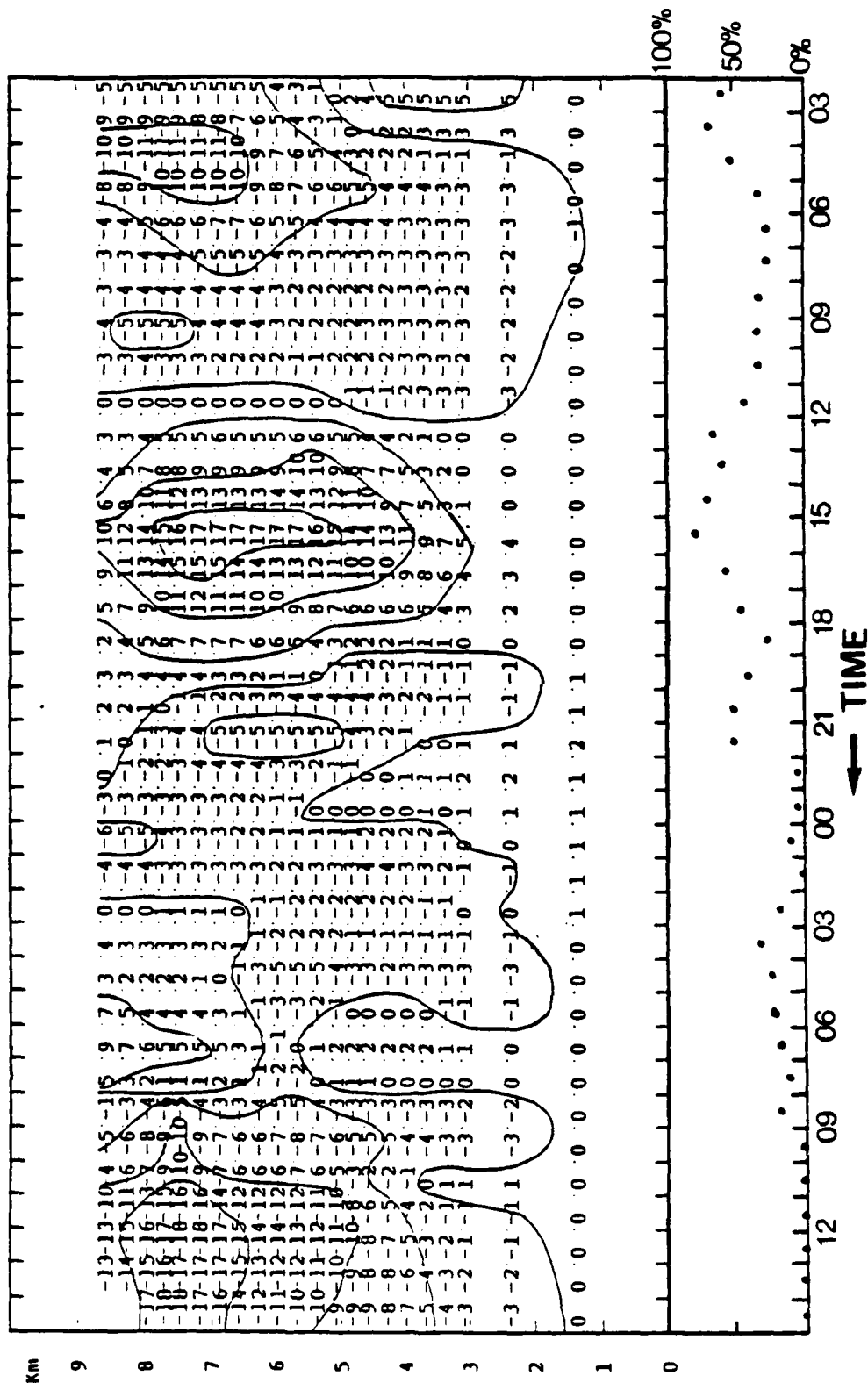


Figure 4.14 Time-height section of profiler-derived kinematic vertical velocities (cm/s) during the period from 0300 UT 22 September 1985 to 1500 UT 23 September 1985, and a plot of percent areal coverage of the profiler triangle by precipitation echo from the Limon, Co. weather radar. Positive values denote upward motion and negative values denote downward motion.

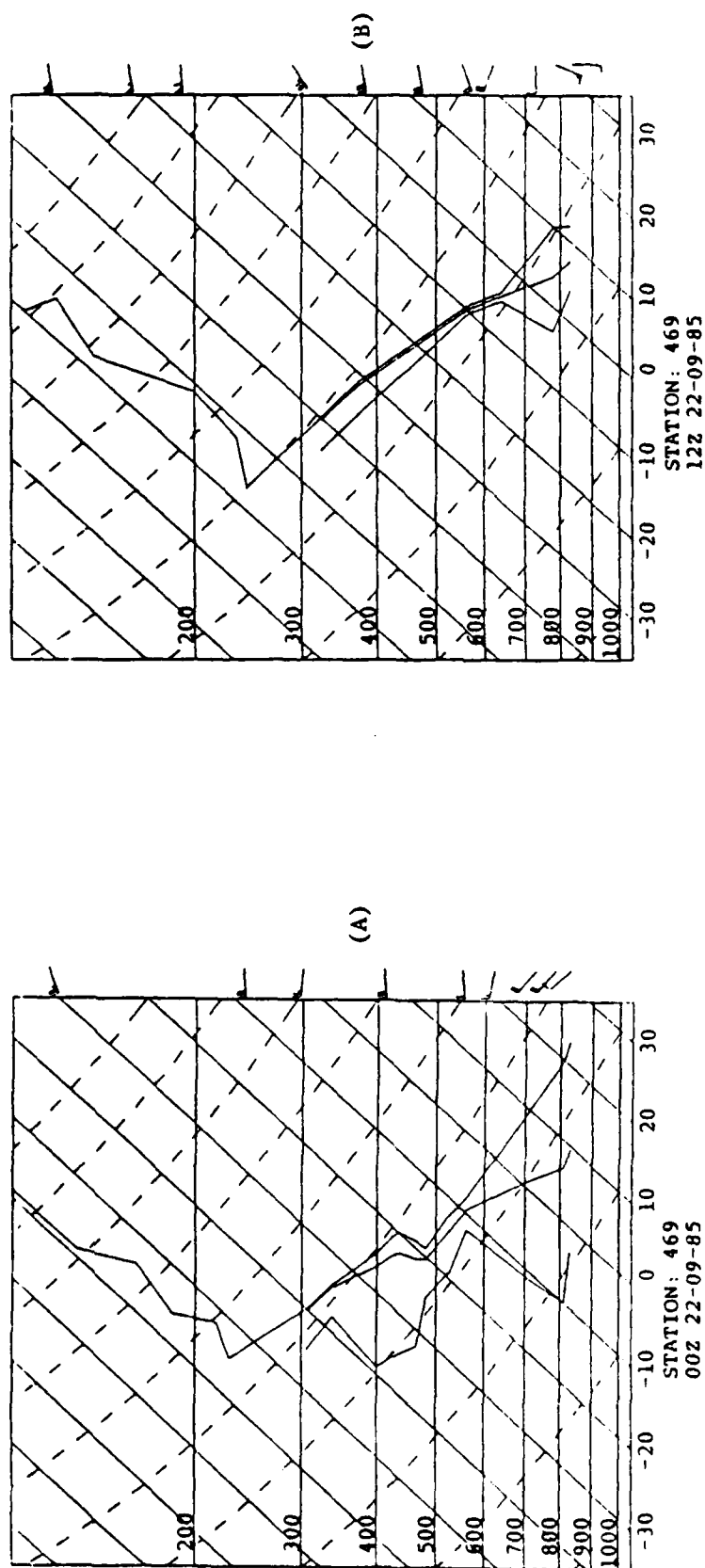


Figure 4.15 Skew-T log-P diagrams from Denver, Co. Rightmost profile is air temperature; leftmost is dew point temperature. (A) 0000 UT 22 September 1985, (B) 1200 UT 22 September 1985, (C) 0000 UT 23 September 1985, and (D) 1200 UT 23 September 1985.

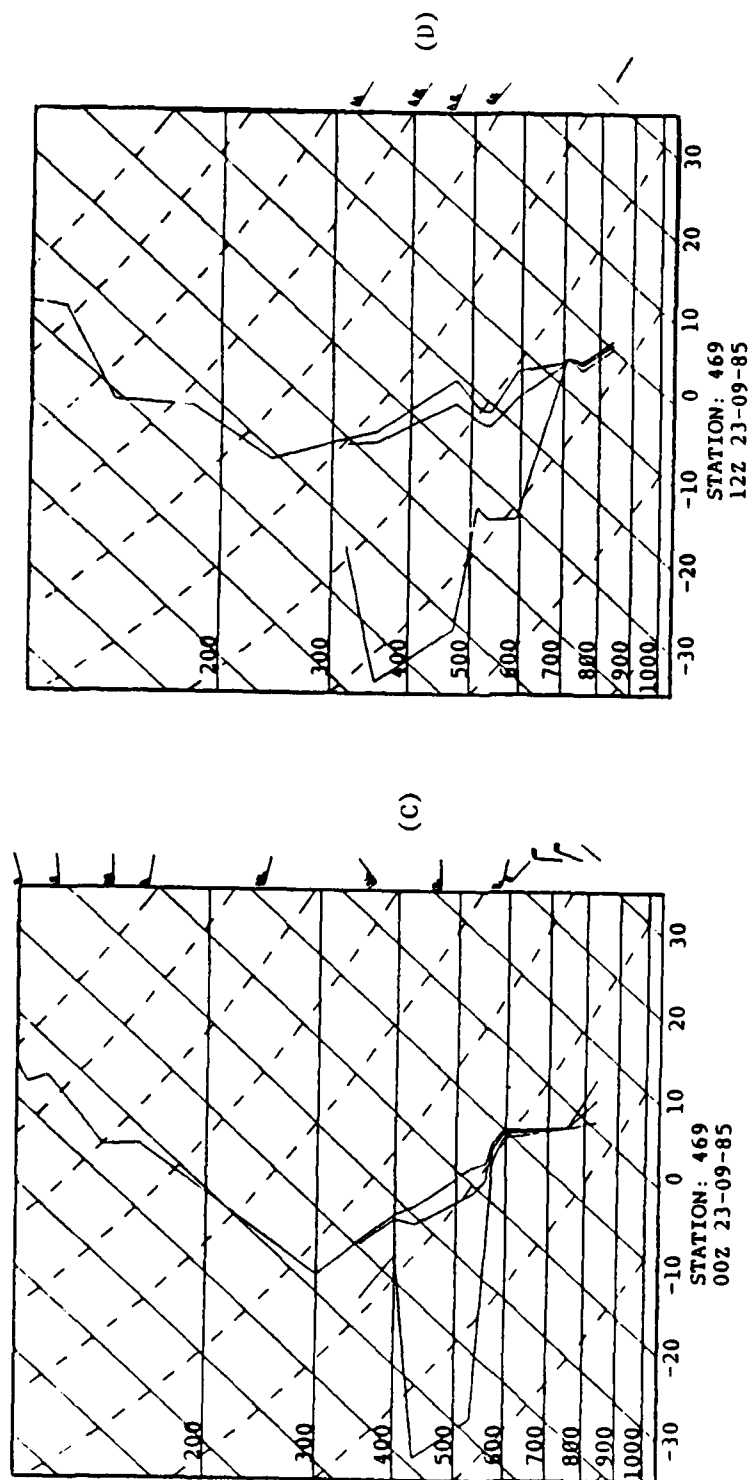


Figure 4.15 (C) and (D)

profiler triangle which covered 50% of the triangle area for the same period. The relatively dry sounding, and the character of the echoes, indicate that these were showers of convective origin, forming with the assistance of the release of potential instability by the upward motion and low-level convergence in the vicinity of the weak cold front.

Strong sinking motion above 6 km moved into the network at 0500/22, and at that time the areal coverage of the precipitation echoes decreased. At 0800/22, the intensity of the sinking motion decreased, and the percentage of areal coverage by the precipitation echo increased.

Rising motions were present in the profiler triangle starting at 1300/22 and continuing until 2000/22, as the weak warm front and strong cold front produced low-level convergence. The Denver sounding for 1200/12 showed a deep moist layer from approximately 650 mb to 325 mb, consistent with the convective moistening having occurred. The Limon radar showed an increase in the areal coverage of the precipitation echo over the profiler triangle from 15% at 0730/22 to a maximum at 1530/22 of 80%. This maximum occurred at same time as the maximum upward motion. This time was also when the synoptic-scale cold front entered the profiler triangle.

As the intensity of the upward motion decreased after 1600/22, so did the coverage of the precipitation echo. The vertical velocity remained upward until the passage of the cold front at 2000/22. Sinking motion dominated the vertical motion field for the remainder of the case, with the exception of the period from 0300/23 to 0800/23. The Denver sounding at 0000/23 still showed a

moist layer between 750 mb and 650 mb, but a very dry layer from 650 mb to 400 mb had now appeared, apparently in association with the large-scale subsidence.

The percentage of the areal coverage of the precipitation echo had a small peak at 55% for the time period from 2030/22 to 2130/22 even though the vertical motion was slightly downward. This occurred during the passage of the mid-tropospheric front and during a period of PVA. Invoking quasi-geostrophic concepts, downward vertical velocities in the presence of PVA indicate that cold advection was strong. The precipitation, then, may have occurred due to destabilization by this cold advection aloft. Thereafter, from 2230/22 to 0130/23, the percentage of areal coverage of the precipitation echo was less than 10%.

During the time from 0300/23 to 0800/23, the profiler network was in the left exit region of the jet streak. Upward motion generated by the transverse circulation in this quadrant of the jet streak produced snow showers in the profiler triangle. The greatest areal extent of the precipitation echo, which occurred at 0330/23, was 30%. The Denver sounding at 1200/23 showed a deep layer of dry air over Denver, which had advected in from the northwest in this region west of the upper-air trough axis.

After 0830/23, the vertical velocity became negative and the Limon radar did not show any precipitation echoes in the profiler triangle for the remainder of the case. The switch from upward to downward motion after 0800/23, the secondary vorticity maximum at about 1000/23, and the decrease thereafter, suggest that the jet

stream was beginning to drift eastward across the triangle. From then on the triangle was in the subsiding right exit region.

4.2 Case of September 28-29, 1985

In this case study a Colorado upslope snowstorm, during the period from 1200 on 28 September to 2300 on 29 September 1985, was investigated. Though the low-level flow was generally upslope, important weather systems travelled over the region aloft and exerted appreciable control over the precipitation intensity. These disturbances are studied in detail.

The upslope flow was forced by a strong anticyclone located in the Canadian province of Alberta. Prior to 1200/28, a 1034 mb high pressure system, moving eastward through southern Canada, channeled cold air along the east slopes of the Rockies. The southern portion of this anticyclone can be seen in Fig. 4.16. The cold air became dammed along the east slopes of the Rockies as the anticyclonic flow from the high pressure system combined with the cyclonic flow from a weak low pressure system in northwest Colorado to produce easterly surface winds. Cross-sections of potential temperature, extending from Medford, Oregon, to Centerville, Alabama, in Figs. 4.17a and b, show the tropospheric-depth of the synoptic-scale cold dome accompanying the anticyclone, as well as a more shallow (extending to about 700 mb) cold dome associated with the cold air damming. This cold pocket of air remained over Denver throughout the entire case, and served as an overrunning surface for the southwesterly flow aloft.

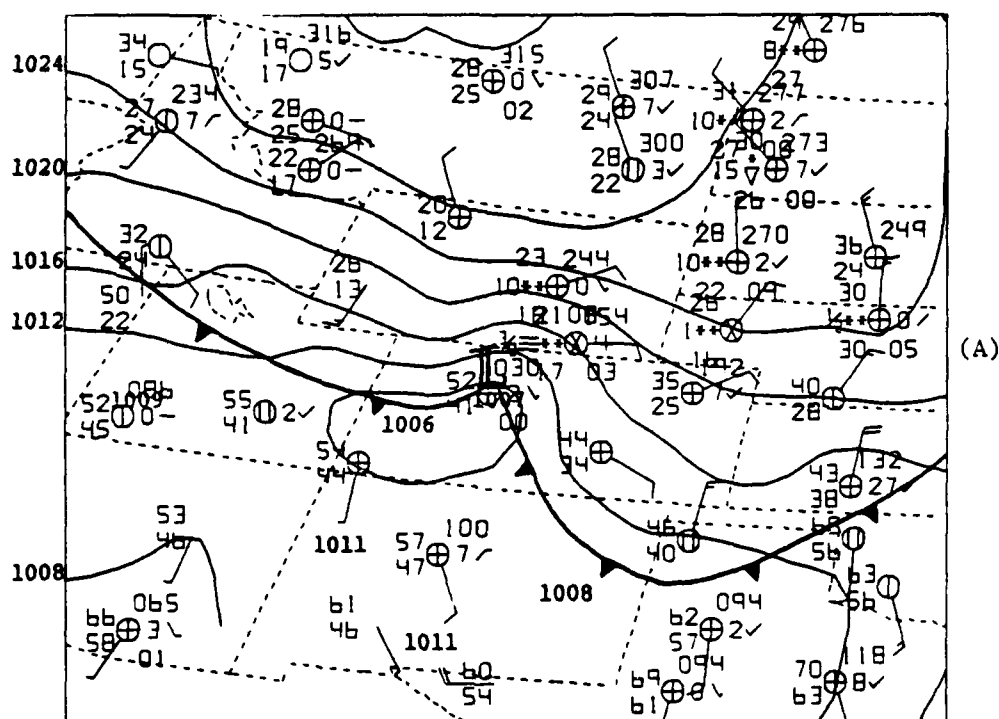


Figure 4.16 Surface pressure analyses. (A) 1200 UT 28 September 1985, (B) 0000 UT 29 September 1985, (C) 1200 UT 29 September 1985, and (D) 0000 UT 30 September 1985.

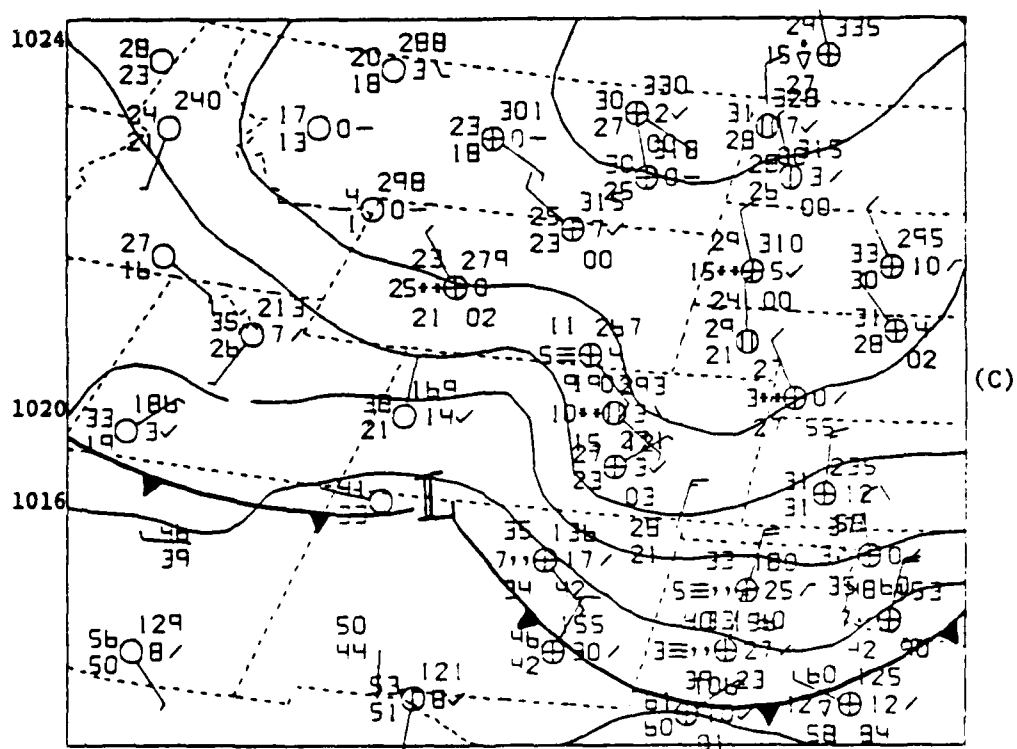
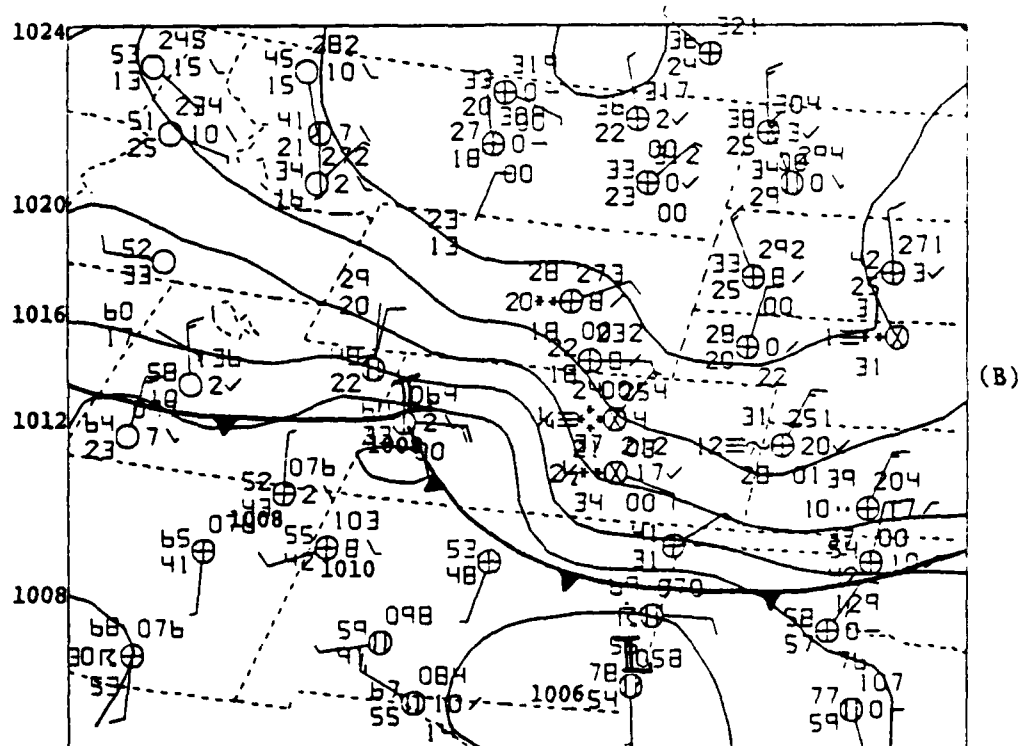


Figure 4.16 (B) and (C)

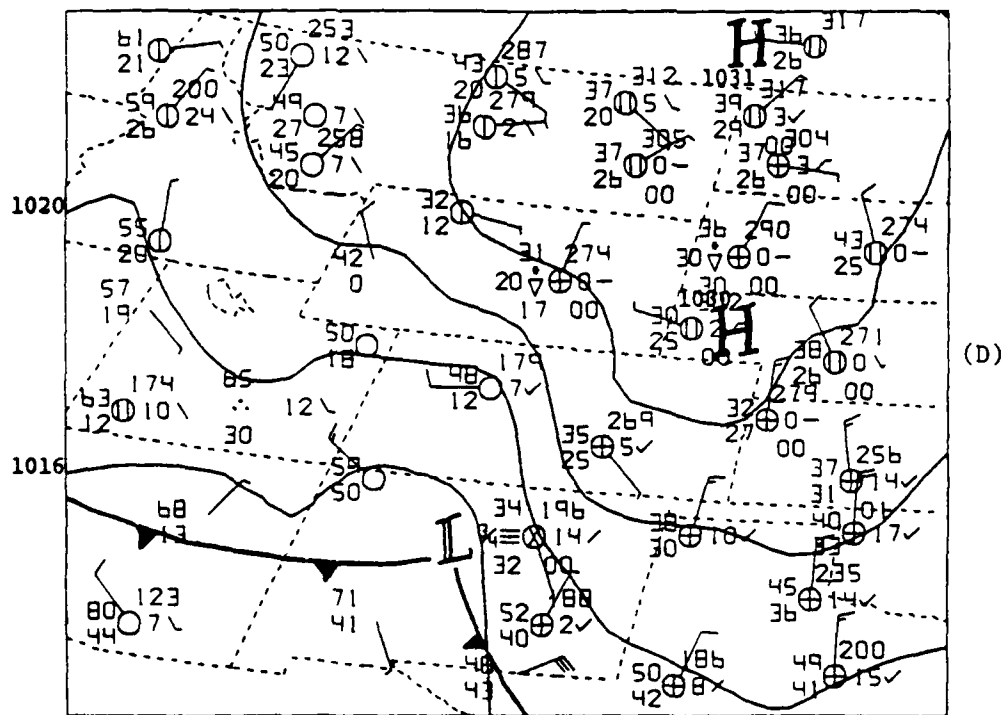


Figure 4.16 (D)

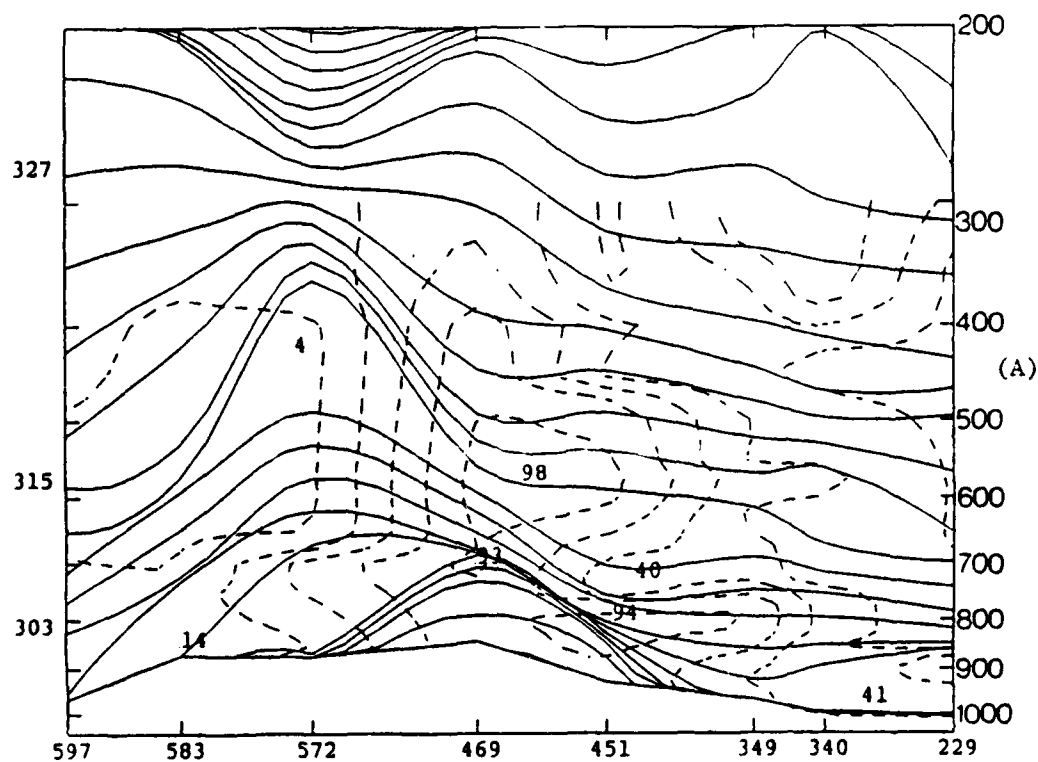


Figure 4.17 WNW-ESE cross-sections of potential temperature (solid lines, K) and relative humidity (dashed lines, %). Observing stations include Medford, Ore. (597), Winnemucca, Nev. (583), Salt Lake City, Utah (572), Denver, Co. (469), Dodge City Ka. (451), Monett, Mo. (349), Little Rock, Ark. (340), and Centerville, Al. (229). (A) 0000 UT 29 September 1985, and (B) 1200 UT 29 September 1985.

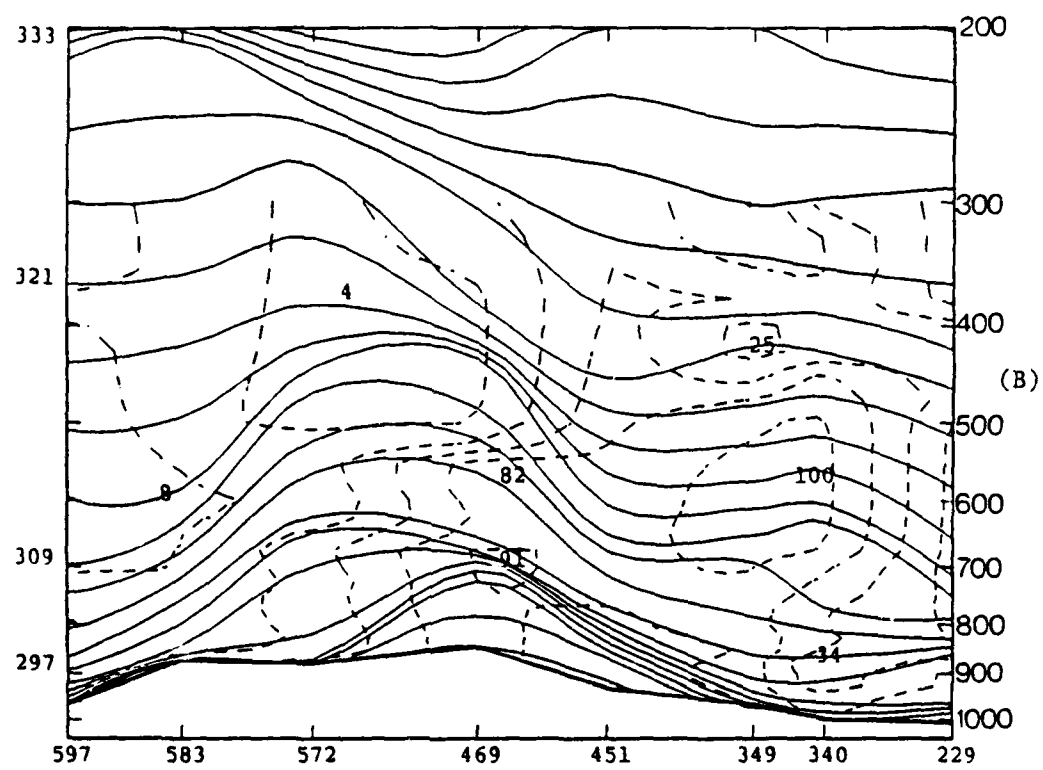


Figure 4.17 (B)

4.2.1 Low-Level Fronts and Troughs

At 1200/28, in Fig. 4.16a, the surface cold front was located north of Amarillo, Texas, and extended from Kansas to New Mexico and back into southern Idaho. A weak low pressure disturbance was located near the cold front in northwestern Colorado at this time. As the cold front proceeded southeastward, the weak disturbance moved with it, and by 0000/29, in Fig. 4.16b, over southeastern New Mexico. It later continued to move southeastward into southern Texas. At 1200/29, in Fig. 4.16c, the cold front had pushed southward into Oklahoma, central New Mexico, and northern Arizona, and continued moving southward in Texas, as shown in Fig. 4.16d. A portion of the original Colorado trough appeared to be left behind in southwestern Colorado and northeastern Arizona, and drifted slowly to central Colorado and New Mexico by 0000/30.

The 700 mb maps are depicted in Figs. 4.18a, b, c, and d. A 700 mb cold front extending from Northern Ontario, to Nebraska, and back into Oregon is shown entering the profiler triangle around 1200/28. By 0000/29, the cold front was located south of the profiler triangle in southeastern Colorado, and it continued to move southeastward extending from Nebraska to Texas into Nevada by 1200/29. At this time, the cold front had become stationary from Omaha, Nebraska, to Sault Ste. Marie, Michigan, and a small wave appeared to be developing near Omaha. As the cold front moved eastward into central Kansas and Oklahoma, the front remained stationary for the next twelve hours over the northern Midwest. A weak 700 mb circulation was present over northwestern Iowa by 0000/30.

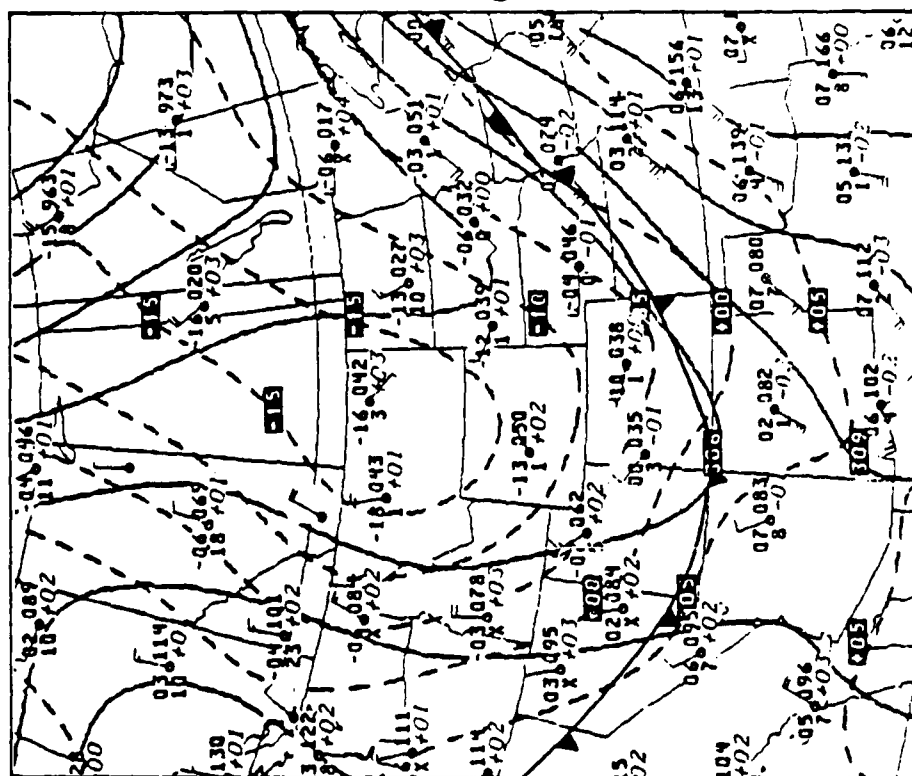
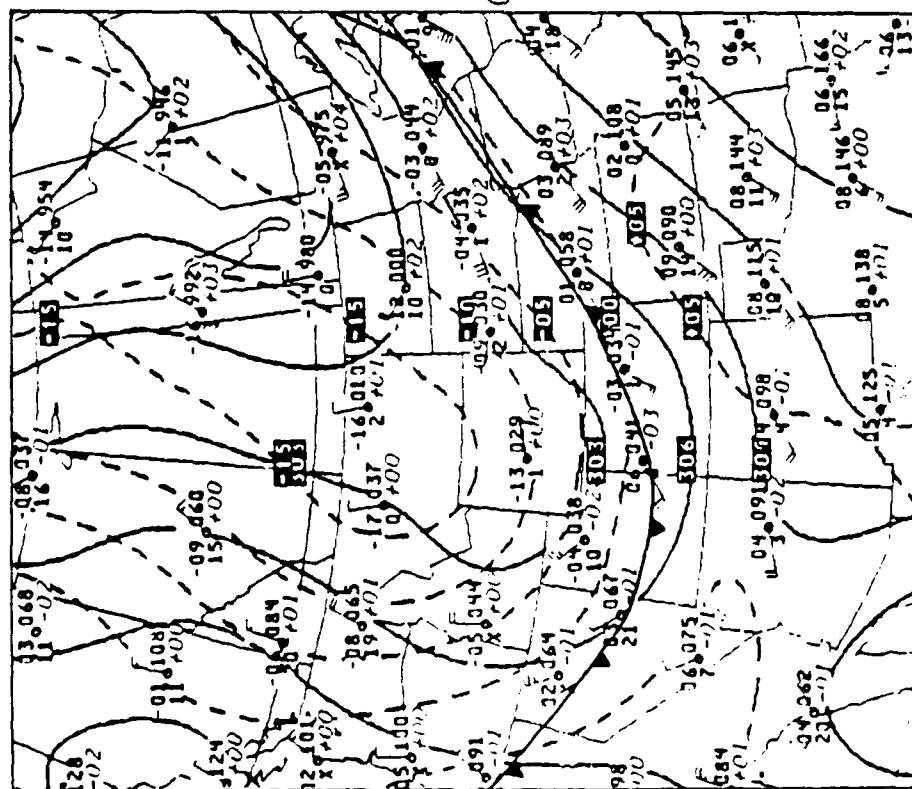
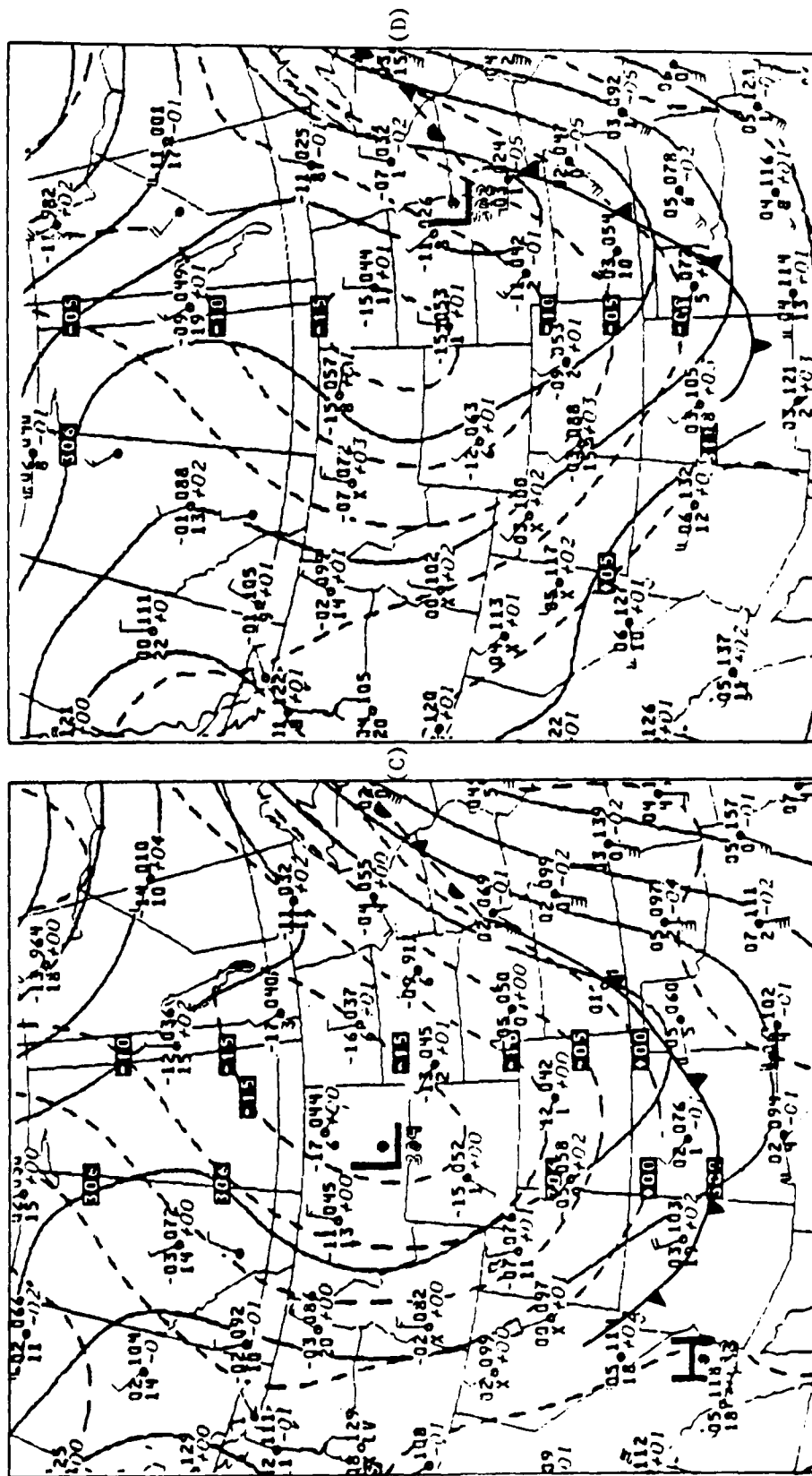


Figure 4.18 NMC objective analyses of 700 mb height and temperature fields. (A) 1200 UT 28 September 1985, (B) 0000 UT 29 September 1985, (C) 1200 UT 29 September 1985, and (D) 0000 UT 30 September 1985.



Two 700 mb short-wave troughs, imbedded within a long-wave trough extending from the Hudson Bay area to Baja, California, are shown in Fig. 4.18a. The first short-wave is located from northeastern North Dakota to southwestern South Dakota, and is of little relevance to this case study. The second trough, located over central Wyoming and northeastern Utah, had a weak cyclonic disturbance located in its northern end. By 0000/29, a third short-wave trough had developed in central Montana over the area where the coldest 700 mb temperatures were found.

The Grand Junction and Denver, Colorado, rawinsonde data showed a wind shift from southwest to northwest during the time period from 1200/28 to 0000/29, indicating that the second trough had passed. The Lander, Wyoming station, on the other hand, was still reporting a northeast wind, indicating that the weak cyclonic disturbance at the northern end of the second trough was still in southern Wyoming. The long-wave trough remained over southern Colorado.

By 1200/29, the second short-wave trough had shifted eastward through southeastern Colorado into northern and western Texas. The weak closed circulation at the northern end of this second trough had disappeared. The long-wave trough over South Dakota had deepened slightly. The short-wave trough over Montana had remained stationary or drifted slowly southward during this time period. By 0000/30, the long-wave trough and the second short-wave trough had phased together in Texas and Oklahoma, forming one major trough extending from Wisconsin to Texas. The short-

wave trough in Montana has appeared to shear apart, with a portion remaining in Montana and a portion moving eastward with the cold pocket of air.

After 1200/28, the 3.3 to 4.8 km profiler winds (Figs. 4.19 to 4.24) shifted from southwest to northwest as the 700 mb trough axis and cold front moved through the profiler triangle. The trough axis began to pass through Platteville by 1700/28, Fleming by 2100/28, and Flagler by 0700/29. The trough axis had virtually stalled between the Fleming and Flagler sites for a period of ten hours after moving rapidly between Platteville and Fleming.

After the front passed and the winds had veered, the 3 to 4 km profiler winds at the two northern sites backed to the south or southwest over a few hours, as depicted in Figs. 4.19, 4.20, and 4.21. The winds at Platteville backed to the south at 0500/29 followed by Fleming at 0900/29. The low-level winds at Flagler were light and, thus, it was difficult to determine if a backing occurred, but it appeared that no backing occurred. The backing at the two northern sites over a 6 to 9 hour period was consistent with the approach of the 700 mb weak cyclonic circulation of the second short-wave, which had been located southeast of Lander, Wyoming.

The cyclonic circulation of the recent short-wave trough moved east but north of the profiler triangle between 0500/29 and 1800/29, trailing the cold front which had surged ahead. Winds remained generally in their backed direction for a few hours. At about 3.5 km, there was then a sharp shift of winds to westerly or northwesterly in a thin layer, which appeared to signal the passage of the center (or a secondary cold front) of the closed

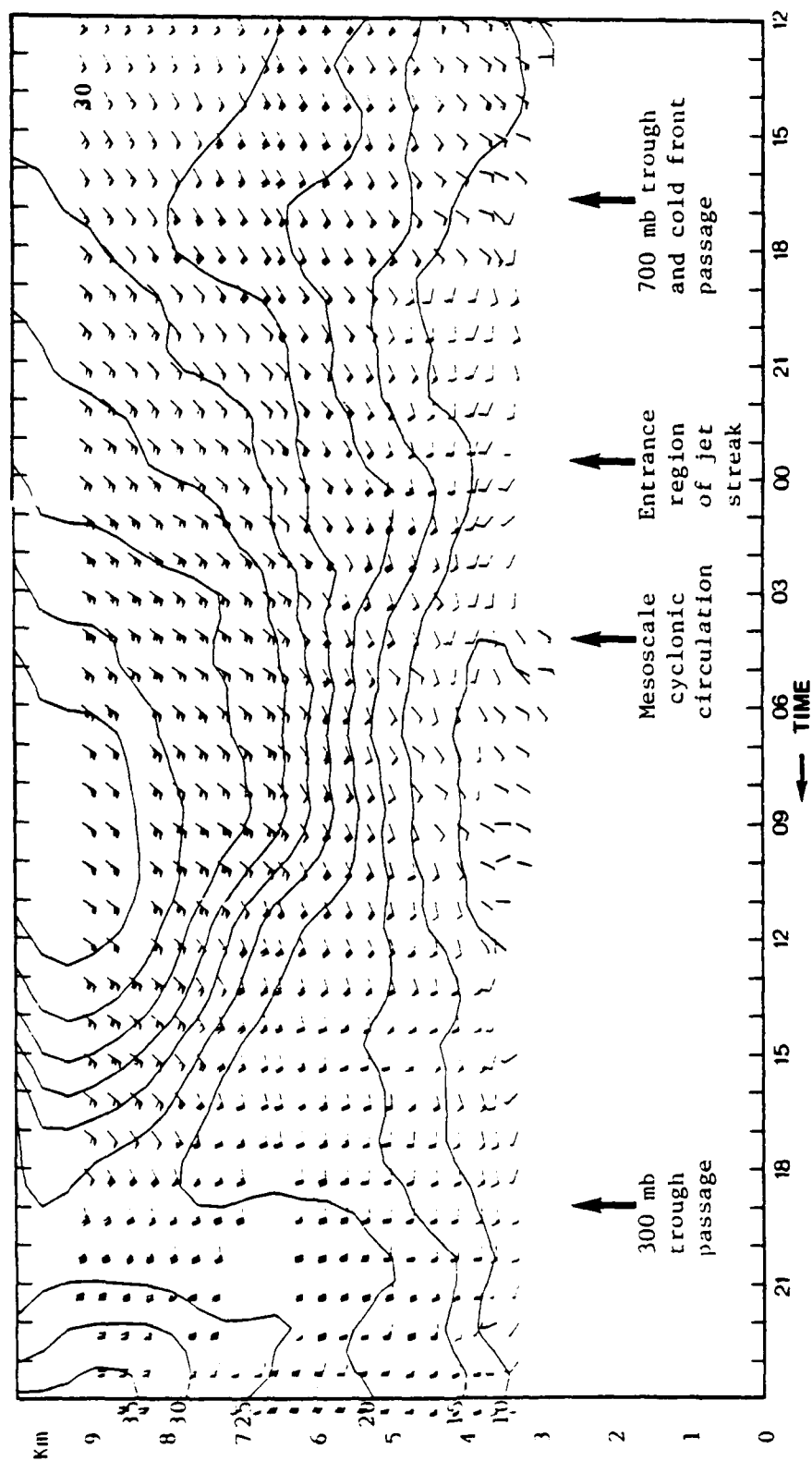


Figure 4.19 Time-height section of observed winds from the Platteville profiler during the period from 1200 UT 28 September 1985 to 0000 UT 30 September 1985. Convention as in Fig. 4.2.

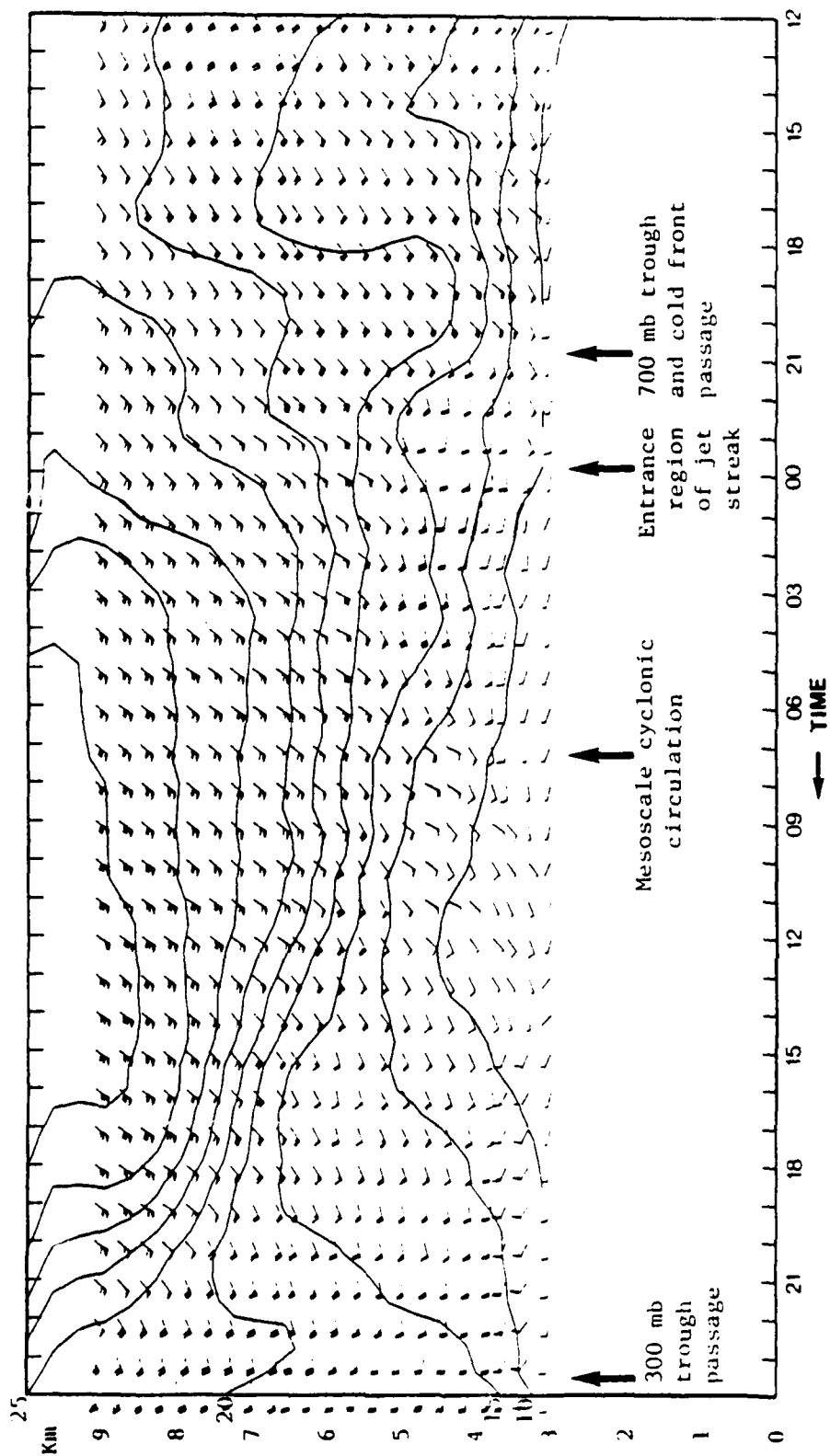


Figure 4.20 Time-height section of observed winds from the Fleming profiler during the period from 1200 UT 28 September 1985 to 0000 UT 30 September 1985. Convention as in Fig. 4.2.

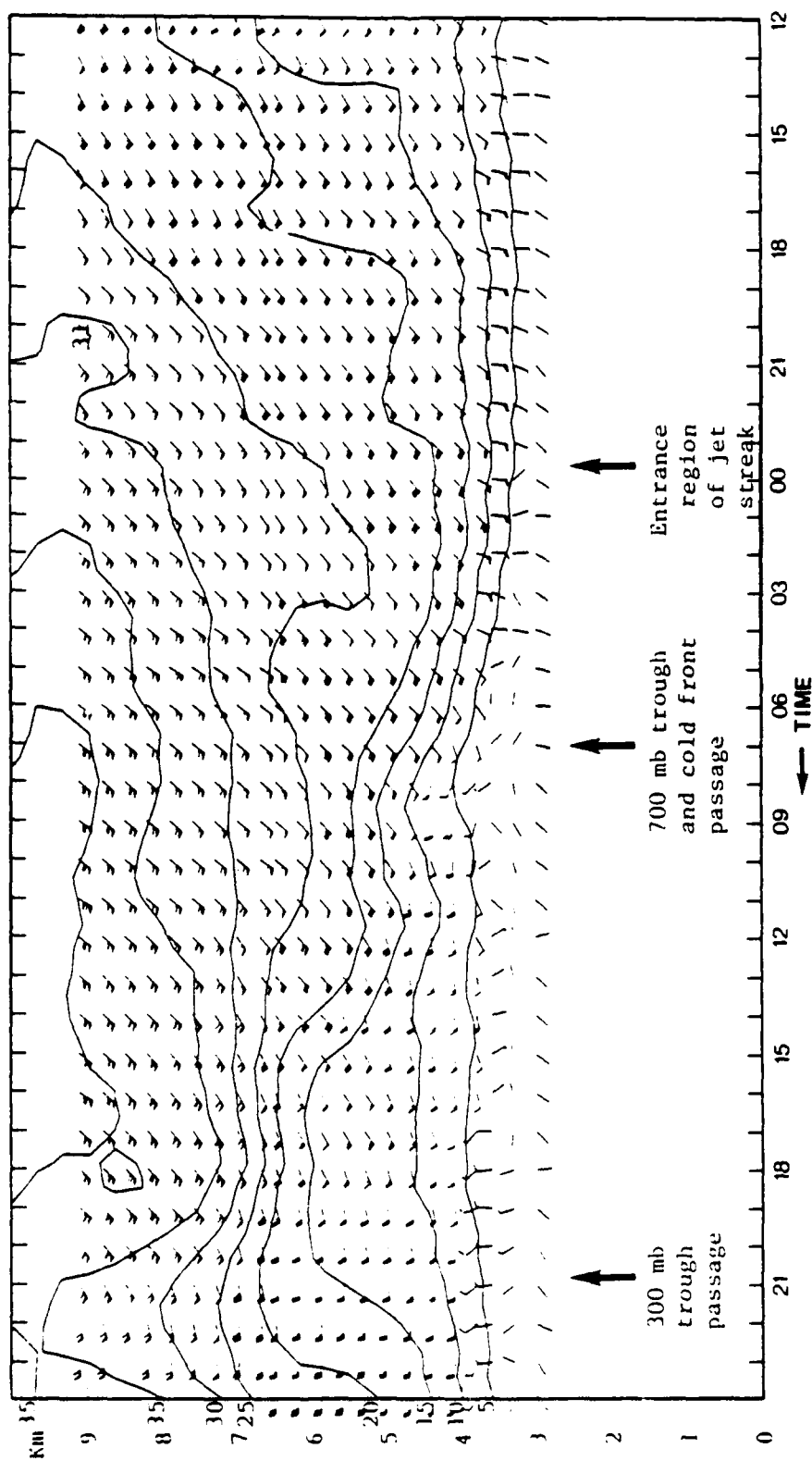


Figure 4.21 Time-height section of observed winds from the Flagler profiler during the period from 1200 UT 28 September 1985 to 0000 UT 30 September 1985. Convention as in Fig. 4.2.

circulation at the north and lagging end of the second short wave. The windshift occurred at Platteville at about 1300/29, Fleming about 1400/29, and Flagler about 1700/29.

The perturbation winds, in Figs. 4.22, 4.23, and 4.24, showed more clear evidence of the cyclonic circulation in the 3.0 to 5.0 km layer between 0800/29 and 1800/29. The Platteville and Fleming low-level perturbation winds showed a southeasterly flow beginning at about 0400/29 and continuing until 1200/29 and 1500 to 1700/29, respectively, when it appeared that a weak cyclonic disturbance center passed through the sites. The Flagler perturbation winds showed only weak and much more shallow cyclonic circulations. The overall pattern suggests the passage of this feature at 3.5 km at about 1700/29.

In this case, profiler data, especially from Platteville and Fleming, confirmed the existence of a meso-alpha-scale system, shaped somewhat like a comma. The tail of this comma-shaped system surged across the profiler network as a cold front on the 29th, dragging slowly past Flagler early on the 29th. A lagging circulation center occupied the head portion of the system, and subsequently affected the northern portion of the profiler triangle on the 29th. Perturbation winds made a cyclonic spiral as this feature passed. While the presence of the feature was detectable in the raw winds in the form of wind shifts, the perturbation winds more clearly revealed the nature of the system.

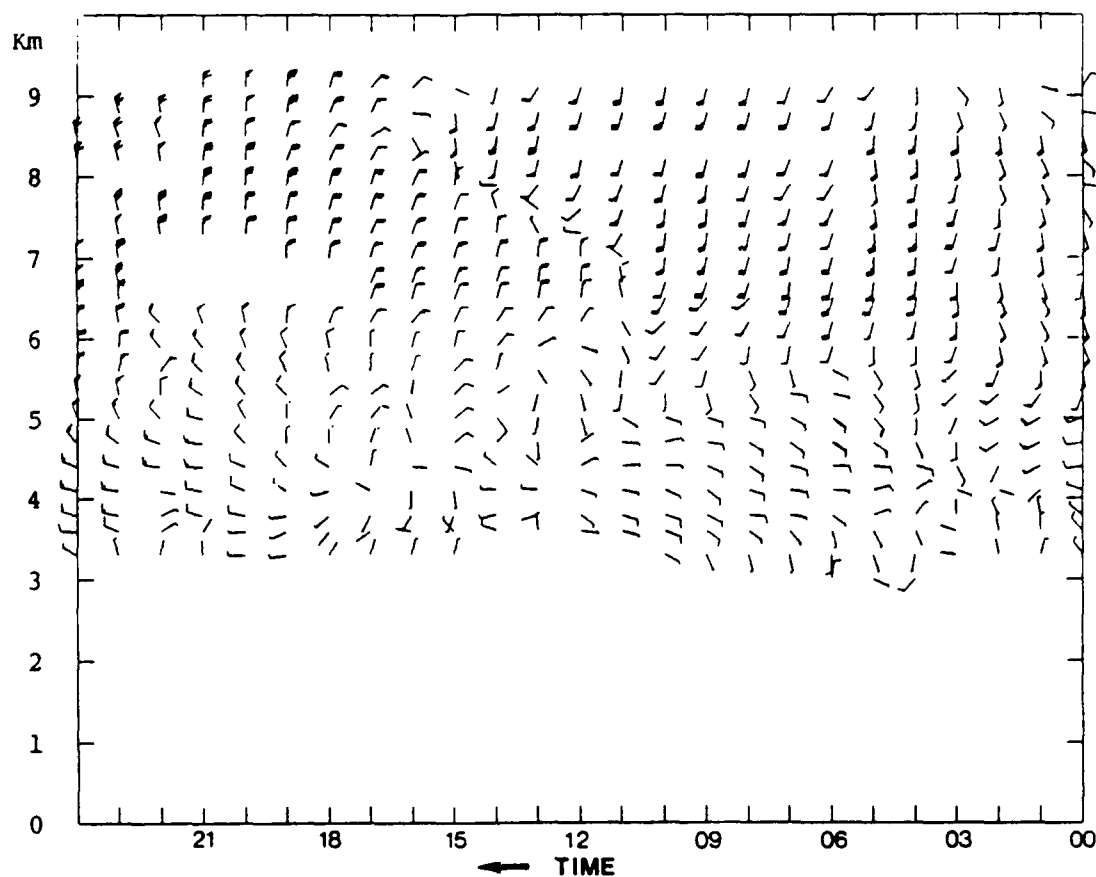


Figure 4.22 Time-height section of perturbation winds from the Platteville profiler during the period from 0000 UT 29 September 1985 to 0000 UT 30 September 1985. Convention as in Fig. 4.2.

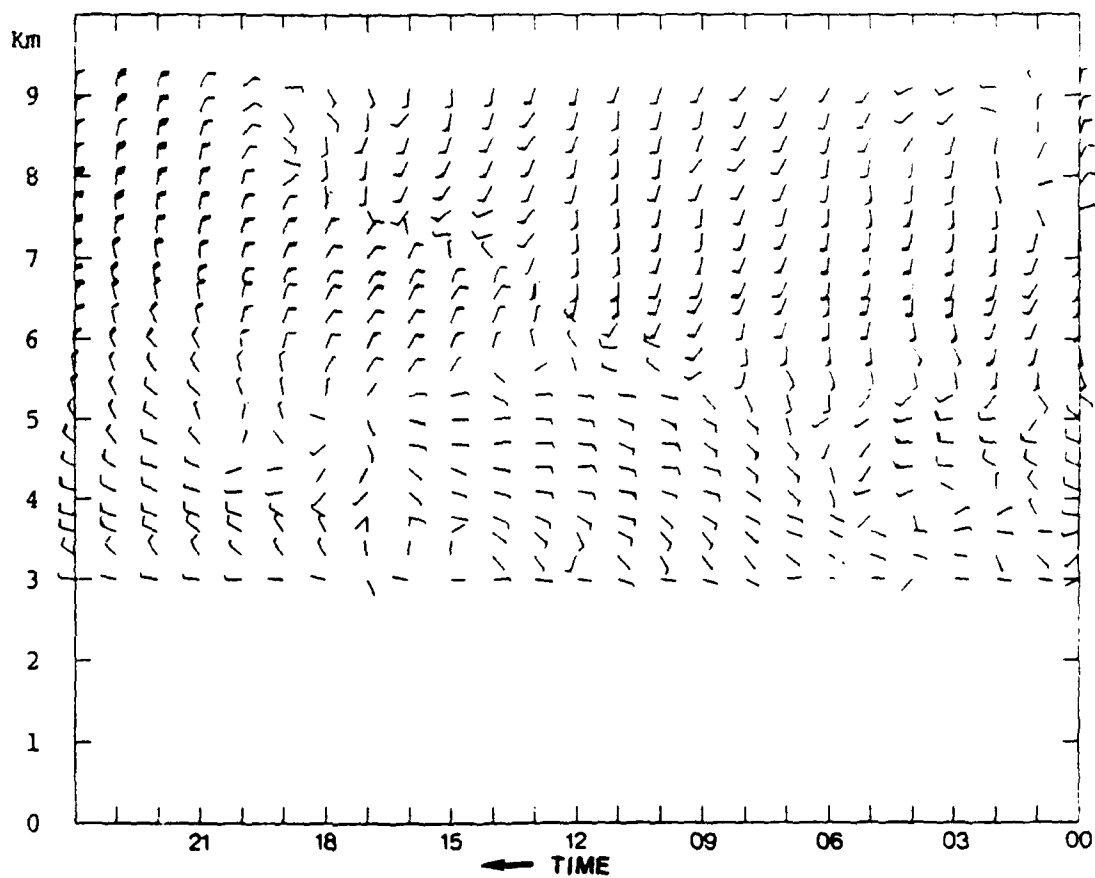


Figure 4.23 Time-height section of perturbation winds from the Fleming profiler during the period from 0000 UT 29 September 1985 to 0000 UT 30 September 1985. Convention as in Fig. 4.2.

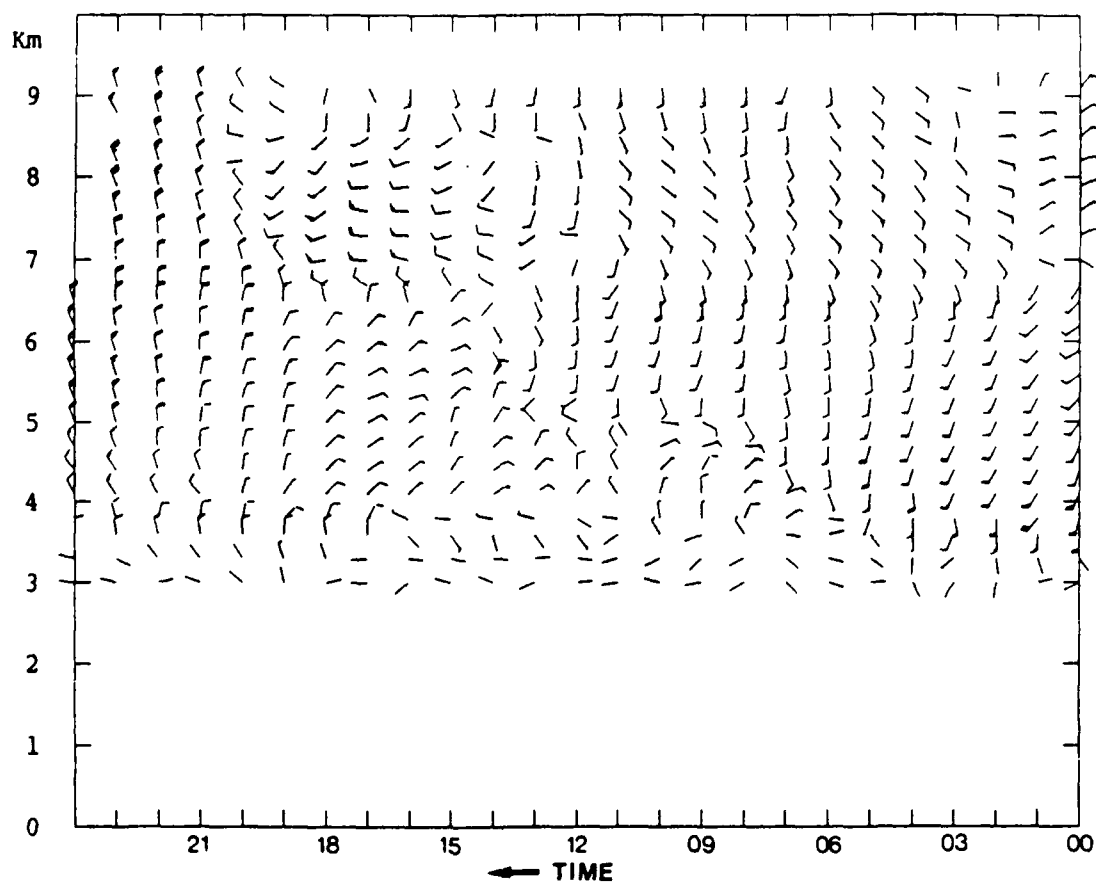


Figure 4.24 Time-height section of the perturbation winds from the Fleming profiler during the period from 0000 UT 29 September 1985 to 0000 UT 30 September 1985. Convention as in Fig. 4.2.

4.2.2 Upper-Level Troughs and Jet Streaks

A 300 mb short-wave trough extending from the Canadian province of Saskatchewan to central Nevada is shown in Fig. 4.25a. Large height falls were occurring in the base of this trough at Lander, Wyoming, Salt Lake City, Utah, and Boise, Idaho, which indicated that the short-wave trough was digging. The 300 mb trough continued to dig south and eastward toward the profiler triangle and by 0000/30 the 300 mb trough axis had passed through Denver.

The wind shifts at the three profiler sites (Figs. 4.19 to 4.21) indicated that the 500 mb and 300 mb troughs had a two-hour time lag between their passages through the profiler triangle. The axis of the weak 500 mb short-wave trough passed Platteville, Flagler, and Fleming at about 1900/29, 2100/29, and 2300/29, respectively. The 300 mb trough was much sharper and passed through Platteville at 2100/29 and Flagler at 2300/29. The winds at Fleming were in the process of veering to the northwest at 0000/30.

The 300 mb short-wave trough had two jet streaks associated with it: one in the northwesterly flow located west of the trough axis, and the other in the southwesterly flow located east of the trough axis. As the 300 mb trough dug further south, the southwesterly jet streak intensified and became more southerly. This jet streak entered the profiler triangle from the west-northwest between 1200/28 and 1200/29 according to the 300 mb analysis, Figs. 4.25a-c.

The southwesterly jet streak appeared to develop stronger winds at its core during this period, from approximately 52 m/s at

AD-A207 542

KINEMATIC QUANTITIES DERIVED FROM A TRIANGLE OF VHF
DOPPLER WIND PROFILER. (U) PENNSYLVANIA STATE UNIV
UNIVERSITY PARK DEPT OF METEOROLOGY. C A CARLSON

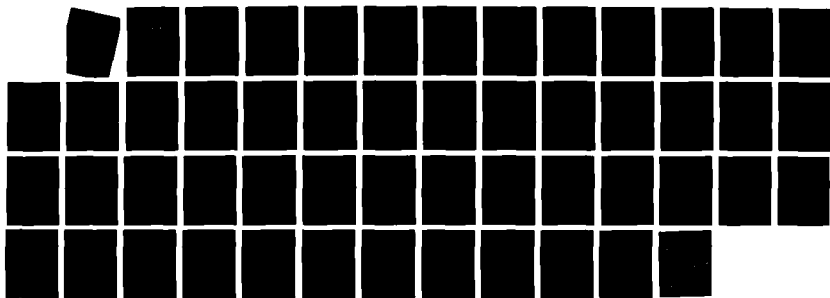
272

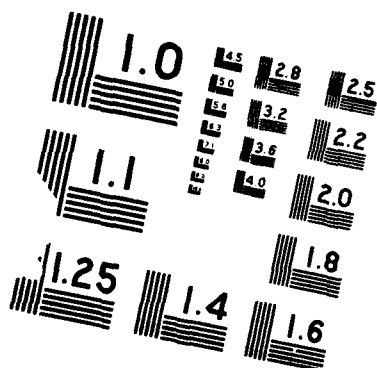
UNCLASSIFIED

AUG 87 SCIENTIFIC-1 AFGL-TR-87-0265

F/G 17/9

NL





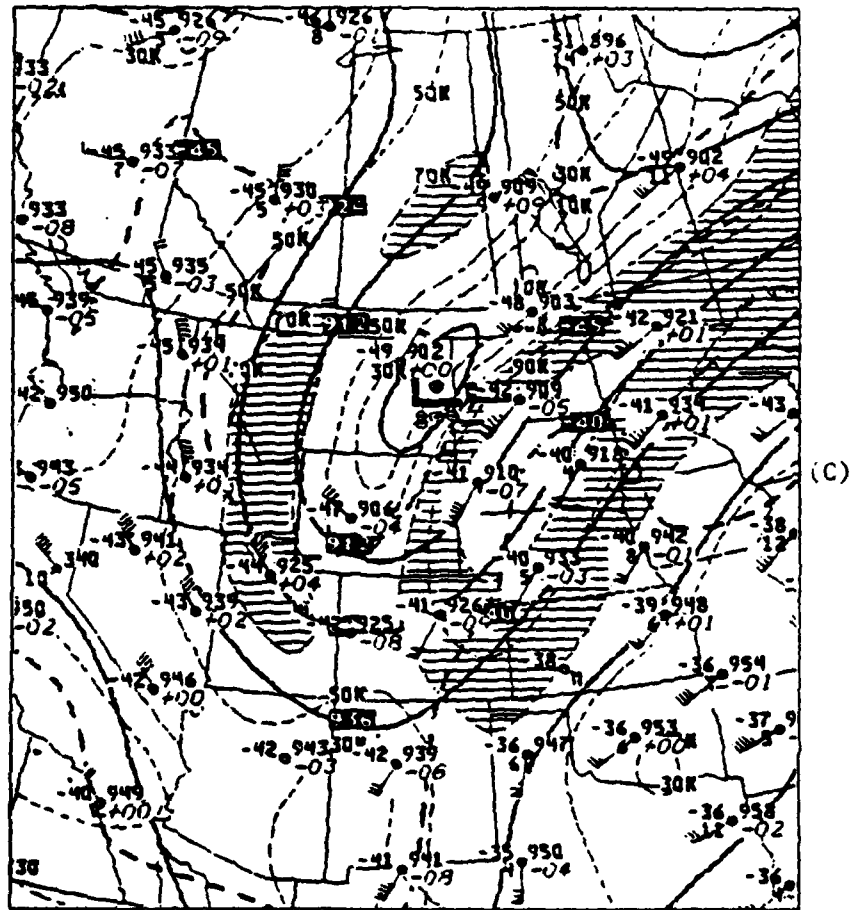


Figure 4.25 (C)

1200/28 to approximately 65 m/s at 1200/29. Between 1200/29 and 0000/30, this southwesterly jet streak moved out of the profiler triangle as the 300 mb trough axis passed through the triangle. The northwesterly jet streak entered the profiler triangle soon after the trough passage, and by 0000/30 it was located over Denver.

The leading edge of the southwesterly jet streak began to move over Platteville, Fleming, and Flagler at about 1800/28, 1900/28 and 2000/28, respectively, as indicated by winds increasing beyond 30 m/s in Figs. 4.19 to 4.21. The profiler triangle was located in the right entrance region of this southwesterly jet streak until approximately 1200/29 when the winds speed peaked at Fleming and began to subside at Platteville. The maximum winds in the profiler triangle occurred at Platteville where the winds speed peaked to 52 m/s from 0800/29 to 1100/29. The wind speed peak was not as distinct at Flagler, but was about 45 m/s at 1600/29.

Following the passage of the southwesterly jet streak, wind speeds decreased and then began to veer as the 300 mb trough approached. The speeds were as low as 23 m/s at Platteville during the trough passage. The northwesterly jet streak began to move over the Platteville profiler at about 2200/29, as indicated by speeds exceeding 30 m/s. At this time, the left exit region of this jet streak began moving over the profiler triangle.

Now that the key features of the case have been studied with observed profiler, rawinsonde, and surface data, the profiler-derived quantities are examined individually. The profiler-derived geostrophic winds, relevant at the center of the triangle, are

depicted in Figure 4.26. For the lower tropospheric features of Section 4.2.1, the geostrophic winds were much like the observed winds. They showed a southwesterly flow for most of the case study. The passage of the second 700 mb short-wave trough at 2200/28 was shown, as was the backing and veering patterns of the low-level winds when the weak 700 mb circulation passed north of the profiler triangle.

As the southwesterly jet streak entered the profiler triangle, the middle and upper tropospheric geostrophic winds differed from the observed winds. The geostrophic winds in the 5 to 8 km layer were faster and more westerly than the observed winds, most notably near 6 to 7 km at 0300/29, indicating that ageostrophic motions were present.

The ageostrophic winds aloft, in Fig. 4.27, developed a strong southeasterly flow by 0000/29, in response to the upper portion of the transverse (direct) circulation in the entrance region of the southwesterly jet streak. Once the core of the southwesterly jet streak began to pass through the profiler triangle, the southeasterly ageostrophic winds subsided. Weak westerly ageostrophic components were occasionally experienced for about a five-hour period.

As the axis of the southwesterly jet stream moved east and the winds weakened and began to veer in association with the approach of the trough axis, ageostrophic winds again became strong. Actually, geostrophic wind speeds increased to more than 65 m/s by about 1800/29. The strong ageostrophic easterlies were almost exactly opposite in direction to the geostrophic winds at this time.

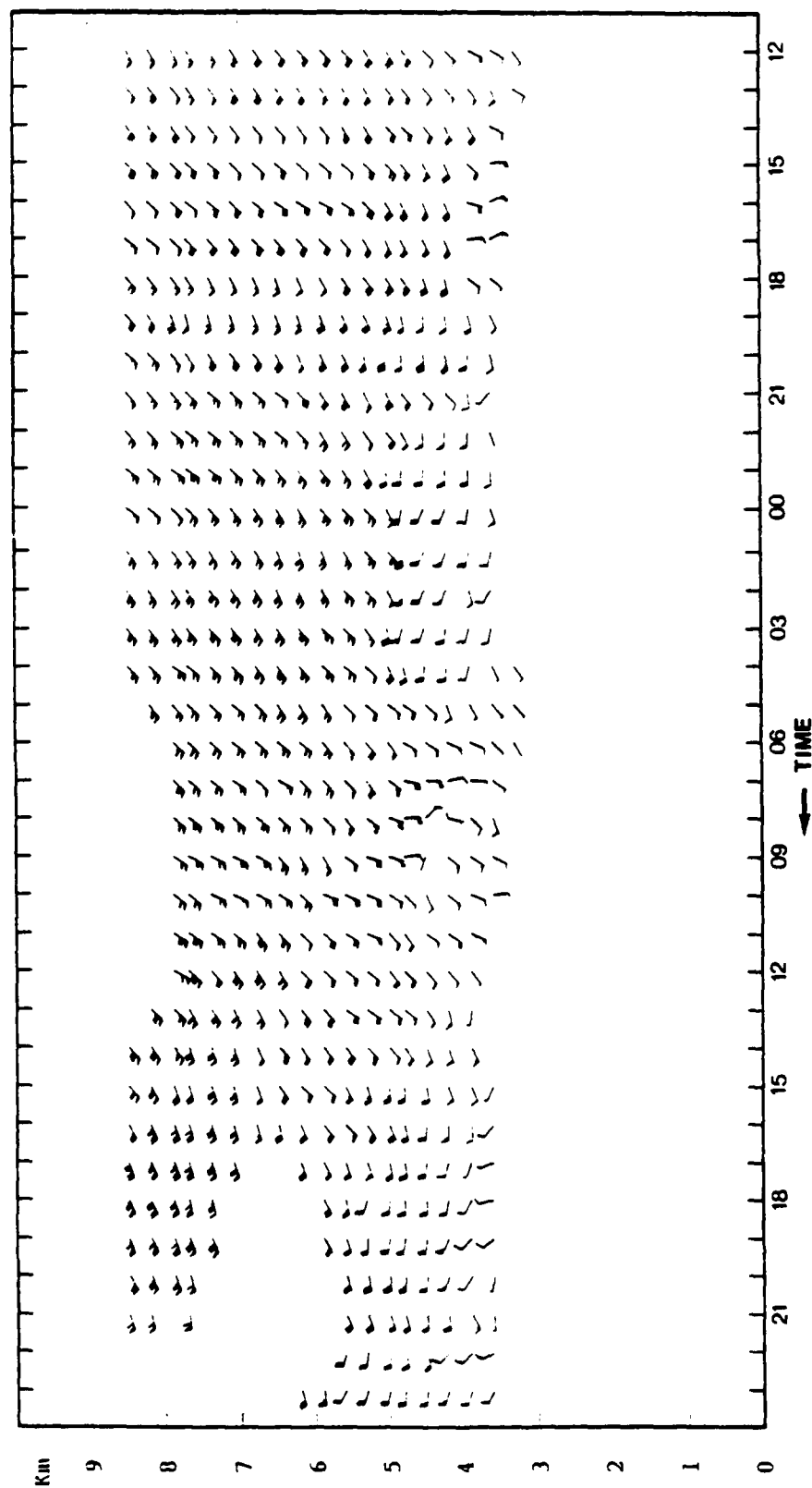


Figure 4.26 Time-height section of the profiler-derived geostrophic winds during the period from 1200 UT 28 September 1985 to 2300 UT 29 September 1985. Convention as in Fig. 4.2.

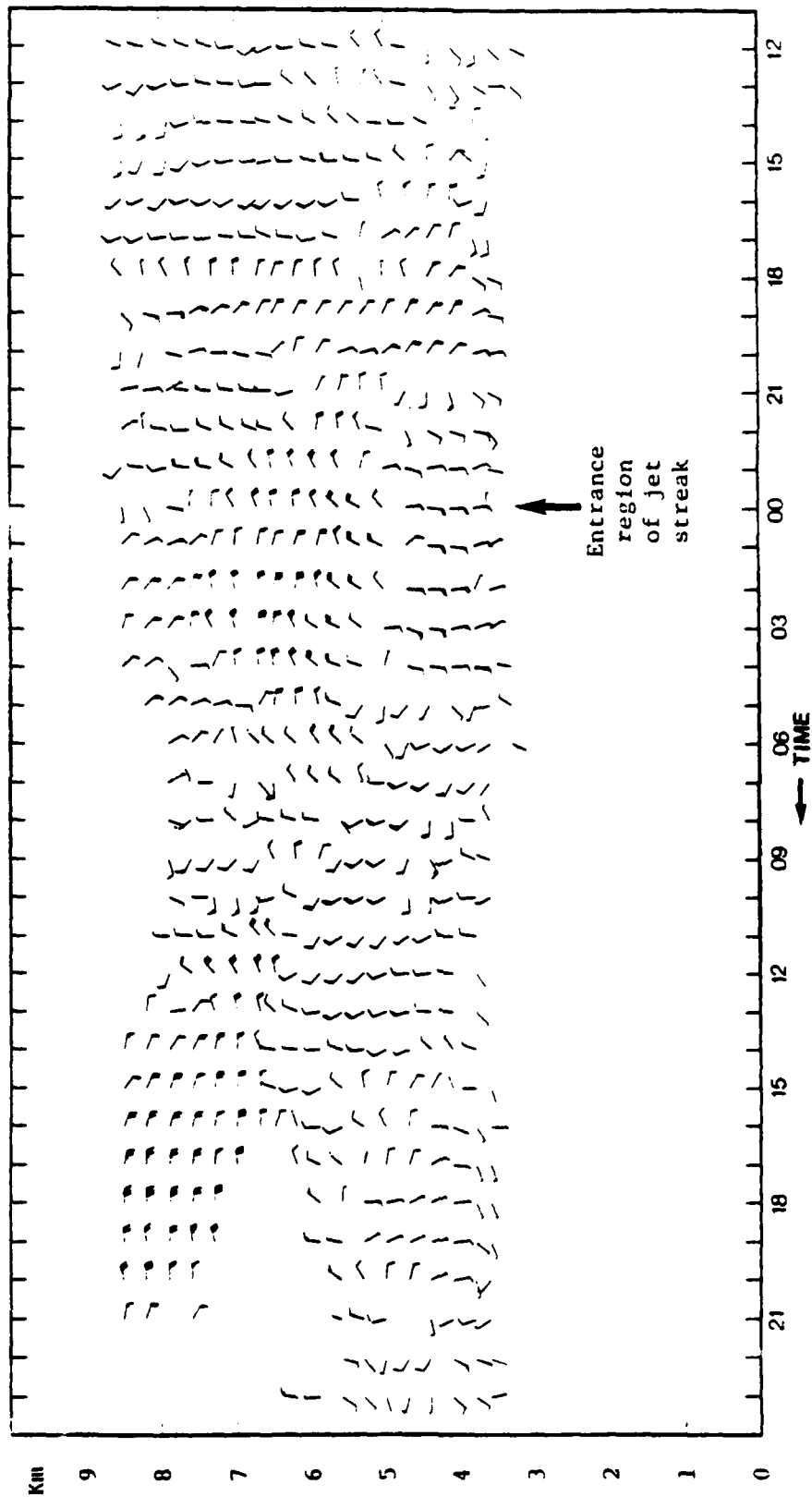


Figure 4.27 Time-height section of the profiler-derived ageostrophic winds during the period from 1200 UT 28 September 1985 to 2300 UT 29 September 1985. Convention as in Fig. 4.2.

They represent the effect of curved flow around the trough, with cyclonically-curved flow being naturally sub-geostrophic.

The profiler-derived relative vorticity field is depicted in Figure 4.28. Below 4 km, the values of relative vorticity remained negative for the entire case. This may reflect a bias at one or more profilers, as discussed later. However, from 1200/28 to 0000/29 and from 0600/29 to 1200/29, the values of relative vorticity became less negative or, in a spatial sense, positive relative vorticity advection (PVA) was occurring. Both these periods preceded the passage of the 700 mb trough and, later in the case, the passage of the weak cyclonic circulation through the profiler triangle. A period of NVA was present between 2000/28 and 0200/29 in the 4 to 5 km layer following the passage of the 700 mb trough.

Three positive relative vorticity maxima were present in the layer between 4 and 6 km, apparently associated with the second short-wave. Maxima of $8 \times 10^{-5} \text{ s}^{-1}$ occurred at 1900/28 near 4.5 km, at 0000/29 near 5.5 km, and at 0400/29 near 6 km. Another maximum of $8 \times 10^{-5} \text{ s}^{-1}$ occurred with the passage of the "head-region" circulation center of the comma-shaped trough, near 4.5 km at 1000/29.

Above 6 km, the values reflected anticyclonic vorticity until 0800/29, when the axis of the southwesterly jet streak moved through the profiler triangle and the upper-air trough began to approach. By 1400/29, the profiler triangle had cyclonic relative vorticity at all levels above 3.5 km. A maximum of $20 \times 10^{-5} \text{ s}^{-1}$ occurred at 2000/29 to 2100/29 when the base of the 300 mb trough passed through the profiler triangle. Strong PVA was present between 0900/29 and 2000/29 prior to the passage of this trough.

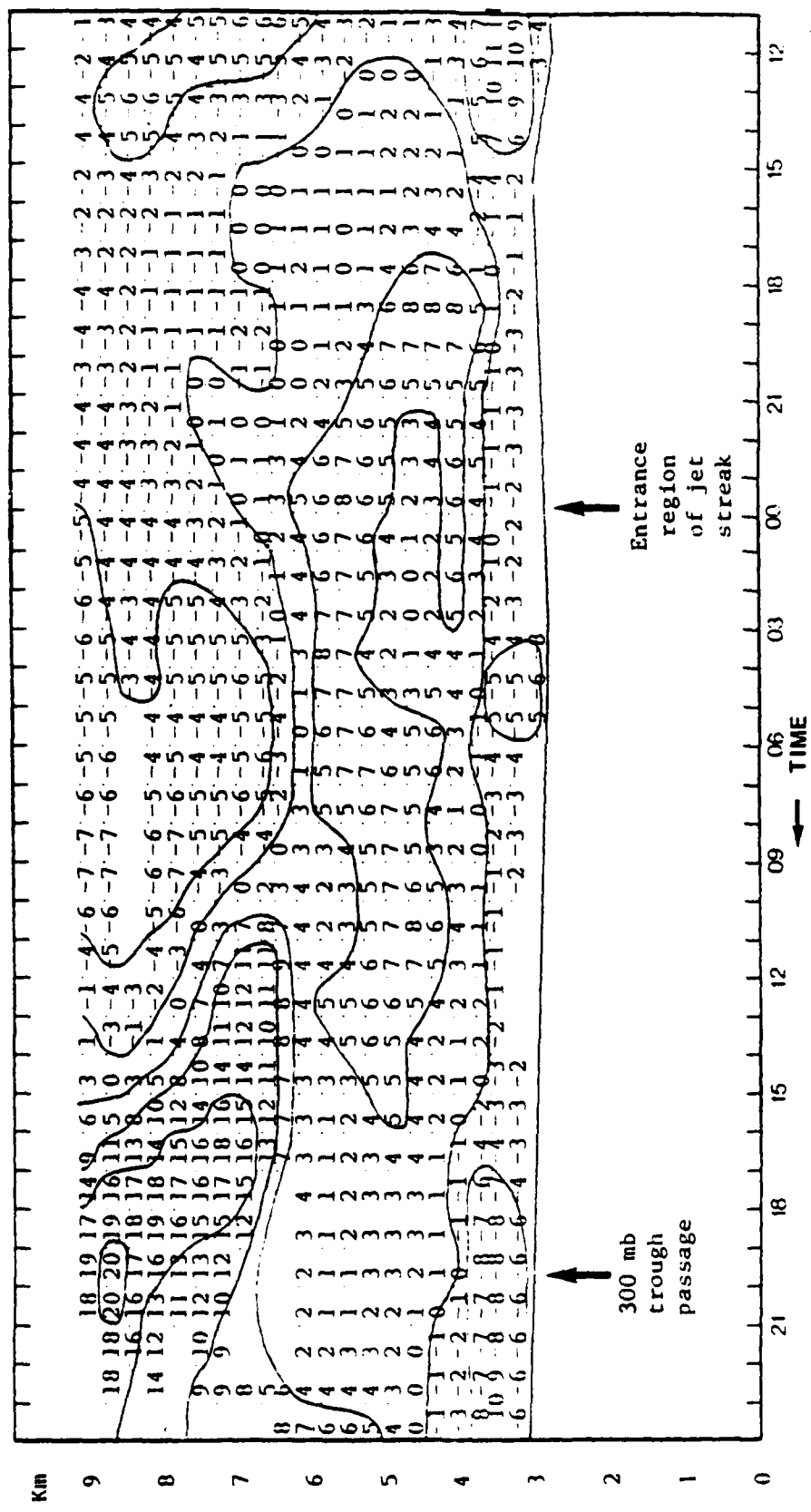


Figure 4.28 Time-height section of the profiler-derived relative vorticity field (units of $1 \times 10^{-5} \text{ s}^{-1}$) during the period from 1200 UT 28 September 1985 to 0000 UT 30 September 1985. Convention as in Fig. 4.11.

The profiler-derived divergence field is depicted in Fig. 4.29. The most striking feature of this diagram is the convergence zone sloping with height to about 6 km, beginning at 1600/28 near 3.5 km. This convergence zone was related to the synoptic-scale cold front of the second short-wave trough which passed through the profiler triangle. The convergence zone was strongest at 4 to 5 km about 0100 to 0200/29. After 0400/29, a period of divergence developed from 3 to 5 km when the low-level winds backed to the southwest. An enhanced area of convergence developed around 0800/29, when the 700 mb cyclonic circulation center of the second short-wave trough was present north of the triangle.

The profiler-derived vorticity and divergence time sections showed that the low-level trough and cold front were not easily connected to the mid- and upper-level trough and front. A break occurred near 5 to 6.5 km. This would not have been easily detected with the rawinsonde data. The 500 mb maps indicated that a front passed through Denver between 0000/29 and 1200/29, as the temperature at 500 mb dropped 7°C and the dewpoint depression decreased by 29°C. The cross-section of potential temperature, in Fig. 4.16a, showed an upper-level front approaching Denver at 0000/29. By 1200/29, the upper-level front had passed Denver up to the 400 mb level. From 400 mb to 300 mb, the cold front appeared to tilt back toward Salt Lake City, Utah. The cold front finally passed Denver at all levels by 0000/30, as indicated in Fig. 4.16c.

The profiler-derived vertical velocities are shown in Fig. 4.30. For the first six hours of the case, subsidence was occurring from 2 to 9 km. However, the near-surface vertical velocities were upward

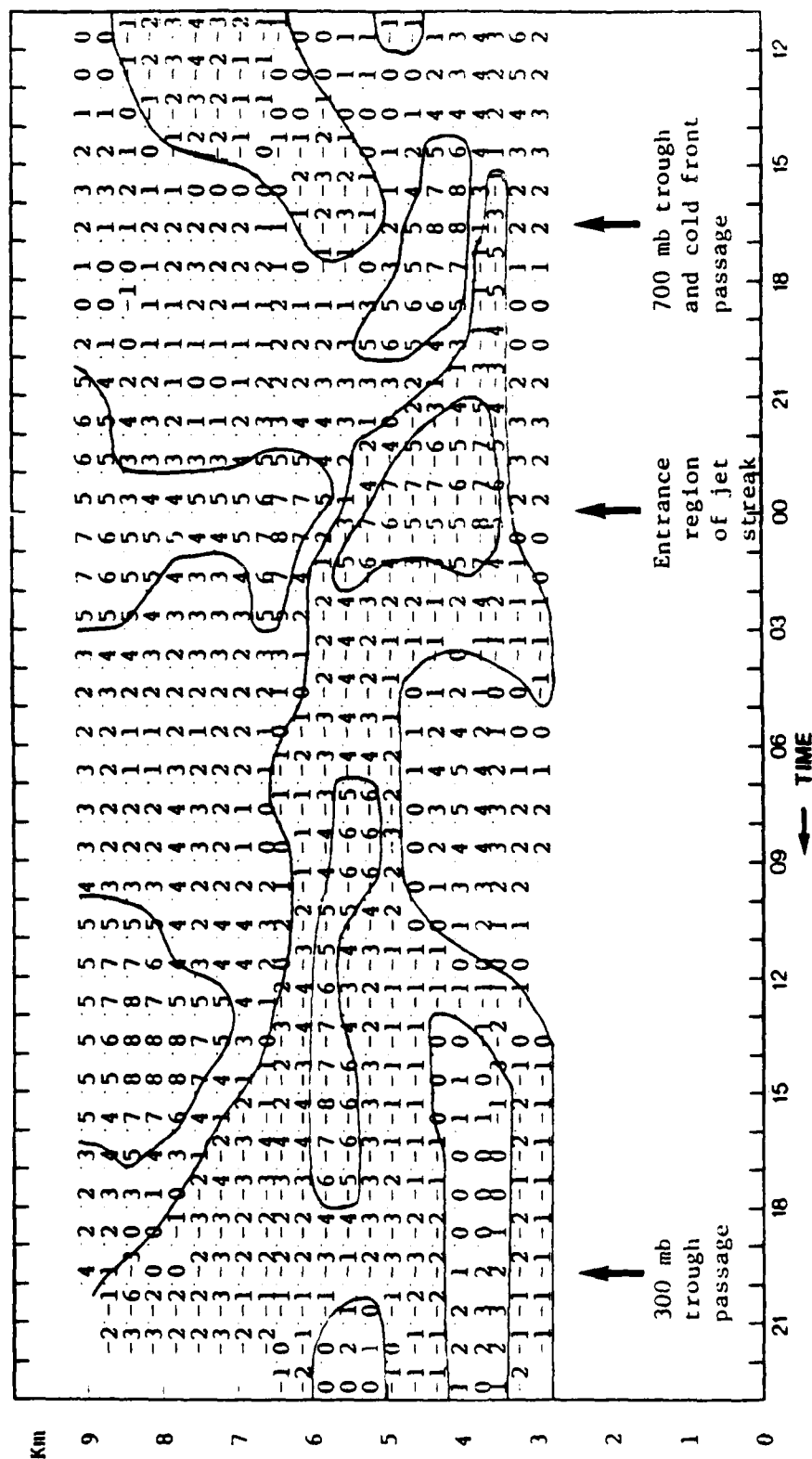


Figure 4.29 Time-height section of profiler-derived horizontal divergence (units of $1 \times 10^{-5} \text{ s}^{-1}$) during the period from 1200 UT 28 September 1985 to 0000 UT 30 September 1985. Convention as in Fig. 4.12.

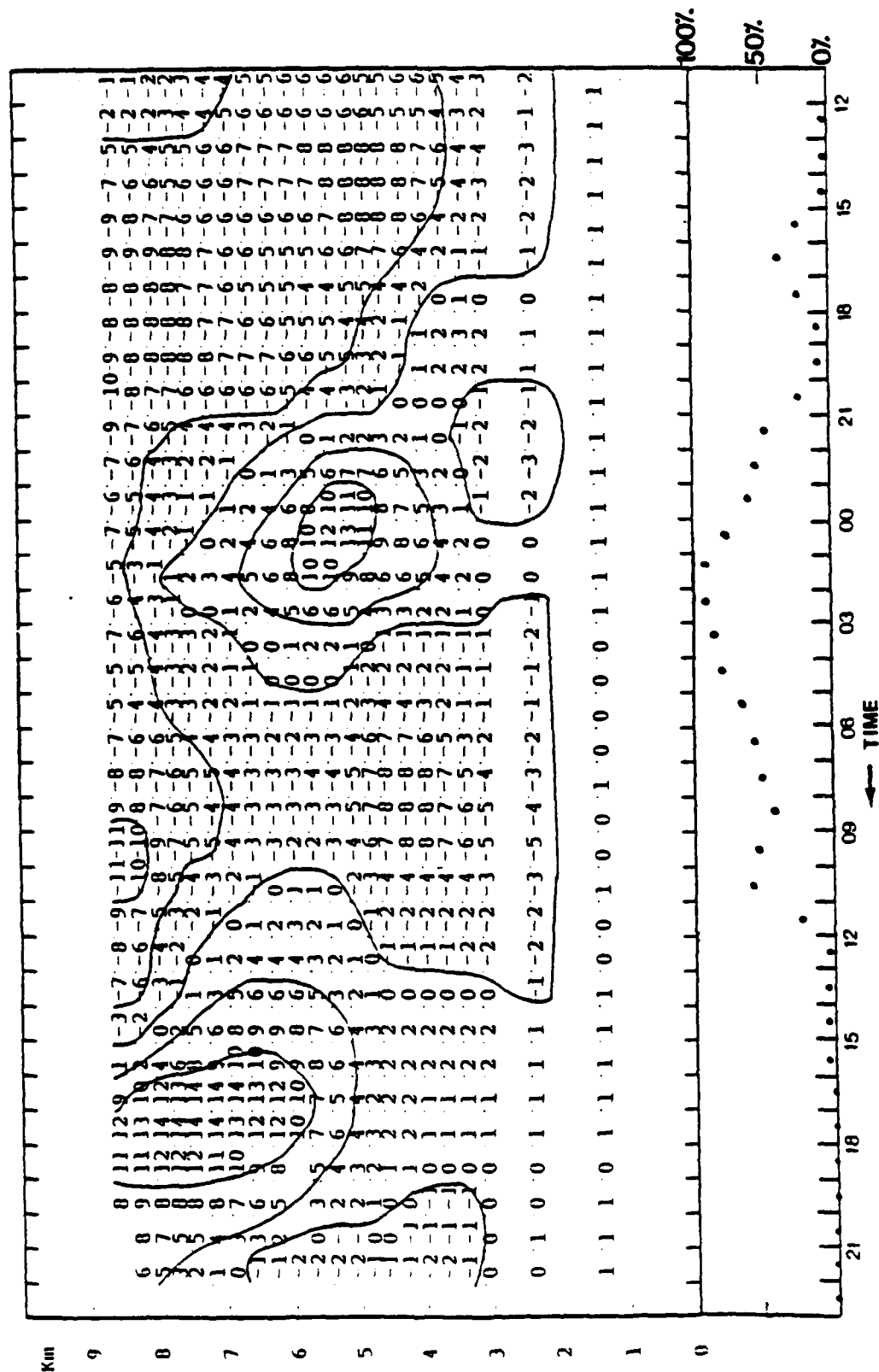


Figure 4.30 Time-height section of the profiler-derived kinematic vertical velocities (cm/s) during the period from 1200 UT 28 September 1985 to 2200 UT 29 September 1985, and a plot of the percent areal coverage of the profiler triangle by the precipitation echo. Convention as in Fig. 4.14.

for this time period due to the easterly surface winds moving up the mountain slopes. The Limon radar indicated that small precipitation echoes were present in the profiler triangle during this time period. A maximum coverage of 30% occurred at 1530/28. The Denver sounding, in Fig. 4.31a, showed a moist layer from 825 mb to 680 mb. An inversion was evident above the moist layer, which is typically present above the dome of cold air in cold air damming events.

During the time period from 1800/28 to 0400/29, associated with the low-level trough and upper-level southwesterly jet streak, the vertical motions were upward, except above 8 km. A maximum vertical velocity of 13 cm/s occurred near 5 km at 0000/29. At this time, Denver's surface station was reporting moderate to heavy snow with one-quarter of a mile visibility. The percentage of areal coverage of the precipitation echo in the profiler triangle was 95% at 0030/29. The Denver sounding, in Fig. 4.31b, indicated that the atmosphere had become more moist above 700 mb, and was now nearly saturated throughout the troposphere.

The upward motions, which were occurring during this time period, were partially forced by the warm, and moist southwesterly flow, above 5 km, overrunning the low-level cold dome and by the upward vertical circulation in the right entrance region of the southwesterly jet streak. The passage of the 700 mb cold front helped to maintain the cold dome at low levels. The transverse (direct) circulation helped to enhance the convergence at low levels and the divergence at upper levels which in turn enabled the already present rising motions to become stronger. Strong ageostrophic winds were present

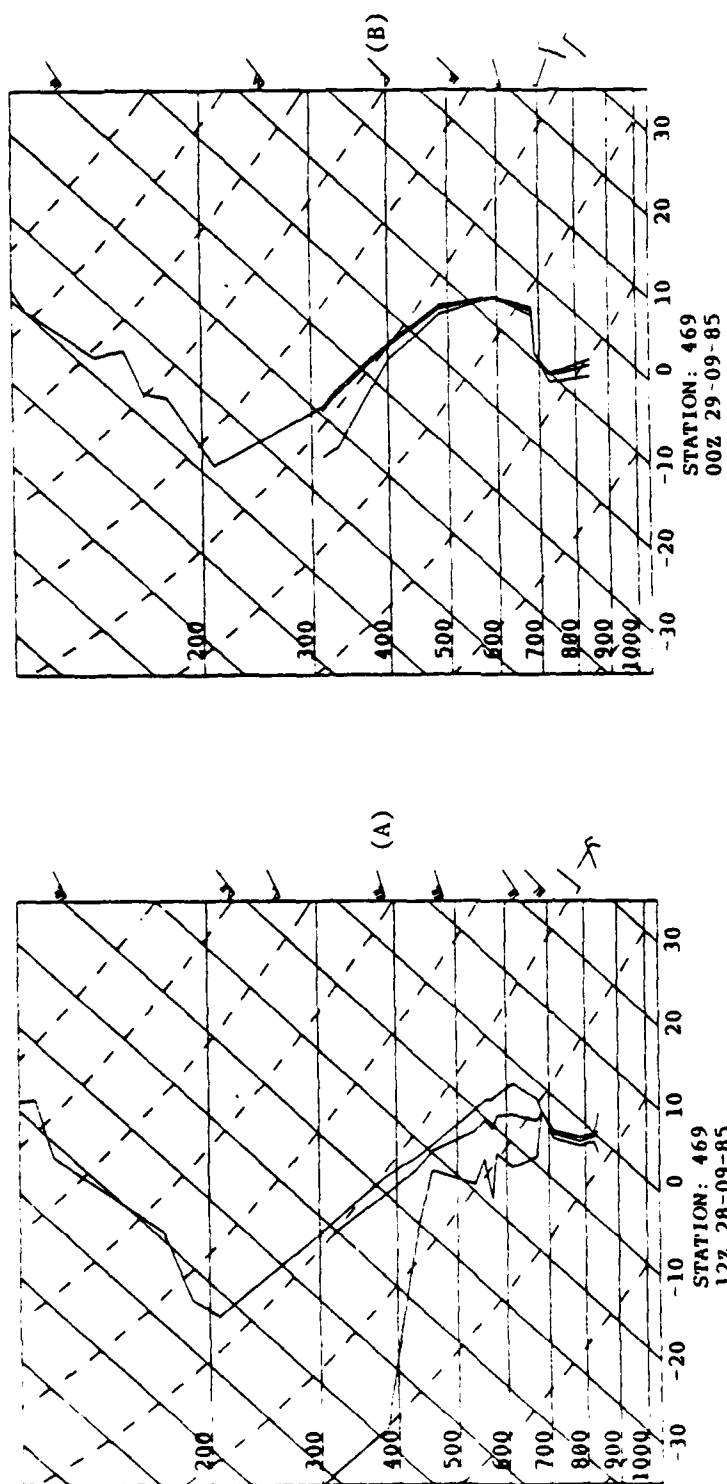


Figure 4.31 Skew-T log-P diagrams from Denver, Co. Convention as in Fig. 4.15. (A) 1200 UT 28 September 1985, (B) 0000 UT 29 September 1985, and (C) 1200 UT 29 September 1985.

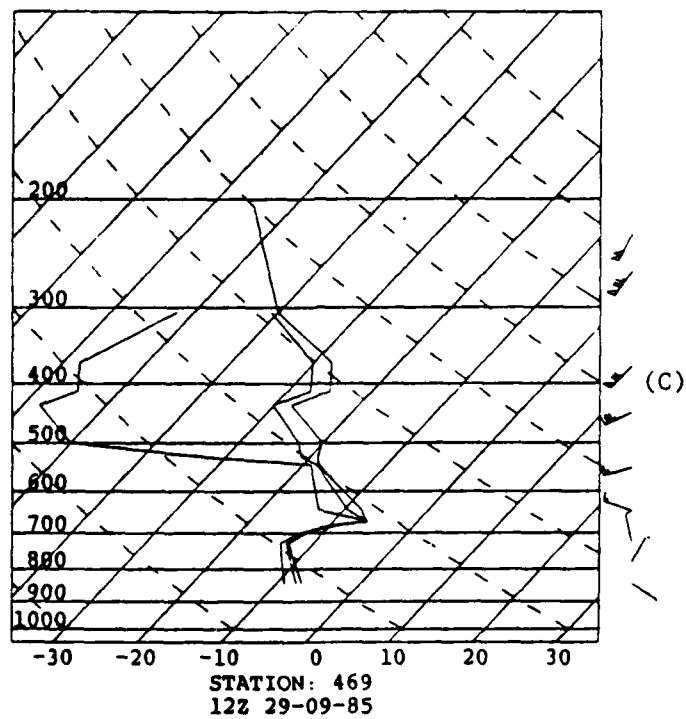


Figure 4.31 (C)

above 5 km, as seen in Fig. 4.27, during the period of rising motions. The influence of PVA was negligible during this time.

Subsidence began after 0500/29 and continued until 1300/29, while the core and left entrance region of the southwesterly jet streak were overhead. Precipitation echoes over the profiler triangle steadily decreased in areal coverage and dropped quickly from 65% at 1030/29 to 20% at 1130/29. The Denver sounding at 1200/29, in Fig. 4.31c, indicated that dry advection and subsidence drying behind the 500 mb cold front were occurring. The low-level moist layer was still present at this time, along with the inversion above the cold dome.

Between 1400/29 and 2200/29, strong rising motions were present above 6 km. Strong PVA, which preceded the passage of the 300 mb trough, was present during this time period. However, the Limon radar indicated that precipitation was not occurring as a result of these rising motions. The Denver soundings at both 1200/29 and 0000/30 showed that the atmosphere was dry in the upper levels and was in the process of drying out (by advection) in the low levels by 0000/30.

In summary, while the near-surface upslope flow provided low-level humidity and upward motion almost continually throughout the case, precipitation was heavy only when a deep layer of the troposphere became involved in the precipitation generation. Specifically, the convergence accompanying a low-level trough/front passage and the ageostrophic circulation in the right entrance region of a southwesterly jet streak provided deep-layer upward motions during the

period of heaviest and most extensive snowfall. Comparable subsequent vertical velocities in dry air did not produce precipitation.

4.3 Case of October 22-23, 1985

This case will investigate four synoptic-scale features which passed through or entered the profiler triangle between 1200 UT on 22 October 1985 and 1200 UT on 23 October 1985. The features of interest are a cold front, a short-wave trough, and two jet streaks. A feature-by-feature discussion will follow in the succeeding paragraphs.

At 1200/22, a surface cold front extending from Saskatchewan, Canada to Arizona moved eastward toward the profiler triangle. The cold front, which was occluded north of the Wyoming-Montana border, entered the profiler triangle between 1500/22 and 1800/22 and had passed through the profiler triangle by 1800/22. The cold frontal passage did not produce precipitation in the profiler triangle, and it did not affect the surface temperatures at the stations surrounding the triangle, as the temperatures remained constant or increased as the cold front passed. However, the dewpoint temperatures dropped approximately 5°C, and the surface winds veered to the northwest after the cold front passed. The surface winds were downslope (northwesterly) behind the cold front, hence the cold air may have been adiabatically warmed.

The passage of the cold front was evident aloft. Denver reported a -3°C to 4°C temperature change at all levels in the 700 mb to 300 mb layer between 1200/22 and 0000/23. The cross-section of potential temperature, in Figure 4.32a, showed a strong

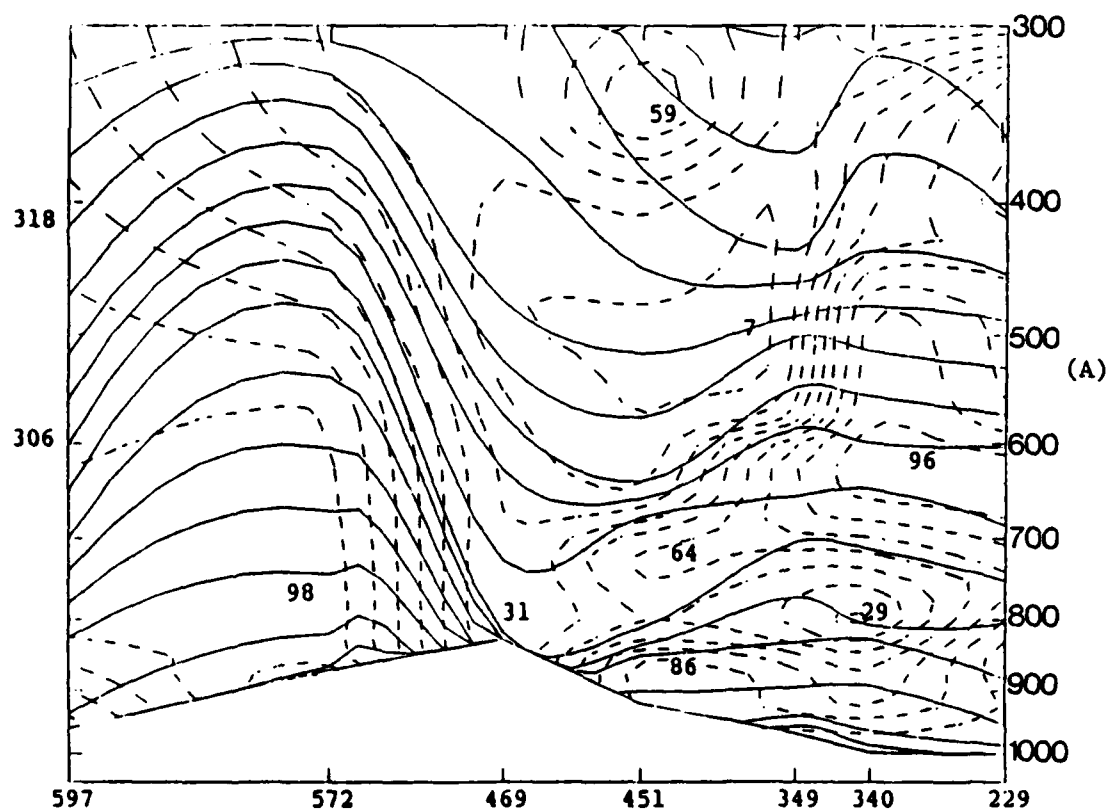


Figure 4.32 WNW-ESE cross-sections of potential temperature (solid lines, K) and relative humidity (dashed lines, %). Observing stations include Medford, Ore. (597), Salt Lake City, Utah (572), Denver, Co. (469), Dodge City, Ka. (451), Monett, Mo. (349), Little Rock, Ark. (340), and Centerville, Al. (229). (A) 1200 UT 22 October 1985, (B) 0000 UT 23 October 1985, and (C) 1200 UT 23 October 1985.

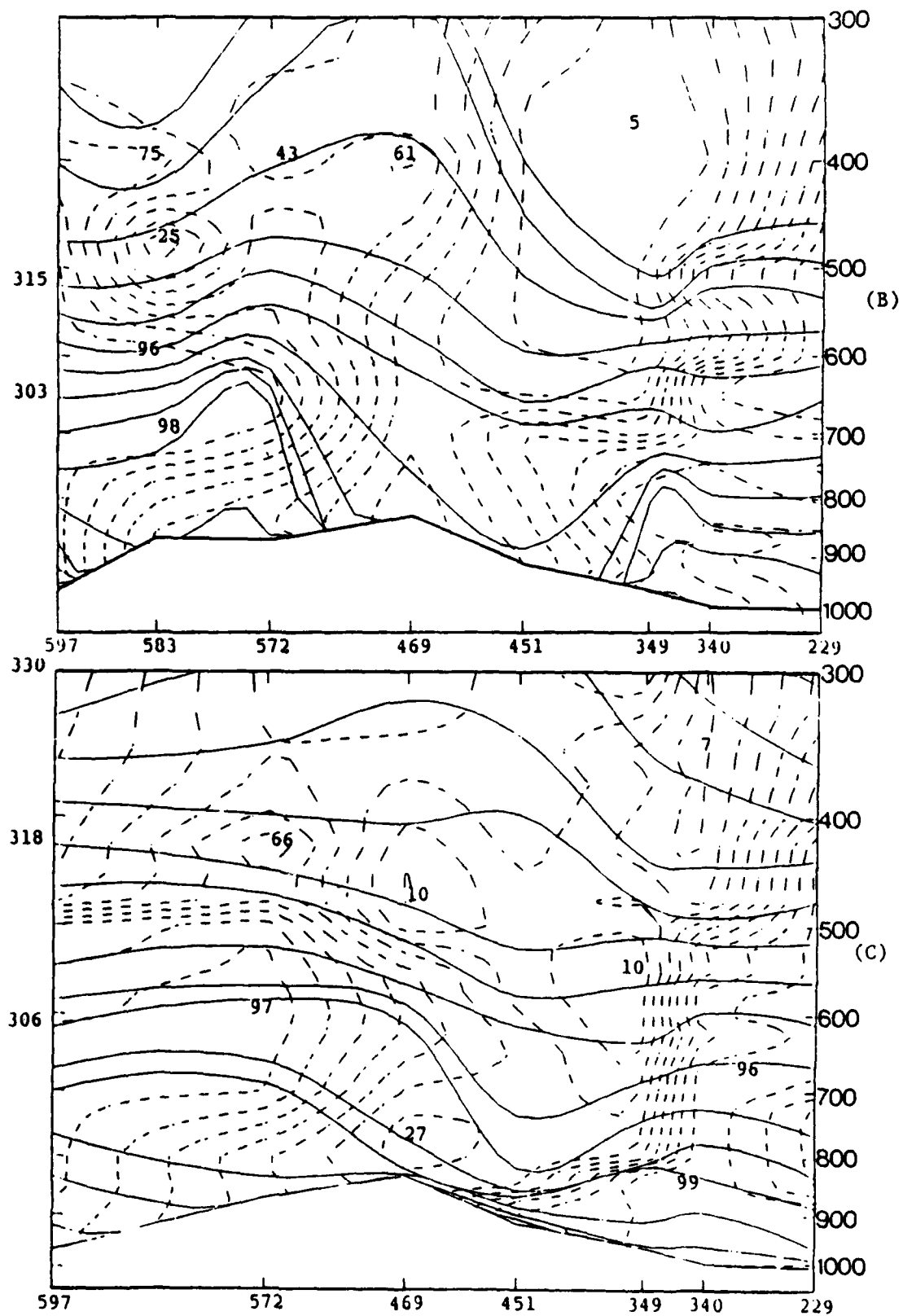


Figure 4.32 (B) and (C)

upper-level front west of Denver at 1200/22. During the previous twelve hours, the cold front had experienced local frontogenesis as a short-wave trough with a cold pocket of air at its base approached the Salt Lake City area. By 0000/23, the cold pocket had moved to the northeast with the rapidly moving short-wave trough. Because the front was moving east, and the cold pocket moved toward the northeast, the cold pocket had a component of movement along the front toward the north. This caused the upper-level cold front to weaken locally in the portion that moved over the Rockies toward Denver. Figures 4.32b and c depict the cross-section of potential temperature for 0000/23 and 1200/23.

A short-wave trough passed through the profiler triangle, "loosely" associated with the upper-level cold front of interest. However, the cooling did not follow the shift of the winds from southwest to northwest. Rather, the cooling occurred while the wind directions remained from the south-southwest ahead of the trough. This is consistent with the cooling due to adiabatic ascent and expansion of unsaturated air, rather than from horizontal advection. A key aspect of this case study was, thus, to see if profiler-derived vertical velocities bear this out.

The 300 mb analysis, in Figure 4.33a, showed a short-wave trough located over Utah at 1200/22. Large 300 mb height falls, from 170 to 190 meters in 12 hours, occurred east of the trough axis over Salt Lake City, Utah, Lander, Wyoming, and Grand Junction, Colorado. These height falls indicated that the short-wave trough had been digging southeastward during the previous twelve hours.

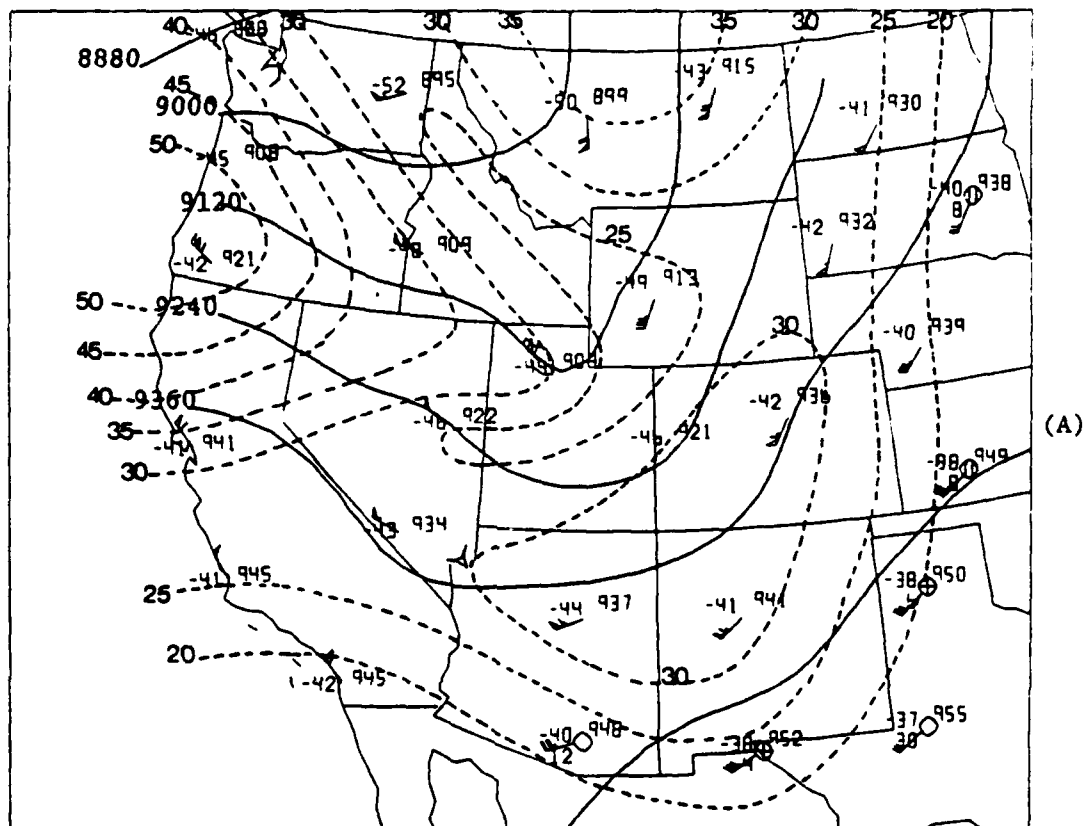


Figure 4.33 300 mb height (solid lines, m) and isotach (dashed lines, m/s) analyses. Contour interval of the height field is 120 m and the contour interval of the wind field is 5 m/s. (A) 1200 UT 22 October 1985, and (B) 0000 UT 23 October 1985.

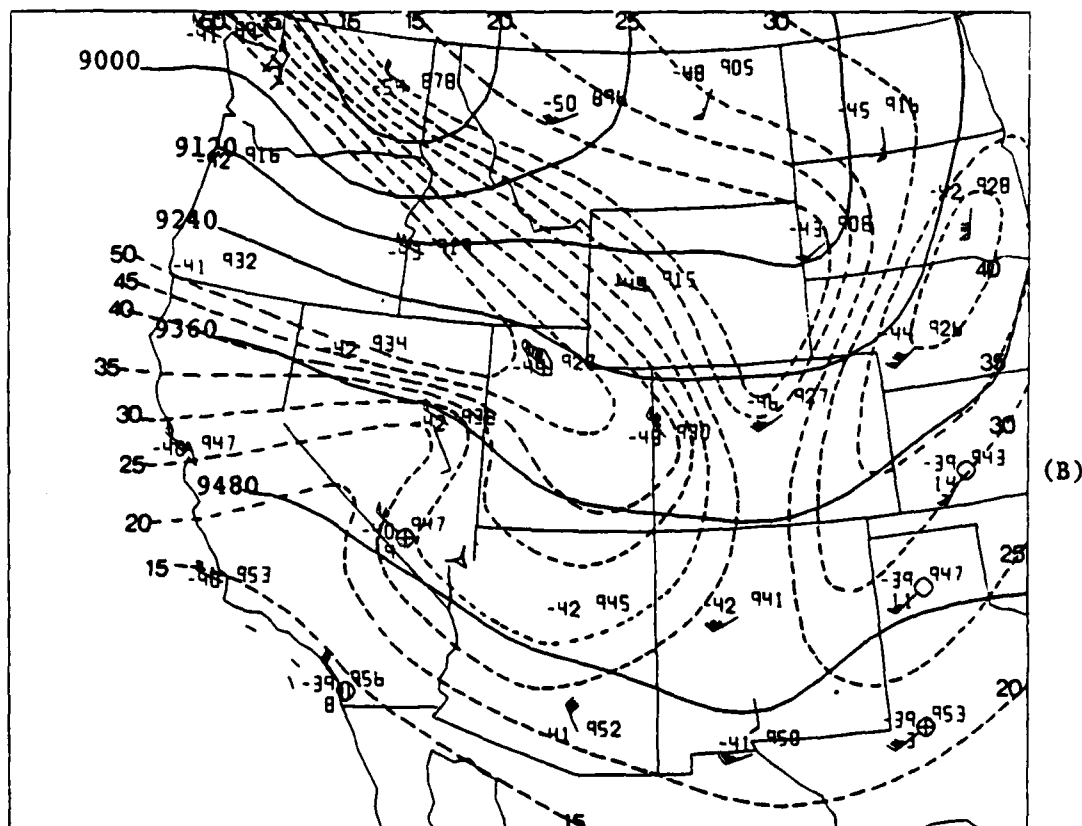


Figure 4.33 (B)

Denver's winds showed a wind shift from southwest to northwest at the 700 mb and 500 mb levels by 0000/23. However, the 300 mb winds at Denver did not shift until after 0000/23. Denver, at this time, reported a 90 m height fall, while Rapid City, South Dakota, reported a 240 m height fall. This large height fall indicated that the trough was now lifting out of Colorado and moving rapidly toward the northeast.

At 3 to 4 km, profiler winds showed a wind shift from southwest to northwest by 1900/22, 2300/22 and 2300/22 for the Platteville, Flagler, and Fleming profiler sites, respectively. The winds shifted in response to the passage of the 700 mb trough axis through the profiler triangle. The 5.6 km Platteville winds shifted to the west at 2000/22, while the 5.6 km Flagler and Fleming winds shifted to the west-northwest 7 hours later, by 0300/23. The wind shift was not always dramatic, and occurred earlier at other levels at some of the stations.

The 500 mb short-wave trough appeared to have slowed down as it passed through the profiler triangle. The 700 mb and 500 mb trough axes passed Platteville at the same time. However, a 3 to 5 hour lag occurred as the trough axes passed over Flagler and Fleming.

Additionally, Platteville had a 3 to 4 hour period of weak northerly-component winds after the passage of the 500 mb trough. This period of weak northerly winds was not evident at either Flagler or Fleming. The 500 mb short-wave trough had turned northeastward over the Rockies. Platteville, which is the profiler closest to the mountains, was close to the trough as it changed course. However, Fleming and Flagler were farther to the east and south, so as the

trough moved northeastward it took the trough axis longer to swing through these stations.

The 300 mb trough axis passed through Platteville at 0000/23, 4 hours after the 500 mb trough axis had passed. The 300 mb trough axis passed Flagler and Fleming at the same time as the 500 mb trough axis. The 300 mb trough had begun lifting out toward the northeast prior to its passage near Platteville.

Each station actually had one previous cyclonic shift at levels above 5 km. The most notable occurred at Platteville between 1400/22 at 6 km and 1700/22 at 9 km. At Fleming, this shift was most easily seen near 8 km between 1900 and 2000/22, and at Flagler, the shift was strongest above 7 km between 1800/22 and 1900/22. This shift may have been confluence related to the upper frontogenesis and jet streak genesis occurring at this time.

As the 300 mb short-wave trough approached the profiler triangle, the synoptic-scale charts indicated that a southerly jet streak began to develop and move over the profiler triangle. Figures 4.33a and b depicted the translation of the jet streak over the profiler triangle. The jet streak intensified between 1200/22 and 0000/23 as the 300 mb short-wave trough turned northeastward and deepened. At 1200/22, the profiler triangle is clearly in the right exit region of the jet streak. It is not quite clear after 1200/22 whether the left exit region of the jet streak ever passed over the profiler triangle. However, by 0000/23 the profiler was located under the left entrance region of the jet streak.

Above 6 km the profiler winds depicted in Figs. 4.34 to 4.36 had a strong southerly component for the time period from 1200/22

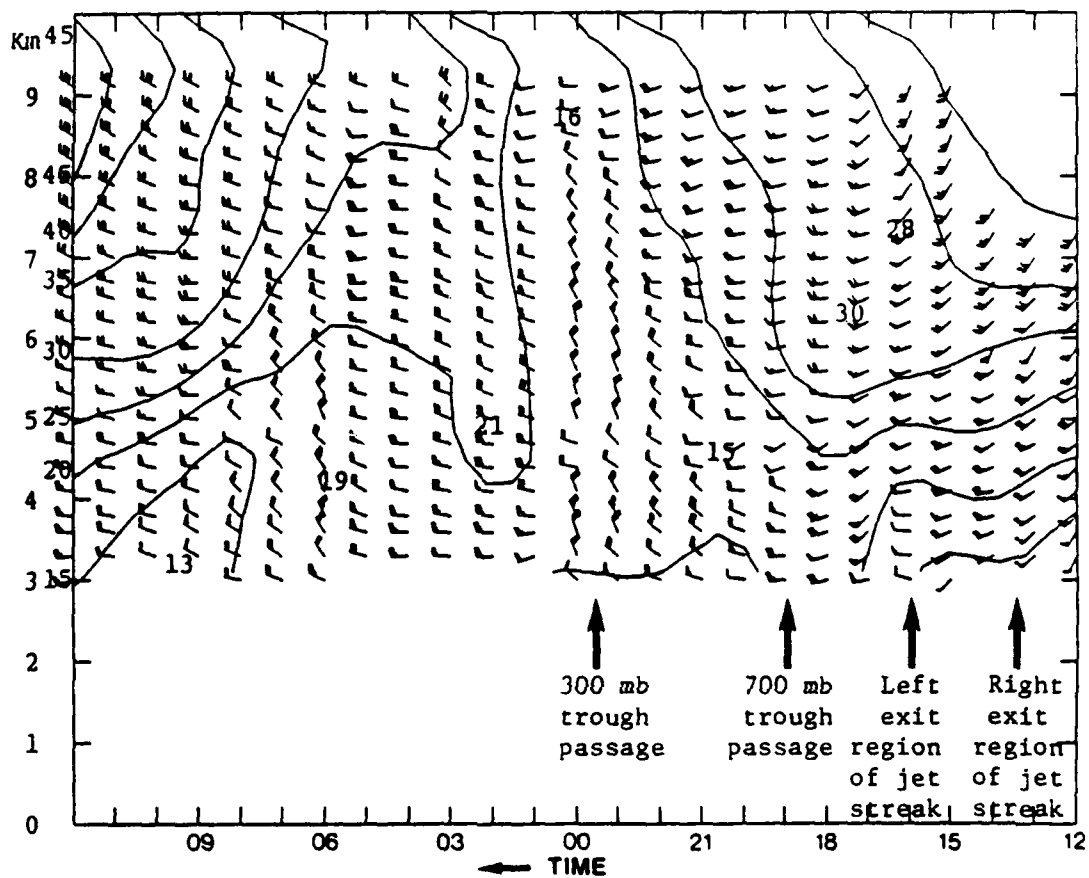


Figure 4.34 Time-height section of the observed winds from the Platteville profiler during the period from 1200 UT 22 October 1985 to 1200 UT 23 October 1985. Convention as in Fig. 4.2.

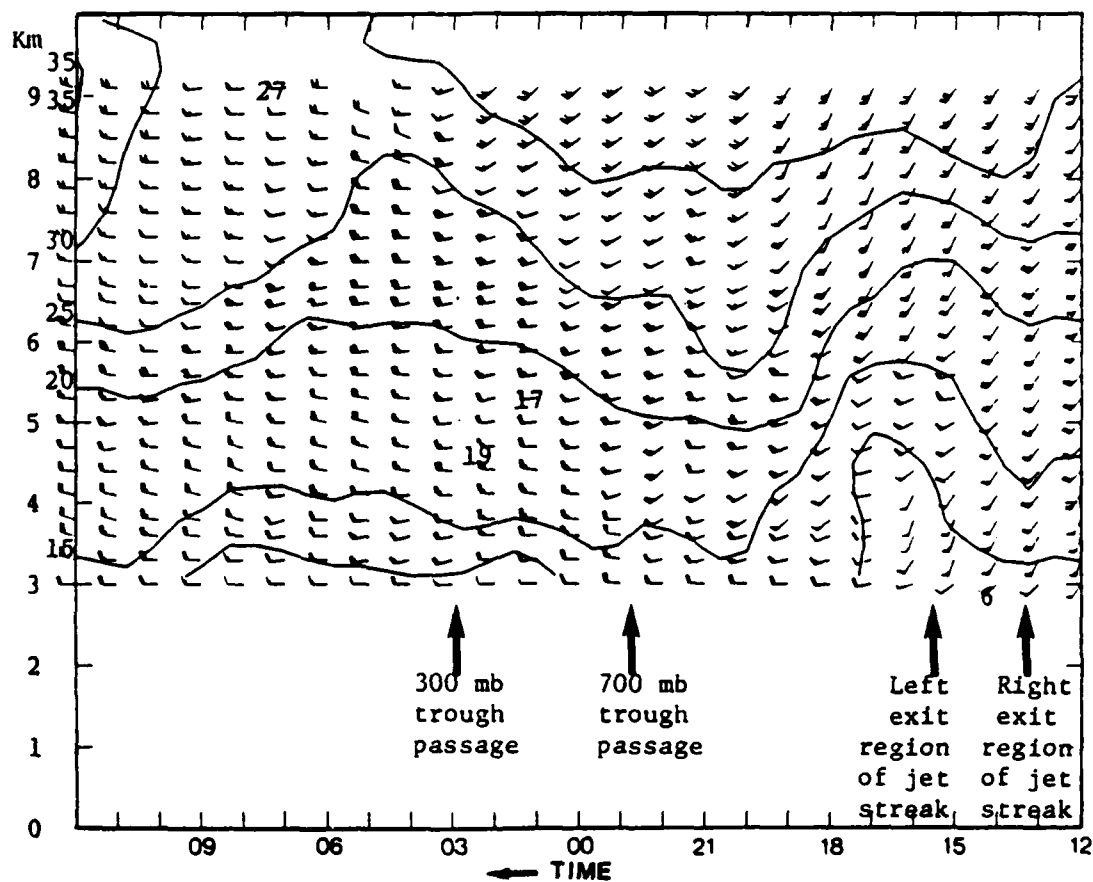


Figure 4.35 Time-height section of the observed winds from the Fleming profiler during the period from 1200 UT 22 October 1985 to 1200 UT 23 October 1985. Convention as in Fig. 4.2.

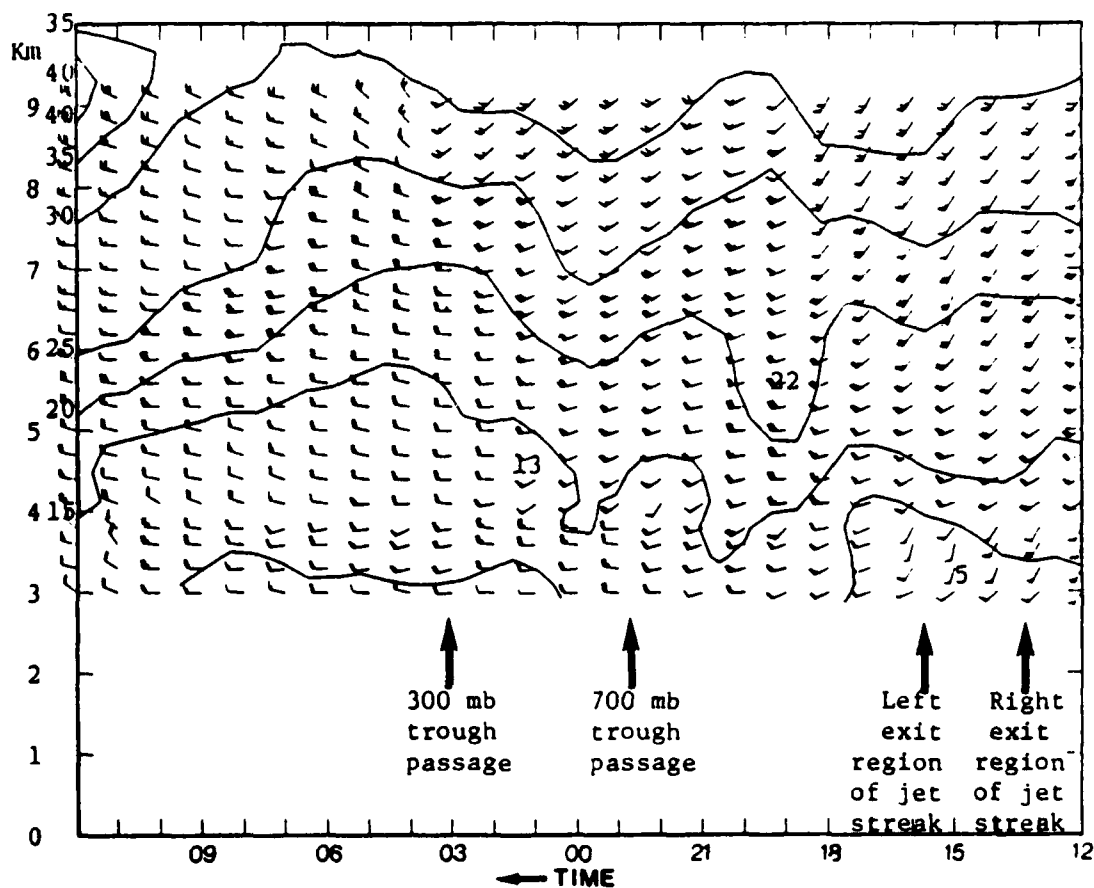


Figure 4.36 Time-height section of the observed winds from the Flagler profiler during the period from 1200 UT 22 October 1985 to 1200 UT 23 October 1985. Convention as in Fig. 4.2.

to 1900/22 at all three sites and were somewhat variable in speed. Unfortunately, the Platteville winds were missing above 7 km for the first three hours. With the early Platteville winds missing, it is difficult to determine when the wind speed peaked at levels above 7.5 km. The 5.5 to 7.5 km winds at Platteville peaked between 1300 and 1500/22, placing the axis of the jet streak over Platteville at that time. Above 5 km the winds also reached a maximum several hours later, after having shifted to a west-southwest direction. The winds above 7 km at Fleming peaked at about 1400/22 from the south-southwest and also at 1800/22. The Fleming winds also peaked from a west-southwest direction in the 5 to 8 km layer at 2000/22, and several levels above 8 km subsequently had minima peaks from a southwest direction. These variations may have been related to waves or other jet stream substructure.

The observed profiler winds do not give any indication of whether or not the left exit region of the jet streak passed over the profiler triangle. However, the ageostrophic winds, which will be discussed later in this section, may offer some information.

After the 300 mb short-wave trough axis passed through the profiler triangle, a northwesterly jet streak entered the profiler triangle. Although the 1200/23 300 mb analysis is not shown due to incompleteness of data, the core of the northwesterly jet streak could be determined to have moved north of the profiler triangle. With this placement, the triangle was located in the right exit region of the northerly jet streak during the time period from 0000/23 and 1200/23.

The 9 km winds at Platteville had a 10 m/s minimum prior to the passage of the 300 mb trough. The 9 km profiler winds at Flagler and Fleming did not show wind speeds this low, as these sites were in the region where the jet streak was intensifying. However, the 0000/23 300 mb isotach analysis showed a wind speed minimum between the two jet streaks, and the profiler time sections also showed a minimum.

After the passage of the 300 mb trough, the profiler wind speeds continued to increase. By 1200/23, the wind speeds were approximately 45, 40, and 35 m/s at Platteville, Flagler, and Fleming, respectively.

The geostrophic winds, relevant at the center of the triangle, are depicted in Fig. 4.37. For this case study, the geostrophic winds were much stronger than the observed winds at the three profiler sites. The observed winds, at all three sites, had a 5 to 6 km wind maximum of 22 to 30 m/s as the southerly jet streak traversed the profiler triangle. The geostrophic winds, at that time, showed a south to southwest 40 m/s maximum in the same layer. Above 8 km, the geostrophic winds exceeded 50 m/s as the southerly jet streak passed, while the observed profiler winds at that level were approximately 40 m/s.

Following the first cyclonic wind shift, the 3.5 to 8.5 km geostrophic winds were very strong during the time period from 2100/22 and 0100/23, and were from a westerly direction. At 0000/23, the geostrophic wind speeds ranged from 20 m/s to 55 m/s, and the observed wind speeds were much lighter ranging from 10 m/s to 35 m/s.

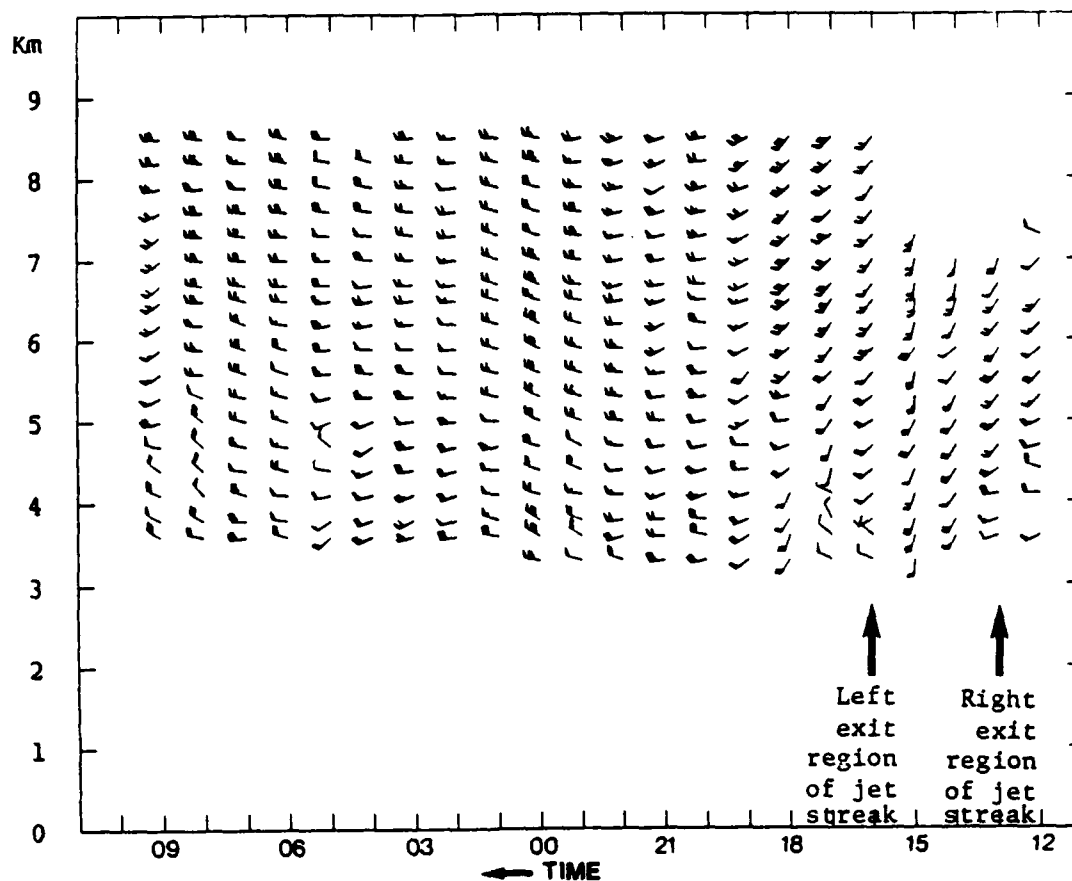


Figure 4.37 Time-height section of profiler-derived geostrophic winds during the period from 1200 UT 22 October 1985 to 0900 UT 23 October 1985. Convention as in Fig. 4.2.

After 0600/23, geostrophic wind speeds above 7 km were as large as 55 m/s, from a westerly direction. Observed wind speeds were not greater than 45 m/s. Strong ageostrophic winds must have been present for such large differences to exist between the geostrophic and observed winds in these periods.

Figure 4.38 depicts the profiler-derived ageostrophic winds for this case. For the first two hours of the case, southeasterly ageostrophic winds were present below 5 km, and northeasterly ageostrophic winds were present up to 7 km. Above 7 km, the ageostrophic winds could not be computed because the Platteville data were missing for the initial three hours of the case. As shown previously, the profiler triangle was at this time in the right exit region of the jet streak. The clockwise transverse circulation present in this exit region of the southwesterly jet streak would produce a southeasterly ageostrophic wind at low levels and a northwesterly ageostrophic wind at upper levels. After 1300/22, a strong upper-level northwesterly ageostrophic wind developed for a period of two hours, which may have indicated the arrival of the left exit region. The low-level ageostrophic winds also backed to the north at this time, suggesting a movement of the jet streak axis and entrance region over the triangle at this time. Thus, the movement of the core of the jet streak remains somewhat uncertain.

At 1600/22, the upper-level ageostrophic winds veered to the northeast, and the low-level ageostrophic winds veered to the south-southeast. These ageostrophic winds gradually shifted to the south-east aloft and to the northwest at low levels by 2000/22. The

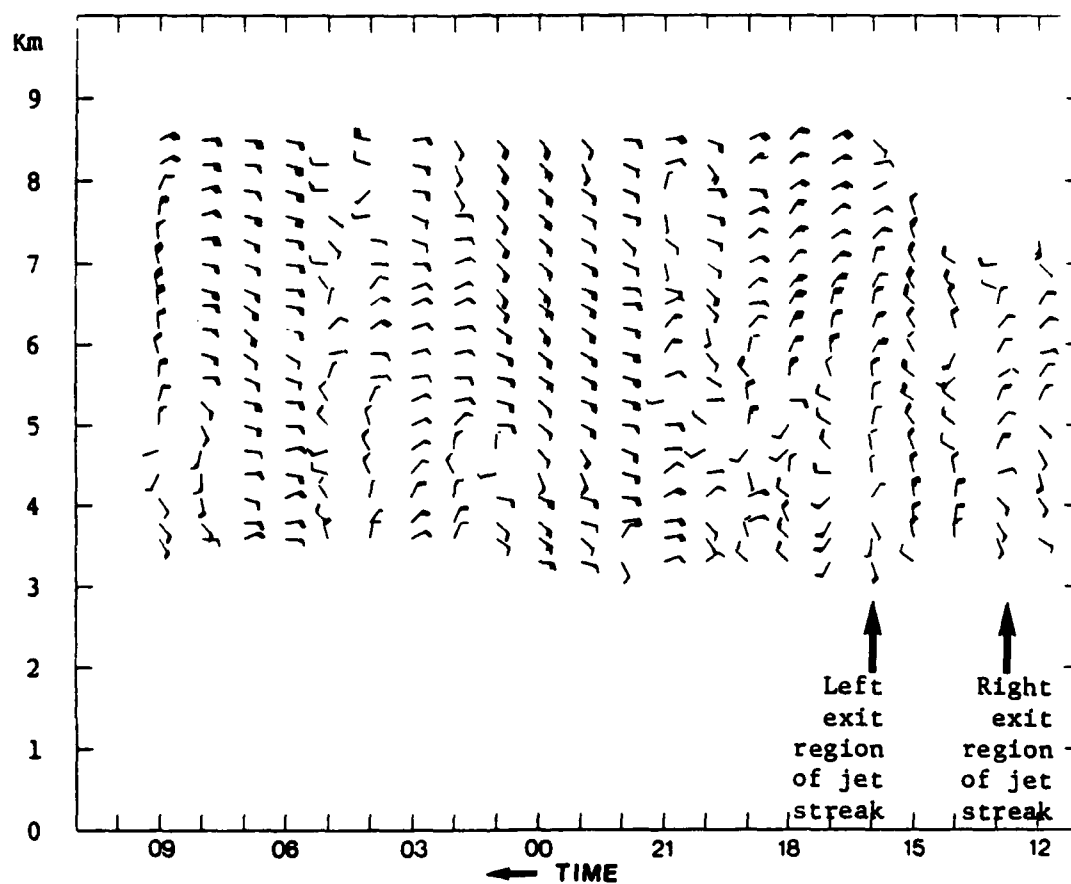


Figure 4.38 Time-height section of the profiler-derived ageostrophic winds during the period from 1200 UT 22 October to 0900 UT 23 October 1985. Convention as in Fig. 4.2.

entrance region of the jet streak may have started to move over the profiler triangle at 1600/22, and was clearly over the profiler triangle by 2000/22. The ageostrophic winds at 2000/22 were consistent with the counter-clockwise circulation and sub-geostrophic winds present in the entrance region of the south-southwesterly jet streak.

Between 2100/22 and about 0300/23, the ageostrophic winds possessed a strong easterly component at all levels. Part of this must be due to the sub-geostrophic winds which occur in a cyclonic flow as the trough axis passed. After about 0300/23 at most levels, the ageostrophic wind speed and direction above 5 km became light and variable for a few hours until the west-northwesterly jet streak entered the profiler triangle.

As the jet streak approached the profiler triangle from the west-northwest, the ageostrophic winds became easterly or east-southeasterly from 3.5 to 8.5 km. These winds remained southeasterly until 0900/23 when the upper-level ageostrophic winds backed to the north and northeast. These ageostrophic winds were partially consistent with the transverse circulation located in the exit region of the west-northwest jet streak, in that there was generally a component of the ageostrophic winds across the jet streak axis from left to right. In contradiction to the jet streak model in straight flow, however, wind speeds in the exit regions were subgeostrophic. This must have been the case because the streak was entering the cyclonically curved trough where curvature effects cause subgeostrophic wind speeds.

The profiler-derived relative vorticity field is depicted in Fig. 4.39. For the first four hours of the case, the relative

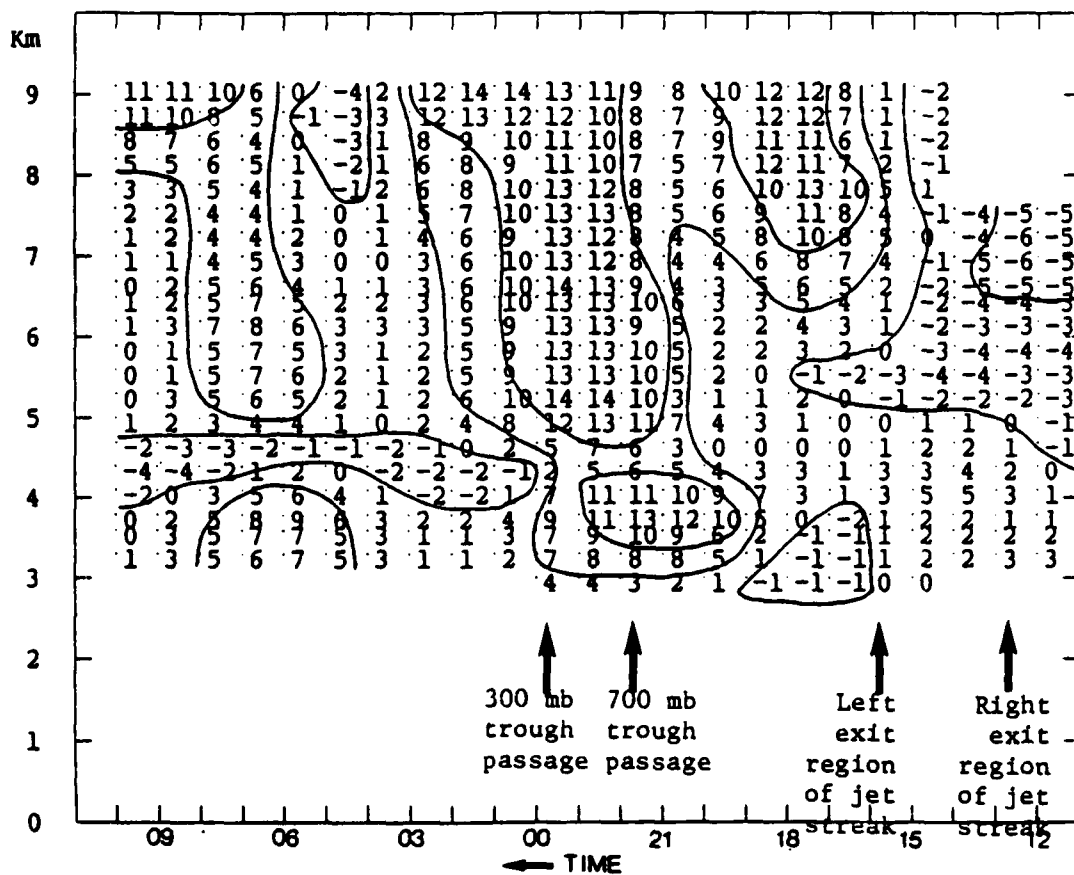


Figure 4.39 Time-height section of the profiler-derived relative vorticity field (units of $1 \times 10^{-5} \text{ s}^{-1}$) during the period from 1200 UT 22 October 1985 to 1000 UT 23 October 1985. Convention as in Fig. 4.11.

vorticity values were negative, which is consistent with the profiler triangle being located on the anticyclonic side of the southerly jet streak. After 1500/22, strong PVA occurred from 3 to 9 km with the exception of three hour period below 4 km. Two positive relative vorticity maxima occurred: one at 1800/22 at 8 km and the other in a broad sloping trough between 2300/22 at 5 km and 0100/23 at 9 km. The first maximum was related to the southerly jet streak as the cyclonic shear side of the jet streak passed over the profiler triangle. This maximum suggested that the left exit region of the jet streak had moved over the profiler triangle after 1500/22. The second maximum was related to the short-wave trough as it passed through the profiler triangle from 3 to 9 km. The relative vorticity pattern indicated that the 700 mb, 500 mb and 300 mb short-wave troughs passed through the profiler triangle at about one hour intervals.

After the passage of the short-wave trough, a period of NVA occurred for five hours. A thin layer of negative relative vorticity appeared at 4.5 km after 0000/23, and was present for the rest of the case. It is not apparent as to why this layer was present.

From 0500/23 to 0800/23, PVA was evident at the 3 to 4 km level and above 5 km. The profiler winds at 3 to 4 km and above 5 km backed to the west or west-southwest during this time period at Fleming and Flagler, after the sharp trough axis had passed. During this same time period, the Platteville profiler winds veered to the northwest as the jet streak approached. The relative vorticity showed an increase at all levels above 5 km at this time.

The upper portion of this increase certainly related to the approach of the left exit region of the west-northwest jet streak. The maximum from 5 to 8 km, however, suggests that there may have been a small trough at the leading edge of the jet streak.

The profiler-derived divergences are depicted in Fig. 4.40. A deep layer of convergence, extending to 8.7 km, was present from 1200/22 to 1900/22. This convergence zone was a result of confluence and speed convergence occurring with the presence of the developing southerly jet streak in the profiler triangle. A maximum value of convergence of $-8 \times 10^{-5} \text{ s}^{-1}$ occurred around the 6 km layer between 1500/22 and 1600/22, which correlated with the wind speed maximum at Platteville. Divergence was present above 8 km after 1900/22, accompanying the trough. At lower levels, the broad "area" of convergence was at least partially due to the approach and passage of the cold front, and its associated pressure trough through the profiler triangle. This convergence zone was present below 5 km until 0700/22.

The vertical velocities, depicted in Fig. 4.41, clearly revealed the circulation associated with the southerly jet streak. For the initial three hours of the period, the upper-level vertical velocities could not be computed because Platteville winds were missing. However, the low level vertical velocities indicated that weak downward motions were occurring in association with the direct circulation in the right exit region of the jet streak. After 1400/22, strong rising motions were present above 5 km for a four-hour period. The profiler triangle must have been located beneath the left exit region of the jet streak at this time.

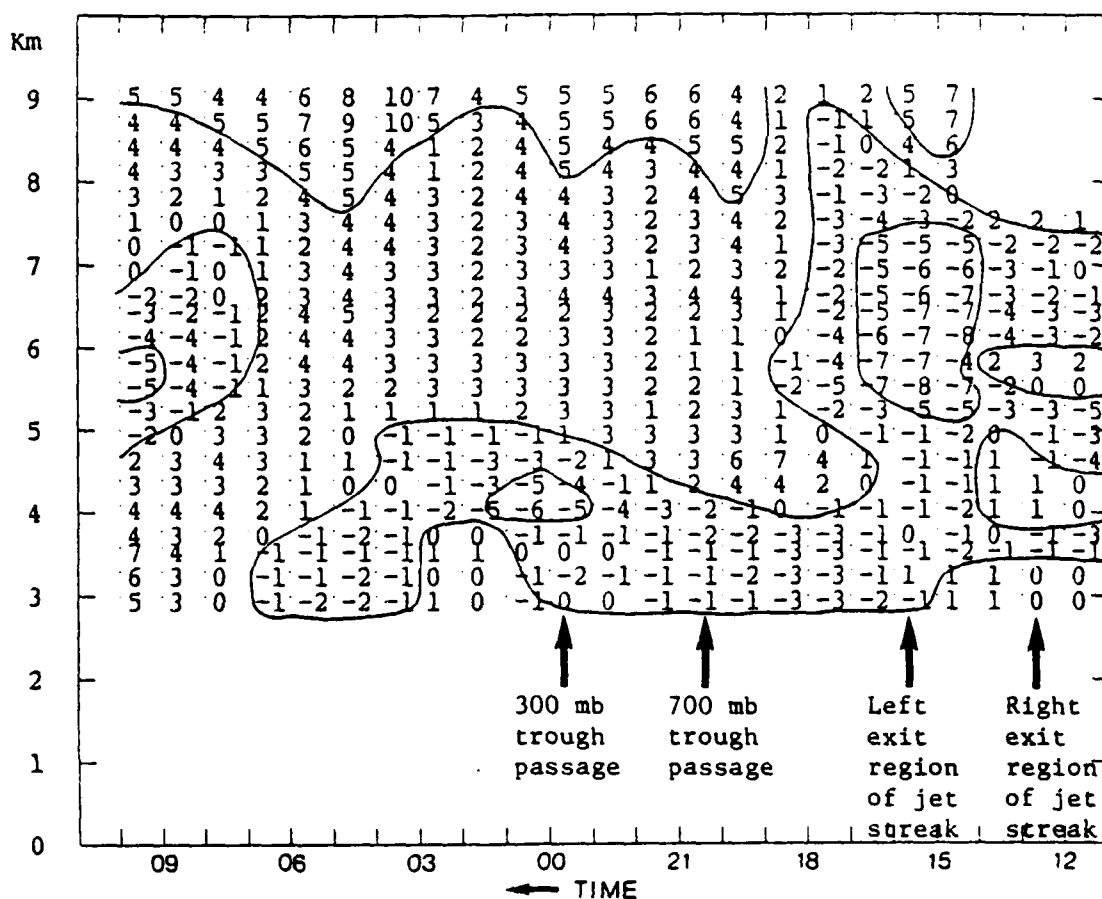


Figure 4.40 Time-height section of the profiler-derived horizontal divergence (units of $1 \times 10^{-5} \text{ s}^{-1}$) during the period from 1200 UT 22 October 1985 to 1000 UT 23 October 1985. Convention as in Fig. 4.12.

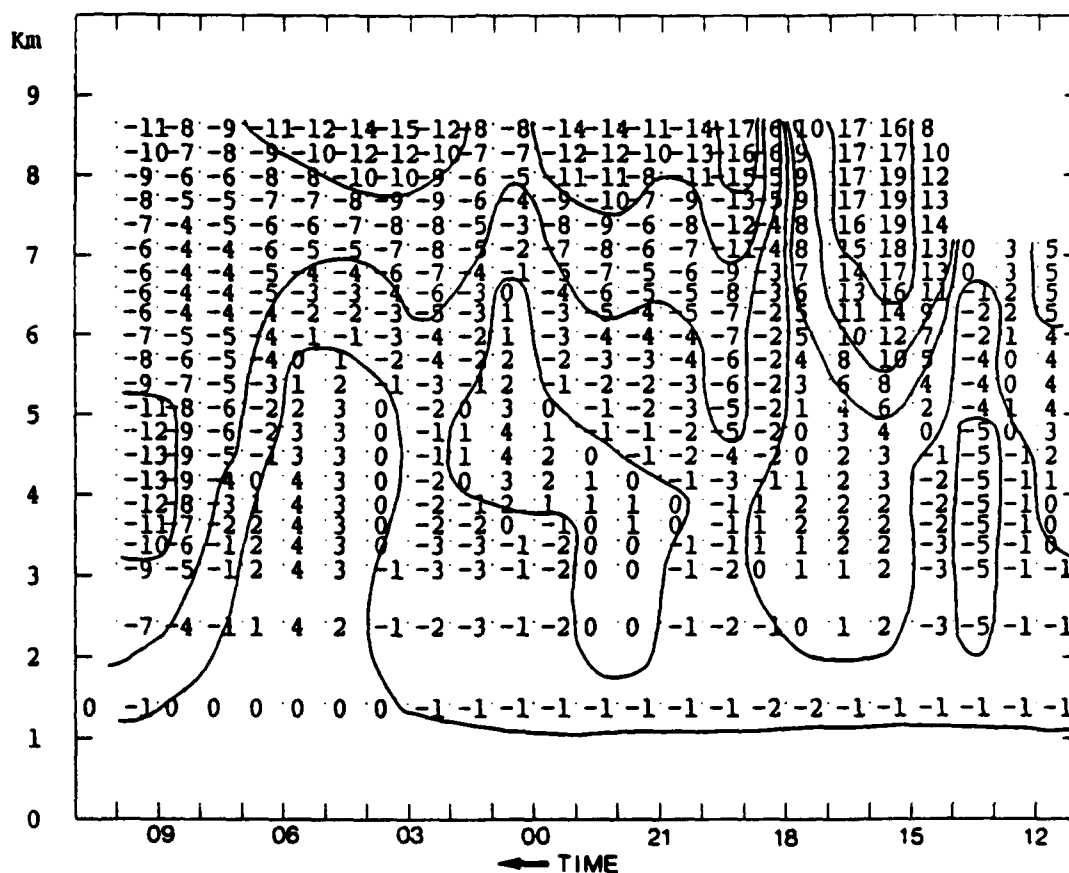


Figure 4.41 Time-height section of the profiler-derived kinematic vertical velocities (cm/s) during the period from 1200 UT 22 October 1985 to 1000 UT 23 October 1985. Convention as in Fig. 4.14.

Between 1800/22 and 1900/22, the vertical velocities abruptly changed sign from strong positive (upward) to strong negative (downward). By 2000/22, a maximum value of sinking motion of -17 cm/s occurred at 8.7 km. This sudden change was related to the movement of the jet streak, such that the triangle went from being beneath the left exit region to below the left entrance region of the jet streak.

Strong sinking motions prevailed for the remainder of the case, except for two periods of weak rising motion. The first period of weak rising motions occurred between 2100/22 and 0200/23 in association with the passage of the short-wave trough. The second period occurred between 0500/23 and 0700/23. This upward motion may have been forced by the small trough feature which the vorticity field suggested was occurring on the leading edge of the west-northwest jet streak.

The 1200/22 thermodynamic sounding at Denver, in Fig. 4.42a, indicated that the atmosphere was extremely dry at all levels, and the Limon radar indicated that precipitation echoes were not present over the profiler network during this period of upward motion. The thermodynamic soundings for Denver at 0000/23 and 1200/23, in Figs. 4.42b and c, indicated that the atmosphere remained dry, with an exception of a small layer around 400 mb at 0000/23. This is consistent with the lack of low-level southerlies which would supply Gulf of Mexico moisture.

As a final bit of analysis, we return to the question of the cooling ahead of the trough axis, between the axis of the jet streak and the upper-air trough axis. It cannot be proved, since

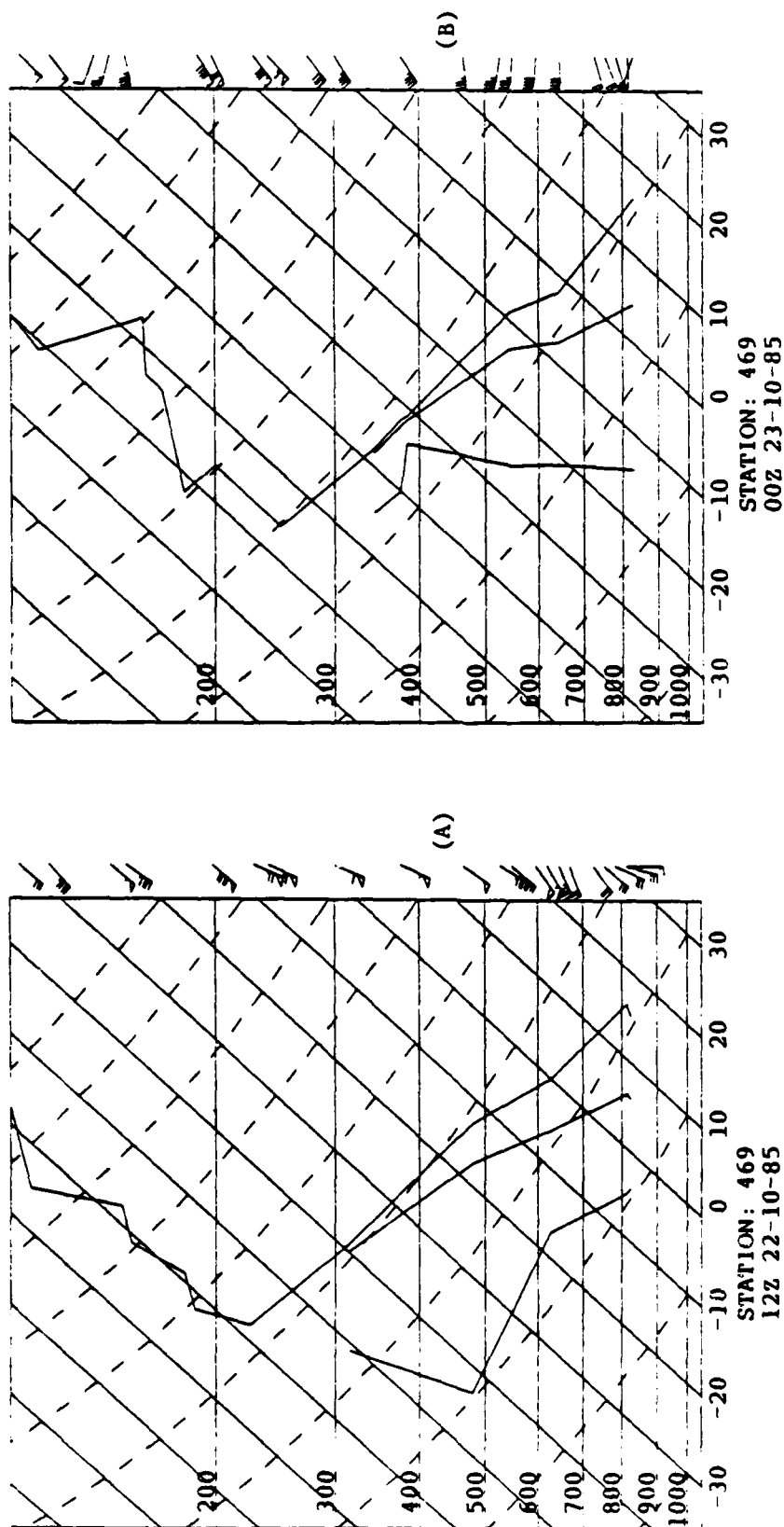


Figure 4.42 Skew-T log-P diagrams from Denver Co. Convention as in Fig. 4.15. (A) 1200 UT 22 October 1985, (B) 0000 UT 23 October 1985, and (C) 1200 UT 23 October 1985.

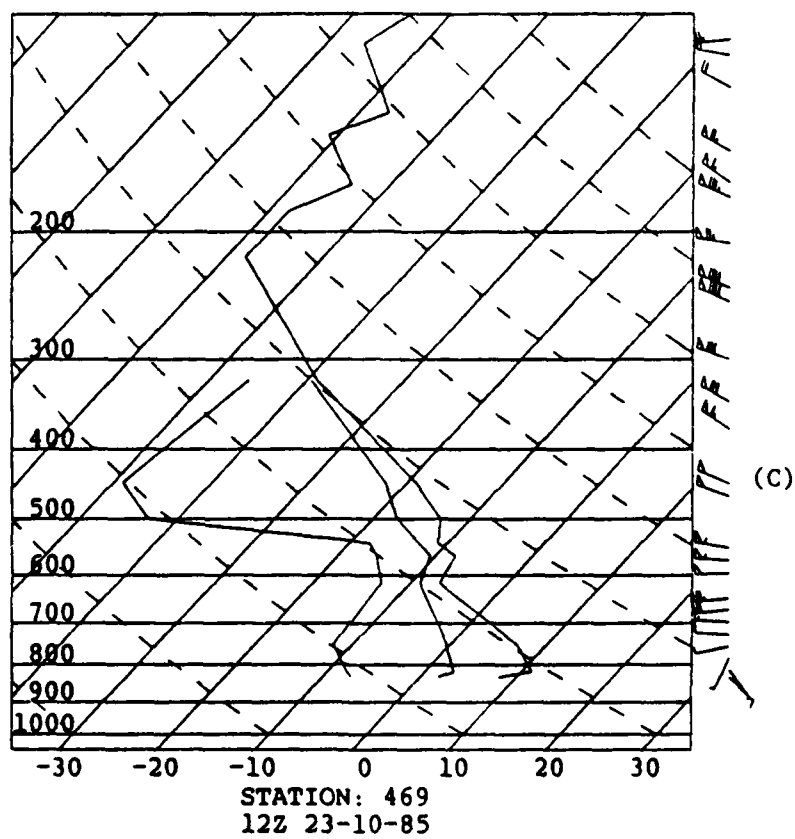


Figure 4.42 (C)

high-temporal and spatial resolution temperature data were not available, but it would appear that two processes may have contributed. Both were related to the developing jet streak. First, there was a deep layer of upward motion in the left exit region of the streak, especially strong aloft. Since the air was dry, rapid cooling would result. Second, during the period when subsidence occurred in the left entrance region, winds had shifted to west-southwest in the confluence of the entrance region. Horizontal cold advection accompanying this wind shift may have prevented the subsidence from "destroying" all of the cold air previously created in the ascent.

CHAPTER 5

SUMMARY AND CONCLUSIONS

5.1 Assessment of Quality of the Derived Kinematic Quantities

Using a triangle of Doppler radar wind profilers, a variety of kinematic quantities were computed in order to investigate the synoptic-scale and mesoscale structure of jet streams, fronts, and synoptic-scale troughs. Hourly high-resolution data from the Fleming, Platteville, and Flagler systems of the Colorado wind profiler network were used. Any "bad" horizontal winds were eliminated if their consensus numbers in either beam were less than seven. A linear interpolation was implemented if one or two consecutive data points were missing. A 1-3-5-3-1 low pass filter was then applied to the time varying horizontal winds. No vertical smoothing was performed.

Horizontal divergence and relative vorticity were calculated using both a line integral method and a finite differencing technique. These techniques were found to give virtually identical results. However, the finite differencing technique was easier to generalize for use with other triangles.

The relative vorticity field revealed a strong bias toward negative values in the lowest three to four range gates of the profiler data. Positive relative vorticity was only rarely indicated. Orographic factors and detection of ground clutter may have contributed to this bias. One symptom of the problem was that the Platteville (northwest station) winds had a tendency to be much stronger than either of the other two sites, due possibly to channelling effects by the Rockies. When using the line integral method, a westerly

component at both Fleming and Platteville produced a clockwise (anticyclonic) component along the side of the triangle defined by the two sites. For the three cases, the wind direction at Fleming and Platteville was typically from the southwest or northwest, and the wind speeds were much stronger at Platteville and Fleming than at the Flagler. Another symptom was that the Flagler (southeast station) winds in the lowest four gates were light for all three cases when meteorological conditions indicated otherwise. Ground clutter probably contaminated the lowest gates which then caused the wind speeds to appear lighter than were really present.

The finite differencing technique for calculating relative vorticity was sensitive to the large negative gradient of the v component of the wind in the x direction resulting from the difference in the wind speeds between Flagler and Platteville, and to the large positive gradient of u in the y direction resulting from the difference in the wind speeds between Flagler and the two northern stations. The orientation of the triangle plus the speed differential contributed to the negative bias in the line integral method.

Vertical velocities were computed by vertically integrating the continuity equation, assuming the atmosphere to be incompressible. Orographic and frictional effects were applied as lower boundary conditions. Three methods were implemented to account for frictional effects; one method used surface divergence in the vertical integration to indirectly compute frictional effects, and the other two methods applied parameterized equations to determine w at the top

of the planetary boundary layer based upon either observed or geostrophic relative vorticity. The indirect method (using divergence) was applied due to the negative bias in the profiler-derived relative vorticity values.

As an upper boundary condition, the vertical velocity was forced to equal zero at the 14 km level (in the stratosphere) by subtracting or adding a constant correction factor to the profiler-derived divergence field. The values of the correction factors ranged from $-1 \times 10^{-5} \text{ s}^{-1}$ to $2.5 \times 10^{-5} \text{ s}^{-1}$. These correction factors compensated for vertical accumulation of errors in the inferred horizontal divergences.

Ageostrophic winds were computed by evaluating the derivatives of the horizontal equations of motion. The derivatives were determined by use of the aforementioned finite differencing technique. The geostrophic winds were then computed by subtracting the calculated ageostrophic wind from the observed wind field.

No independent data set exists by which the above parameters can be evaluated rigorously. In general, however, the fields appeared realistic. First, the values exhibited considerable vertical and temporal coherence rather than random noise. Secondly, the values changed in a manner consistent with conceptual and theoretical models of the flow field of various meteorological phenomena. Thirdly, the winds and derived quantities were generally consistent with synoptic-scale data.

Strauch et al. (1984) estimated that the uncertainty in the measurement of the horizontal wind by Doppler wind profilers was $\pm 1 \text{ m/s}$. Using a scale analysis, this uncertainty would cause an

uncertainty of approximately $\pm 1.0 \times 10^{-5} \text{ s}^{-1}$ in the horizontal divergence and relative vorticity fields, an uncertainty of approximately $\pm 3 \text{ cm/s}$ in the vertical velocity field, and an uncertainty of approximately $\pm 3 \text{ m/s}$ in the ageostrophic and geostrophic winds.

Although the uncertainty appears to be large for the estimation of the vertical velocity field, the patterns of the vertical motions in two of the cases were nearly identical to the percentage of areal coverage of the precipitation echo over the profiler triangle. There were periods of upward motion where no precipitation occurred; however, inspection of the moisture profile from the Denver rawinsonde station indicated that the atmosphere was very dry during these time periods. Also, the relative magnitudes of the profiler-derived horizontal divergences, relative vorticities, vertical velocities, and geostrophic and ageostrophic winds were consistent with the profiler-derived quantities discussed in the literature by Zamora and Shapiro (1984), Smith and Schlatter (1986), and Zamora et al. (1986).

5.2 Summary of Meteorological Observations with the Profiler Data

The observed horizontal winds from the three profiler sites revealed mesoscale and synoptic-scale wind shifts and speed variations while cold fronts, short-wave troughs, and jet streaks passed through the profiler triangle. Rapid increases and decreases in wind speeds were observed as jet streaks imbedded in the jet stream moved over the profiler triangle. Green et al. (1978) also observed such speed variations as a jet streak passed over the Sunset

profiler. Strong vertical wind shears were observed below the jet streaks in a 1 to 2 km layer. Rüster and Czechowsky (1979), and Shapiro et al. (1984) also observed similar strong vertical wind shears with the SOUSY and Colorado network profilers, respectively. The observed horizontal winds from the profiler triangle also precisely revealed the location and intensity of the core of jet streams and jet streaks in northeastern Colorado. The objective analyses of the rawinsonde network data misrepresented both the location and intensity of these features in the case of September 22-23, 1985.

The horizontal spatial resolution of the profiler triangle aided in the observation of mesoscale features through northeastern Colorado. The combination of the time and horizontal spatial resolution of the observed winds and profiler-derived quantities revealed two meso-alpha-scale cyclonic circulations which passed through the profiler network. These meso-alpha-scale features were not evident in either the surface station or conventional rawinsonde networks. The meso-alpha-scale cyclone present in the September 22, 1985 case enhanced the low-level convergence which, in turn, forced stronger upward motions and heavier precipitation.

The profiler-derived quantities revealed synoptic-scale and mesoscale characteristics of lower and upper-level fronts, synoptic-scale troughs, and jet-stream-related features. For example, the profiler-derived relative vorticity field showed the anticyclonic and cyclonic shear related to the passage of jet streams and jet streaks over the profiler triangle, the cyclonic curvature associated

with synoptic-scale troughs, the time variation of relative vorticity or, in a spatial sense, the PVA and NVA related to upper-level trough passages, and the positive vorticity maxima related to two meso-alpha-scale cyclonic circulations. The profiler-derived horizontal divergence field illustrated convergence associated with lower and upper-level fronts, divergence and convergence patterns related to the transverse circulations found in jet streaks, and convergence related to the two meso-alpha-scale cyclonic circulations. The profiler-derived vertical velocities correlated well with the areal coverage of the precipitation echoes over the profiler triangle measured by the Limon, Colorado, WSR-57 radar. They revealed vertical circulations related to jet streaks, the vertical circulation associated with frontal and trough passages, and the enhanced vertical motion associated with the passage of a meso-alpha-scale cyclone.

The profiler-derived geostrophic winds revealed the meso-alpha-scale cyclonic circulation in the September 22-23, 1985 case. The profiler-derived ageostrophic winds identified the transverse circulations in both the exit and entrance regions of jet streaks, and the sub-geostrophic winds located in the curved flow of the trough axes. Zamora et al. (1986) also reported that the ageostrophic winds calculated using a linear vector point function with a triangle of profilers were also consistent with conceptual and theoretical models of jet stream dynamics. However, they pointed out that the magnitudes of the ageostrophic winds and other kinematic quantities are suspect when non-linear variations in the horizontal winds are occurring.

The patterns of the areally averaged profiler-derived relative vorticity, horizontal divergence, and vertical velocity fields, were consistent with patterns of the same quantities computed by Stankov and Shapiro (1986) during a passage of low-level cold front. They deduced positive vorticity, convergence, and rising motion prior to a low-level cold frontal passage, and negative vorticity, divergence and sinking motion after the low-level cold front passed, using a single profiler. However, the profiler-derived quantities computed in this thesis were two orders of magnitude less than those computed by Stankov and Shapiro because hourly averaged data were applied to the computations instead of the 1.2-minute data used by them.

5.3 Overall Conclusions

The conclusions from this study are:

- (1) Kinematic quantities derived from a triangle of VHF Doppler wind profilers show coherent patterns with the use of minimal filtering and smoothing techniques.
- (2) The temporal patterns of the profiler-derived kinematic quantities are consistent with the synoptic-scale and mesoscale patterns associated with cold fronts, upper-level troughs, and jet stream-related features, making the methods used in this study valuable diagnostic tools for research and possibly for nowcasting.
- (3) The patterns of the kinematic vertical velocities are well correlated with the pattern of areal coverage of precipitation echoes over the profiler triangle, when

precipitation occurs, although the magnitudes of the kinematic vertical velocities have fairly large uncertainties. Of course, upward motion can occur in dry air, so that moisture information from radiosondes, moisture profilers, or satellites should be used in conjunction with the profiler-derived kinematic vertical velocities to determine the likelihood of occurrence of precipitation.

BIBLIOGRAPHY

- Balsley, B. B., 1981: The MST technique - a brief review. J. Atmos. Terr. Phys., 43, 495-509.
- Balsley, B. B., and K. S. Gage, 1982: On the use of radars for operational wind profiling. Bull. Am. Meteor. Soc., 63, 1009-1018.
- Blackadar, A. K., 1957: Boundary layer wind maxima and their significance for the growth of nocturnal inversions. Bull. Am. Meteor. Soc., 38, 283-290.
- Cressman, G. P., 1959: An operational objective analysis system. Mon. Wea. Rev., 87, 367-374.
- Dutton, J. A., 1976: The Ceaseless Wind, McGraw-Hill, New York, 579 pp.
- Forbes, G. S., 1986: Examples of mesoscale structures and short-term wind variations detected by VHF Doppler radar. In Handbook for MAP, edited by S. A. Bowhill and B. Edwards, SCOSTEP Secretariat, University of Illinois, Urbana, IL, 17-29.
- Gage, K. S., and B. B. Balsley, 1978: Doppler radar probing of the clear atmosphere. Bull. Am. Meteor. Soc., 59, 1074-1093.
- Green, J. L., K. S. Gage, and T. E. Van Zandt, 1978: Three dimensional wind observations of a jet stream using a VHF Doppler radar. Preprint Vol., 18th Conf. on Radar Meteorology, Atlanta, GA, USA, Amer. Meteor. Soc., 184-189.
- Hogg, D. C., et al., 1983: An automatic profiler of the temperature, wind and humidity in the troposphere. J. Climate Appl. Meteor., 22, 807-831.
- Holton, J. R., 1979: An Introduction to Dynamic Meteorology, Academic Press, Inc., New York, 391 pp.
- Larsen, M. F., and J. Röttger, 1982: VHF and UHF Doppler radars as tools for synoptic research. Bull. Am. Meteor. Soc., 63, 996-1008.
- Murray, R., and S. M. Daniels, 1953: Transverse flow at entrance and exit to jet streams. Quart. J. Roy. Meteor. Soc., 79, 236-241.

- Nastrom, G. D., W. L. Ecklund, and K. S. Gage, 1985: Direct measurement of large scale vertical velocities using clear-air radars. Mon. Wea. Rev., 113, 708-718.
- Neiman, P., 1987: Wind profiler-derived temperature gradients and advections, M.S. Thesis, The Pennsylvania State University, August 1987.
- O'Brien, J. J., 1970: Alternative solutions to the classical vertical velocity problem. J. Appl. Meteor., 9, 197-203.
- Röttger, J., 1979: VHF radar observations of a frontal passage. J. Appl. Meteor., 18, 85-91.
- Röttger, J., and G. Schmidt, 1981: Characteristics of frontal zones determined from spaced antenna VHF radar observations. Preprint Vol., 20th Conf. on Radar Meteorology, Boston, MA, USA, Amer. Meteor. Soc., 30-37.
- Rüster, R., and P. Czechowsky, 1980: VHF radar measurements during a jet stream passage. Radio Sci., 15, 363-369.
- Shapiro, M. A., 1974: A multiple-structured frontal zone jet stream system as revealed by meteorologically instrumented aircraft. Mon. Wea. Rev., 102, 244-253.
- Shapiro, M. A., 1978: Further evidence of the mesoscale and turbulent structure of upper level jet stream-frontal zone systems. Mon. Wea. Rev., 106, 1100-1111.
- Shapiro, M. A., and P. J. Kennedy, 1981: Research aircraft measurements of jet stream geostrophic and ageostrophic winds. J. Atmos. Sci., 38, 2642-2652.
- Shapiro, M. A., and P. J. Kennedy, 1982: Airborne radar altimeter measurements of geostrophic and ageostrophic winds over irregular topography. J. Appl. Meteor., 21, 1739-1746.
- Shapiro, M. A., T. Hampel, and D. W. van de Kamp, 1984: Radar wind profiler observations of fronts and jet streams. Mon. Wea. Rev., 112, 1263-1266.
- Smith, T. L., and T. W. Schlatter, 1986: The real-time use of wind profilers in nowcasting. In Handbook for MAP, edited by S. A. Bowhill and B. Edwards, SCOSTEP Secretariat, University of Illinois, Urbana, IL, 53-59.
- Stankov, B. B., and M. A. Shapiro, 1986: High frequency (~2 min) profiler measurements of wind and thermodynamic profiles during a surface cold front passage. Profiler Forum, December 1986.

- Strauch, R. G., et al., 1984: The Colorado wind-profiling network. J. Atmos. Oceanic Tech., 1, 37-49.
- Syrett, W., 1987: Some applications of 50 MHZ wind profiler data: Detailed observations of the jet stream, M.S. Thesis, The Pennsylvania State University, August 1987.
- Uccellini, L. W., and D. R. Johnson, 1979: The coupling of upper and lower tropospheric jet streaks and implications for the development of severe convective storms. Mon. Wea. Rev., 107, 682-703.
- Zamora, R. J., and M. A. Shapiro, 1984: Diagnostic divergence and vorticity calculations using a network of mesoscale wind profilers. Preprint Vol., 10th Conf. on Weather Forecasting and Analysis, Clearwater Beach, FL, USA, Amer. Meteor. Soc., 386-391.
- Zamora, R. J., M. A. Shapiro, and C. A. Doswell III, 1987: The diagnosis of upper tropospheric divergence and ageostrophic wind using profiler wind observations. Mon. Wea. Rev., 115, accepted.

END

6-89

DTIC